N° d'ordre NUM_ORDRE
Année 2014

Thèse

Non-Linear Mechanics of Generalized Continua and Applications to Composite Materials

Présentée devant
L'institut national des sciences appliquées de Lyon
et
L'Université de L'Aquila, Italie

Pour obtenir
Le grade de docteur

Formation doctorale
Ecole doctorale Mécanique, Energétique, Génie Civil, Acoustique (MEGA)
Spécialité : Mécanique, génie mécanique, génie civil

Par
Manuel FERRETTI

Soutenue le 07 Novembre 2014 devant la Commission d'examen

Jury

BOISSE Philippe	Professor (INSA Lyon)	Directeur
DELL'ISOLA Francesco	Professor (La Sapienza, Italie)	Examinateur
LUONGO Angelo	Professor (Univ. de L'Aquila, Italie)	Directeur
MADEO Angela	Maitre de Conférences (INSA Lyon)	Co-encadrante
NEFF Patrizio	Professor (Univ. de Duisburg-Essen, Allemagne)	Rapporteur
REMOND Yves	Professor (Univ. de Strasbourg)	Rapporteur
RUBINO Bruno	Professor (Univ. de L'Aquila, Italie)	Examinateur

LaMCoS - UMR CNRS 5259 - INSA de Lyon

20, avenue Albert Einstein, 69621 Villeurbanne Cedex (FRANCE)

INSA Direction de la Recherche - Ecoles Doctorales – Quinquennal 2011-2015

SIGLE	ECOLE DOCTORALE	NOM ET COORDONNEES DU RESPONSABLE
CHIMIE	**CHIMIE DE LYON** **http://www.edchimie-lyon.fr** Sec : Renée EL MELHEM Bat Blaise Pascal 3e etage 04 72 43 80 46 Insa : R. GOURDON	M. Jean Marc LANCELIN Université de Lyon – Collège Doctoral Bât ESCPE 43 bd du 11 novembre 1918 69622 VILLEURBANNE Cedex Tél : 04.72.43 13 95 directeur@edchimie-lyon.fr
E.E.A.	**ELECTRONIQUE, ELECTROTECHNIQUE, AUTOMATIQUE** **http://edeea.ec-lyon.fr** Sec : M.C. HAVGOUDOUKIAN eea@ec-lyon.fr	M. Gérard SCORLETTI Ecole Centrale de Lyon 36 avenue Guy de Collongue 69134 ECULLY Tél : 04.72.18 60.97 Fax : 04 78 43 37 17 Gerard.scorletti@ec-lyon.fr
E2M2	**EVOLUTION, ECOSYSTEME, MICROBIOLOGIE, MODELISATION** **http://e2m2.universite-lyon.fr** Sec : Safia AIT CHALAL Bat Darwin - UCB Lyon 1 04.72.43.28.91 Insa : H. CHARLES	Mme Gudrun BORNETTE CNRS UMR 5023 LEHNA Université Claude Bernard Lyon 1 Bât Forel 43 bd du 11 novembre 1918 69622 VILLEURBANNE Cédex Tél : 06.07.53.89.13 e2m2@ univ-lyon1.fr
EDISS	**INTERDISCIPLINAIRE SCIENCES-SANTE** **http://www.ediss-lyon.fr** Sec : Safia AIT CHALAL Hôpital Louis Pradel - Bron 04 72 68 49 09 Insa : M. LAGARDE Safia.ait-chalal@univ-lyon1.fr	Mme Emmanuelle CANET-SOULAS INSERM U1060, CarMeN lab, Univ. Lyon 1 Bâtiment IMBL 11 avenue Jean Capelle INSA de Lyon 696621 Villeurbanne Tél : 04.72.68.49.09 Fax :04 72 68 49 16 Emmanuelle.canet@univ-lyon1.fr
INFOMATHS	**INFORMATIQUE ET MATHEMATIQUES** **http://infomaths.univ-lyon1.fr** Sec :Renée EL MELHEM Bat Blaise Pascal 3e etage infomaths@univ-lyon1.fr	Mme Sylvie CALABRETTO LIRIS – INSA de Lyon Bat Blaise Pascal 7 avenue Jean Capelle 69622 VILLEURBANNE Cedex Tél : 04.72. 43. 80. 46 Fax 04 72 43 16 87 Sylvie.calabretto@insa-lyon.fr
Matériaux	**MATERIAUX DE LYON** **http://ed34.universite-lyon.fr** Sec : M. LABOUNE PM : 71.70 –Fax : 87.12 Bat. Saint Exupéry Ed.materiaux@insa-lyon.fr	M. Jean-Yves BUFFIERE INSA de Lyon MATEIS Bâtiment Saint Exupéry 7 avenue Jean Capelle 69621 VILLEURBANNE Cedex Tél : 04.72.43 83 18 Fax 04 72 43 85 28 Jean-yves.buffiere@insa-lyon.fr
MEGA	**MECANIQUE, ENERGETIQUE, GENIE CIVIL, ACOUSTIQUE** **http://mega.universite-lyon.fr** Sec : M. LABOUNE PM : 71.70 –Fax : 87.12 Bat. Saint Exupéry mega@insa-lyon.fr	M. Philippe BOISSE INSA de Lyon Laboratoire LAMCOS Bâtiment Jacquard 25 bis avenue Jean Capelle 69621 VILLEURBANNE Cedex Tél :04.72 .43.71.70 Fax : 04 72 43 72 37 Philippe.boisse@insa-lyon.fr
ScSo	**ScSo*** **http://recherche.univ-lyon2.fr/scso/** Sec : Viviane POLSINELLI Brigitte DUBOIS Insa : J.Y. TOUSSAINT	Mme Isabelle VON BUELTZINGLOEWEN Université Lyon 2 86 rue Pasteur 69365 LYON Cedex 07 Tél : 04.78.77.23.86 Fax : 04.37.28.04.48 viviane.polsinelli@univ-lyon2.fr

*ScSo : Histoire, Géographie, Aménagement, Urbanisme, Archéologie, Science politique, Sociologie, Anthropologie

Non-Linear Mechanics of Generalized Continua and Applications to Composite Materials

Abstract

The micro-structure of materials is an essential feature for the design of engineering structures with improved performances. Generalized continuum theories are able to account for the effect of microstructure on the overall mechanical behavior of architectured materials. Indeed, one of the most promising fields of application of generalized continuum theories is that of the study of the mechanical behavior of woven fibrous composite reinforcements. Such metamaterials are constituted by two order of fibers which have very high elongation stiffness, but very low shear stiffness. This strong contrast in the mechanical properties of the mesostructure is such that the homogenized material must necessarily be described at least in the framework of second gradient theories. As a matter of fact, classical Cauchy theories are not sufficient for the description of specific deformation patterns usually observed in such fibrous composites such as concentration of high gradients of strains in thin boundary layers which can be seen to be related to flexural strains of the fibers. It is worth to stress the fact that a classical Cauchy continuum theory is not able in any case to take into account the effect of flexural bending stiffness of the yarns on the overall mechanical behavior of fibrous composite reinforcements. On the other hand, it is easy to understand that such a mesoscopic deformation mechanism may have an important macroscopic effect on the overall deformation of the considered material, at least for particular boundary conditions and/or applied external loads. It can be easily understood that the bending of the yarns, which takes place at lower scales, must be necessarily taken into account if one wants to fully characterize the behavior of fibrous composite reinforcements from a mechanical point of view. The macroscopic manifestation of mesostructure could indeed play an important role when considering the molding process of the reinforcement which may sometimes take complicated shapes so allowing the conception of complex engineering structural elements. It is clear that, during the forming process of the raw woven composite, the flexural rigidity of the yarns may play an important role on the final deformation of the blade. It is for this reason that a generalized continuum theory is mandatory if one wants to correctly predict the final deformed shape of the considered fiber reinforcements while remaining in a continuum framework.

In the light on such considerations, we propose to use a second gradient continuum theory to completely describe the mechanical behavior of woven fibrous composite reinforcements. The introduced second gradient model is used to simulate the so-called bias extension test on 2D woven reinforcements and a three point bending test on thick composite interlocks. In both cases, the effect of the bending of the yarns at the mesoscopic level is seen to be essential to correctly describe the deformation of the specimens at higher scales.

Keywords: Woven fibrous composite reinforcements, second gradient theories, generalized continua, bias extension test, three point bending of composite interlocks.

Mécanique non-linéaire des milieux continus généralisés et applications aux matériaux composites

Résumé

La microstructure des matériaux est un levier essentiel pour l'optimisation des propriétés mécaniques des structures. Le passage à la description continue de la matière conduit souvent à une simplification trop drastique de la réalité et à une perte significative d'informations. Les développements de la mécanique des milieux continus, des moyens de calcul numérique et des techniques expérimentales permettent aujourd'hui de rendre compte des effets d'échelle observés en mécanique des matériaux et des structures. Le but primaire de cette thèse a été celui de développer un modèle continu de gradient supérieur pour intégrer dans la modélisation continue la morphologie complexe des microstructures ainsi que les longueurs caractéristiques associées. Ce modèle continu généralisé a ensuite été utilisé pour décrire en détail le comportement mécanique des renforts de composites textiles. Des simulations numériques qui montrent l'importance des termes de deuxième gradient pour la correcte description du comportement mécanique de ces matériaux ont été développées dans le cadre de cette thèse à l'aide du software COMSOL Multiphysics. Il a été montré que des théories de deuxième gradient sont nécessaires pour intégrer dans la modélisation continue l'effet de la flexion des mèches au niveau mesoscopique. Ceci a été mis en évidence pour le cas du "bias extension test" et de la flexion trois points d'un interlock 3D de composite. Pour le cas du "bias extension test", les termes de deuxième gradient permettent la description de certaines couches limites qui déterminent une zone de transition entre deux régions à angle de cisaillement constant. Pour ce qui concerne la flexion trois points des interlocks de composite, il a été montré que les termes de deuxième gradient sont nécessaires pour décrire correctement la déformée des deux extrémités de la poutre et la courbure au milieu de l'échantillon. Dans les deux exemples traités, l'effet de la flexion des mèches à l'échelle mesoscopique est le mécanisme principal donnant lieu aux effets de deuxième gradient.

Mots-Clés: Renforts fibreux de composite, théories de second gradient, milieux continus généralisés, bias extension test, flexion trois points d'un interlock de composite.

Contents

List of Figures

List of Tables

General Introduction

It is nowadays well accepted that the microstructure of materials can be suitably tailored in order to design engineering metamaterials which show better performances and new functionalities. In this optic, a class of materials which is gaining more and more attention is that of so-called complex materials, e.g. materials exhibiting different mechanical responses at different scales due to different levels of heterogeneity. In fact, the overall mechanical behavior of such materials is macroscopically influenced by the underlying microstructure especially in presence of particular loading and/or boundary conditions. Therefore, understanding the mechanics of meso- and micro-structured materials is becoming a fundamental issue in engineering.

Complex metamaterials may exhibit superior mechanical properties with respect to more commonly used engineering materials, also providing some advantages as easy formability processes, light weight and exotic behavior with respect to wave propagation. In this manuscript we address the problem of the description of the mechanical behavior of a class of complex engineering materials which are known as woven fibrous composite reinforcements. These materials possess a hierarchical microstructure, since they are constituted by woven tows which are themselves made up of thousand of fibers. We will show that the meso- and micro-structure of fibrous composites actually have a strong impact on the overall mechanical behavior of the macroscopic engineering piece. In particular, the macroscopic manifestation of the microstructure of such materials is accounted for by i) the use of suitable orthotropic constitutive laws which allow for the description of two privileged directions in the material corresponding to warp and weft and ii) the introduction of second gradient terms in the strain energy density which permit to take into account the bending stiffness of the yarns.

A first gradient continuum orthotropic model is not able, alone, to take into account all the possible effects that the microstructure of considered materials have on their macroscopic deformation. More precisely, some particular loading conditions, associated to particular types of boundary conditions may cause some microstructure-related deformation modes which are not fully taken into account in first gradient continuum theories. This is the case, for example, when observing some regions inside the materials in which high gradients of deformation occur, concentrated in relatively narrow regions. One way to deal with the description of such boundary layers, while remaining in the framework of a macroscopic theory, is to consider so-called "generalized continuum theories". Such generalized theories allow for the introduction of a class of internal actions which is wider than the one which is accounted for by classical first gradient Cauchy continuum theory. These more general contact actions excite additional deformation modes which can be seen to be directly related with the properties of the microstructure of considered materials.

The main aim of the present work is to explicitly show the interest of using second gradient theories for the modeling of the mechanical behavior of fibrous composite reinforcements. This task will be accomplished by presenting a second gradient modeling for two important experimental tests on such materials, namely the "bias extension test" on 2D woven fabrics and the three point bending of thick composite interlocks. We will show, by presenting suitable numerical simulations, that in both cases the second gradient elastic moduli are able to describe the effect of the bending stiffness of the yarn on the macroscopical behavior of considered materials.

This manuscript is constituted by six chapters. In the first one the hierarchical microstructure of fibrous composite reinforcements is described in detail and some elementary tests, usually performed in order to characterize the mesoscopic and macroscopic behavior of these materials, are presented.

In chapter 2 the fundamental concepts and methods of the first gradient theory are recalled: representation theorems, some classical constitutive laws for isotropic materials and the strong form of the equations of motion are presented.

In the chapter 3 the basic kinematics of the micro-structured continua in the framework of nonlinear regime is presented and the linear theory proposed by Mindlin [MIN64] is discussed through a comparison with some new models recently proposed in the literature [NEF13, MAD13]. It is also shown how to obtain a particular generalized theory by constraining a more general one by imposing suitable constraints. We finally derive the equations of motion in strong form for a micromorphic continuum by means of a suitable variational procedure.

In chapter 4 some well-established facts about second gradient theories are recalled and, in particular, the general equations of motion in strong form for a hyperelastic, second gradient material are presented. Finally, a generalized Hooke's law for linear second gradient material is presented to the sake of introducing some basic tools about constitutive modeling in second gradient theories.

In chapter 5 a technologically important class of fibrous composite reinforcements is considered and their mechanical behavior is described at finite strains by means of a second gradient, hyperelastic, orthotropic continuum theory which is obtained as the limit case of a micromorphic theory. The case of the bias extension test is analyzed and it is shown that second gradient energy terms allow for an effective prediction of the onset of internal shear boundary layers which are related to in-plane bending stiffness of the yarns.

Finally, in chapter 6 we propose to apply a suitable second gradient model to the case of the three point bending of composite interlocks. We show that second gradient terms are able to account for the effect of the out-of-plane bending stiffness of the yarns on the macroscopic bending of the specimen.

Chapter 1

Modeling the mechanical behavior of woven fibrous composite reinforcements

In this chapter we show that fibrous composite reinforcements are materials with hierarchical microstructure. Indeed, different scales of heterogeneities may be identified, namely the microscopic scale (scale of the fiber), the mesoscopic scale (of the yarns) and the macroscopic scale (of the engineering piece). The micro- and meso-structure of the considered materials play a crucial role on the overall mechanical behavior of the material at the macroscopic scale. We try here to specify which are the main characteristics of the micro- and meso-structures which have a macroscopic manifestation on the overall behavior of woven fibrous composite reinforcements. Some simple mechanical tests are presented which allow to characterize some basic macroscopic deformation modes as related to the meso- and microscopic ones. All the considerations exposed in this chapter are at the basis of the conception of suitable macroscopic hyperelastic constitutive laws to be used in the modeling of fibrous composite reinforcements in the framework of a continuum theories.

Contents

1.1 General introduction

By definition, a composite material is a combination of two or more constituents which are not miscible and whose resultant properties are improved with respect to those of the individual components used separately. Composite materials are usually constituted by two phases, namely the reinforcement and the matrix. These two phases posses different functionalities: the reinforcement gives the fundamental mechanical properties to the material and the matrix plays the role of cohesion between the different components. The main advantages which can be found in the use of these materials are light weight, improved strength and stiffness and the possibility of constructing new materials, designed *ad hoc*, by choosing in an appropriate way the mechanical properties of the constituents. There exists several examples of natural or artificial materials which respect the definition given above and which can henceforth be classified as composite materials. Among them we list, for example, wood, bone, mud brick and concrete, etc.

In the context of this manuscript we will be interested in the description of the mechanical behavior of some particular composite materials which are known as **woven fiber-reinforced composites**. Such materials are conceived by molding the raw fiber reinforcement into the desired shape and then injecting a polymeric resin which confers the final stiffness to the engineering piece. In the framework of the present thesis we will consider the study of the mechanical behavior of the raw woven reinforcement alone, before the injection of the polymeric resin. This study is of crucial interest for an accurate description of the forming process of such reinforcements. The tools which are needed to develop a complete theoretical framework for the description of the behavior of such materials are not trivial since different complicated aspects must be taken into account. We will show in the remainder of this thesis how the following points must be addressed when dealing with the modeling of fibrous composite reinforcement:

- development of suitable hyperelastic constitutive laws which allow for the description of an average material behavior at large strains,
- development of a generalized continuum theory which is able to account for the effect of the presence of the mesostructure on the overall mechanical behavior of the considered material.

To approach the first problem, we will follow the efforts made in [CHA11b, ORL12, CHA12] in which suitable hyperelastic, orthotropic constitutive laws are given for fibrous composite reinforcements.

The second problem is the key point of the present work, since different approaches are indeed possible in order to account for the presence of microstructure on the homogenized behavior of the material a higher scales (see e.g. homogenization methods, multi-scale methods etc.). One of the possible approaches is that of remaining in the framework of a continuum theory, while trying at the same time to account somehow for the effect of microstructure on the overall behavior of the considered materials. This can be done (see e.g. [FOR06, ERI01, MIN64]) by using so called generalized continuum theories which will be presented in detail in the body of this manuscript.

Before approaching more closely the problem of the mechanical modeling of fibrous composite reinforcements, we recall in the following subsections some general aspects concerning composite materials.

1.1.1 The Matrix

There are different types of matrix that can be used for conceiving a composite materials and the choice usually depends on different aspects concerning the characteristics that the composite material must posses. In general, all these matrices can be schematically divided in two categories:

- the organics matrices,
- the mineral matrices.

Examples of materials belonging to the first category are thermoplastic polymers, thermosetting polymers and elastomers. On the other hand, examples for the second category are ceramics, metals and graphite. The first category is the most used in the industry, while the second is are generally employed to build advanced materials or when the environment is not suitable for the use of organic matrix (high temperature and/or unfavorable humidity).

1.1.2 The Reinforcements

The reinforcements may be of various type and are generally classified by their geometry. One can henceforth classify them as

- particulate reinforcements: this type of reinforcement consists in a series of inclusions dispersed in the matrix. Such inclusions may be of different type: granular, lamellar or needle-shaped.
- reinforcements with discontinuous fibers: such reinforcementss are constituted by fiber of short length that posses generally a random orientation.
- reinforcement with continuous fibers: this type of reinforcement is constituted by an assembly of continuos fibers which posses a length comparable to the dimensions of the workpiece. These fibers are generally oriented in specific directions in order to confer to the reinforcement specific mechanical properties.

The fibers which constitute the reinforcement (continuous or not) may be of different nature: glass, metal, etc. In this manuscript, as already mentioned above, we will focus our attention on the reinforcements with continuos fibers and, in particular, on the so called class woven fibrous reinforcements.

1.2 Woven fibrous composite reinforcements

The reinforcements that will be the object of the study exposed in this manuscript are classified as woven fibrous reinforcements. Such materials are constituted by packages of fibers, which are called **yarns**, that are woven following more or less complex weaving patterns. In general, one can classify the weaving as:

- 2D weaving;
- 2.5D weaving (interlocks);
- 3D weaving (tridimensional);

A brief description of each of these three classes can be found below.

In this manuscript we will address the problem of the mechanical modeling of such reinforcements and we will present some examples concerning the characterization of the mechanical behavior of 2D and 2.5D fibrous reinforcements.

1.2.1 2D Weaving

This type of weaving is obtained by interleaving two networks (warp and weft), which are the preferred directions of the fabric. There exists three principal patterns for the 2D weaving:

- the *plain weave* is the more simple pattern: each warp yarn passes alternately over and under each weft yarn (see Fig. 1.1);
- the *twill* ($n \times m$): the warp yarn passes alternatively over n and under m yarns in the weft direction by shifting from a given number of yarns at each passage (see Fig. 1.1);

- the *satin*: the binding points of the warp and weft are scattered so as to mitigate the diagonal effect of the twill (see Fig. 1.1).

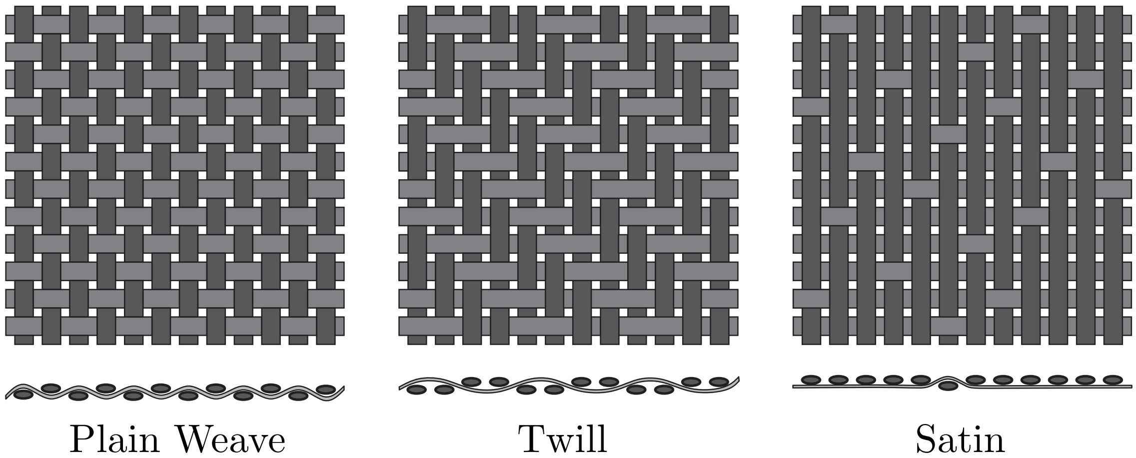

Figure 1.1: Different pattern for the 2D weaving.

1.2.2 2.5D Weaving - Interlock

Interlocks are 2.5D woven reinforcements, in which multiple layers of warp are joined together by a plurality of weft. This structure of interwoven layers avoids the problems of delamination that may occur in multi-layered materials obtained by superimposing independent woven layers and permits the realization of thick reinforcements (see e.g. Fig. 1.2). Such materials are very expensive and are hence reserved for advanced aeronautics and aerospace applications.

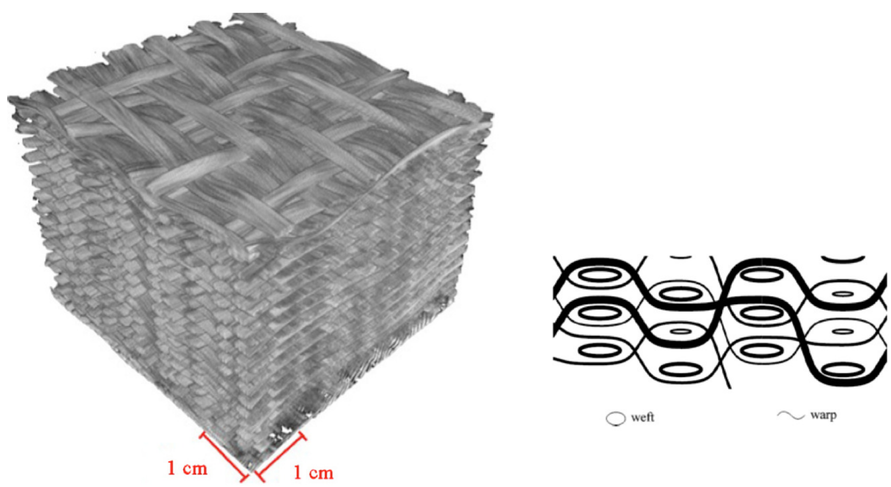

Figure 1.2: Example of 3D woven composite interlock reinforcement [ORL12] and general principle of the interlock weaving pattern.

1.2.3 3D Weaving

This type type of weaving is obtained by adding a complete third direction of weaving to the warp and weft described above. Such materials differ from the 2.5D described above since they are thicker and they present a third material direction. The application of such reinforcements is nowadays rather limited since the third weaving directions usually produces spurious concentrations of stress after the forming process and the subsequent injection of the polymeric matrix. Such problem of stress localization may be deleterious for the engineering structure and is indeed much reduced when using 2.5D reinforcements.

1.3 Multi-scale mechanical behavior of fibrous composite reinforcements

In the light of the aforementioned description, it becomes clearer that woven composite reinforcements are multi-scale materials and that their macroscopic mechanical behavior is influenced by the different scales presented by the material. The hierarchical heterogeneity of composite reinforcements is illustrated in Fig. 1.3, in which three different scales can be recognized:

- the macroscopic scale (left): scale of the specimen;
- the mesoscopic scale (center): scale of the mesh;
- the microscopic scale (right): scale of the fibre.

The study of the mechanical behavior of the material at the different scales itemized above permits a correct characterization of its phenomenological behavior. Indeed, we will show that the mesoscopic scale of the material has a visible effect on the overall mechanical behavior at the macroscopic scale. Such influence of the microstructure on the averaged behavior of the material has a twofold nature related to: i) the orthotropy conferred to the material by the presence of the woven yarns and ii) the effect of some mesostructural properties (as the effect of the bending stiffness of the yarns) on the macroscopic deformation mechanisms. We will show in this manuscript how the first point concerning the orthotropy of the material will be approached by means of the use of suitable hyperelastic constitutive laws, while the second point will be addressed by using generalized, second gradient, continuum theories.

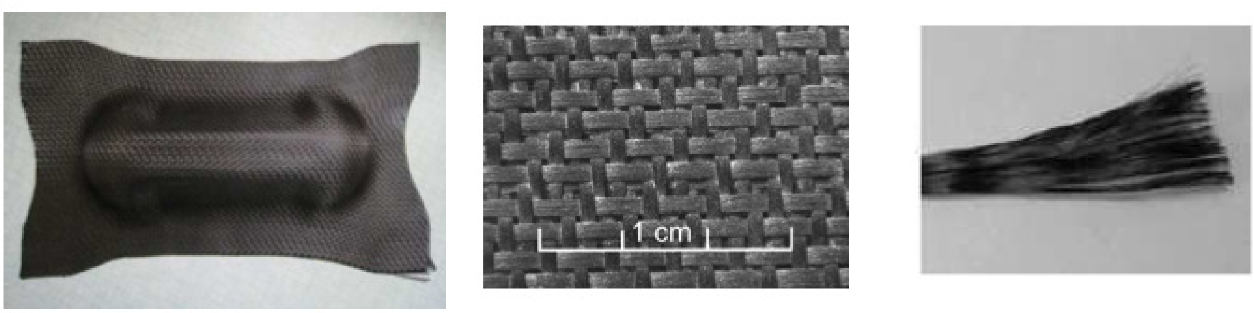

Figure 1.3: Macro, meso and microscopic scale of the composite reinforcement.

1.3.1 Mesoscopic behavior at the scale of the yarns

The macroscopic behavior of the material is influenced by deformations mechanisms associated to the deformation of the yarns at the mesoscopic scale. Such mesoscopic deformation mechanisms are, in turn, influenced by the microscopic structure of the material, i.e. by the behavior of the fibers which constitute the yarns. In the remainder of this manuscript we will try to clarify how the microscopic and above all the mesoscopic properties of the considered material influence the deformation of the macroscopic piece. To do so we will need to

- develop suitable first gradient hyperelastic, orthotropic constitutive laws at the macroscopic scale and

- develop suitable second gradient macroscopic constitutive laws in order to account for the effect of the bending stiffness of the yarns (and hence of the fibers) at the macroscopic scale.

In order to be able to conceive realistic macroscopic constitutive laws one needs to understand deeply which are the deformation mechanisms which take place at the mesoscopic scale. To do so, it is sensible to describe some basic experimental tests which are used in the community of woven fiber reinforcements and which allows for the measurement of simple mechanical parameters related to simple deformation mechanisms at the mesoscopic and microscopic scales. The presentation and description of such experimental tests has then the twofold aim of i) better understanding the deformation mechanisms which may take place at the mesoscopic (and also microscopic) scale and ii) propose some simple procedures to measure some mechanical characteristics of the material at the mesoscopic (or microscopic) scale.

1.3.1.1 Behavior of the Yarn Under Tension

The yarns, as already remarked above, are constituted by many fibers. When a yarn is subjected to tension a nonlinear behavior can be recognized which is due to the fact that the fibers are not all stretched simultaneously. Naturally, the type of nonlinearity also depends on the material which constitutes the yarn (and then the fibers) which may be e.g. glass or carbon, and on the procedure of fabrication. Nevertheless, when reaching a certain threshold load, corresponding to which the fibers are all stretched, the yarn starts showing a very high stiffness. When the transition from the nonlinear behavior to the acquisition of the complete stiffness of the yarn does not have significant effects on the macroscopic material behavior of the woven fabric, one can also consider, as a limit case that the fibers are inextensible. The study of the material behavior of woven composite reinforcements based on such simplifying hypothesis (inextensibility) could be of interest in order to obtain some "reference" material behaviors starting from which one could then conceive more complicated constitutive laws. Nevertheless, such study introduces conceptual difficulties related to the fact that the ratio between the value of the tension stiffness and that of the shear stiffness tends to infinity. If such limit case could be perhaps analyzed by looking for suitable analytical solutions obtained imposing some particular loading and boundary conditions, it is instead very delicate to be treated from a numerical point of view. Indeed, it is known (see [HAM13a, HAM13b]) that when one consider very high tension stiffnesses (of many orders of magnitude higher than the shear stiffness) of the yarns then phenomena of locking can be observed when performing numerical simulations that do not allow to obtain the correct solution to the considered differential problem.

1.3.1.2 Compaction of the Yarn in the Transverse Plane

The compaction of the yarn is defined as the change of the area in the transversal plane to the yarn, which is the plane orthogonal to the fibers directions. When the yarn is compressed in the direction orthogonal to its main direction the internal fibers are more closely packed together and fill the voids initially present in the transversal section of the fibers. We remark that the behavior of the material in compaction presents an asymptotical behavior: after an initial phase in which the fibers organize themselves in such a way that the voids are filled, the material shows an increased stiffness. In particular, the stiffness of the yarn finally tends to the stiffness of the material constituting the fibers. In addition, is it worth noting that this type of mechanism is difficult to characterize from an experimental point of view due to the fact that a pure compaction test is difficult to be realized and reproduced.

1.3.1.3 Shear Behavior of the Yarn

There exist two types of shear modes in the yarns

- the *distortion*: this deformation mode occurs in the transversal plane of the yarn;

- the *transverse shear*: this deformation mode occurs in the direction of the fibers.

The first deformation mode is characterized by the fact that the cross section of the yarn changes its shape without activating compaction deformation modes. Such deformation mode is due to the fact that the fibers constituting the yarn slide one with respect to the other in order to adapt the overall imposed deformation. So, if one considers, for example, a yarn with cross sections which are initially, let us say, vertical and if a bending deformation is imposed to the yarns, the fibers are forced to slide one with respect to the other in order to let the yarn assume the desired form and, at the same time, let the fibers respect the quasi-inextensibility constraint. This internal sliding of the fibers can be interpreted as a motion of the cross sections (for example a rotation). It is worth noting that a coupling mechanism can be recognized between the compaction of the yarn and its distortion: when the yarn is compacted the distortion of the yarn occurs with increased difficulty. This is sensible since when the fibers are compacted friction mechanisms are more pronounced which render sliding more difficult.

The transverse shear is a deformation mode in the direction of the fibers and corresponds in to a sliding between the fibers in the direction of the fibers themselves. As for the distortion, an increased compaction of the yarn causes a stiffening effect on the transversal shear. It can be also understood that, being the two quoted deformation modes of the yarns based on the same microscopic mechanism of fibers', a coupling exists between them. Both these types of deformation are difficult to be characterized from an experimental point of view, in particular the stiffening effects due to compaction.

1.3.1.4 Behavior of the Yarn Subject to Bending

There exist only few studies which concern the behavior of the yarns subjected to bending. This type of studies, however, is interesting since the bending properties of the yarns can affect the macroscopical behavior of the specimen. In particular, as we will see in the next chapters, the fact of neglecting the effect of the bending stiffness of the yarns (and so of the fibers), produces macroscopic models that are not able to describe all the experimental evidences. As it will be shown in detail in the remainder of this manuscript, a Cauchy continuum theory is not able to account for the effect of bending stiffness of the yarns on the macroscopic behavior of the fabric. It is for this reason that generalized continuum theories (second gradient) may be introduced to palliate this inconvenience. Such theories are indeed able to account for the macroscopic manifestation of the mesoscopic bending of the yarns, still remaining in the framework of a continuum theory. In addition to what said, the characterization of the behavior of the yarn subjected to bending is necessary if one wants to realize a macroscopic model by the use of suitable homogenization procedures. These latters, as well-known, start from the characterization of the microstructure and it is evident how the experimental characterization can be fundamental to determine such microscopic properties.

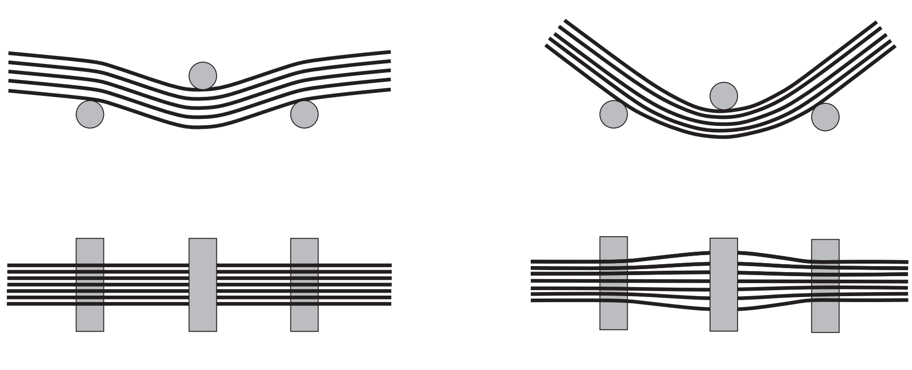

(a) (b)

Figure 1.4: Bending of the yarn before the lateral expansion (a) and after (b).

When the mesh is subjected to a three point bending test, three different types of mechanism are turned on, that are (see Fig. 1.4)

- the transversal shear of the yarn;
- the bending of the fibers which constitute the mesh;
- the lateral expansion of the fibers in correspondence of the central support.

The first mechanism is activated due to the internal sliding of the fibers which takes pace as a consequence of the fact that they are bending together and that they are almost inextensible. The activation of the second mechanism is indeed evidently easy to understand. As for the third mechanism, one can imagine that the contact with the central support can indeed let the fibers rearrange in the horizontal plane.

1.3.2 Macroscopic Behavior

In order to characterize the macroscopic mechanical behavior of woven fibrous composite reinforcements one must start from the conception of suitable elementary material tests that we try to describe in this section. The tests described here will be subsequently used for the identification of the first gradient constitutive laws used to describe the homogenized behavior of the considered material.

1.3.2.1 Uniaxial Extension Test

The behavior of the material subjected to uniaxial tension test results to be nonlinear. This nonlinearity is due to the compaction of the yarns and the undulation of the tissue (with the subsequent straightening). More particularly, when an uniaxial tension test is performed on a given specimen, two successive phenomena can be observed

- a reduction of the undulation in the direction of the solicitation up to arrive to a complete straightening of the yarns,
- the elongation of the yarns in the direction of the solicitation.

These two mechanisms give an easy interpretation of the diagram obtained from experimental measurements in the plane force vs imposed displacement (see [CHA11b, ORL12]). In the first phase, corresponding to the reduction of the undulation of the yarns in the direction of the solicitation, the material possesses a stiffness that increases as the undulation decreases. When the complete straightening of the solicited yarns is reached, the material offers a constant stiffness which corresponds to an increasing force measured in function of the elongation of the yarns.

It is worth noticing that the stiffness at elongation showed by fibrous composite reinforcements strongly depends on the orientation of the yarns with respect to the sides of the considered specimen. Indeed, if one order of yarns is directed as the side of the specimen which is parallel to the applied load, then the tension stiffness of the macroscopic material will be the maximum possible. A small elongation of the macroscopic specimen will be observed due to a reduction of the undulation of the weaving pattern. On the other hand, if the fibers are not parallel to the side of the specimen (and hence to the applied load) the resistance to tension is much lower and significant macroscopic elongations can be observed which are substantially due to pantographic motions of the yarns (see Fig. 6.7).

Such experimental test can be used to characterize the constitutive behavior at elongations of the macroscopic pieces. The macroscopic elongation mechanism can be easily activated when considering standard loading conditions on macroscopic specimens.

1.3.2.2 Biaxial Extension Test

The biaxial extension test is performed by soliciting to tension the material simultaneously in the warp and weft directions. If one denotes the deformation in one of the solicited observed direction as ε_{obs} (i.e. warp or weft) and the deformation in the orthogonal direction as $\varepsilon_{\text{orth}}$, is possible to define the coefficient of the biaxial extension test as

$$k = \frac{\varepsilon_{\text{orth}}}{\varepsilon_{\text{obs}}}, \tag{1.1}$$

from which different cases of solicitation can be classified

- $k = 0$ or $k = \infty$ corresponds to a limit case in which the biaxial test degenerates into an uniaxial one;
- $k = 1$ corresponds to an equal solicitation in both direction;
- $k = r$ with $r \in \mathbb{R}$ corresponds to a solicitation case in which the deformation in the orthogonal direction is r times the deformation in the observed one.

The results of the test, naturally, depend on the chosen value of the coefficient k and one can experimentally observe that when $k = 1$ the deformation in the observed direction is due to the compaction of the yarns, indeed when $k = 0$ or $k = \infty$ the deformation is due to the reduction of the undulation (that involves the shear of the yarns in its transversal plane). When $k = r$ the two mechanism are in competition. The biaxial extension test can be hence used if one wants to understand better which is the effect of such two deformation mechanisms on the overall mechanical behavior of the macroscopic piece.

1.3.2.3 Transversal Compression Test

The transversal compression test is a test realized by compressing a specimen of composite reinforcement between two parallel plates. This test permits the characterization of the behavior of the material in the direction orthogonal to the plane of warp and weft. Performing the test, one can observe that this behavior results to be nonlinear, since the the contact between the yarns and fibers increases when the plates approach one to the other. In oder words, the fact that the two plates approach one to the other produces a compaction of the yarns and, as a consequence, a compaction of the specimen.

Such an experimental test can be used for the constitutive characterization related to compaction. Such deformation mechanism can be easily activated when considering standard loading conditions on macroscopic specimens.

1.3.2.4 Shear Tests in the Plane of the Reinforcement (determination of the shear stiffness)

The shear tests conceived for composite reinforcements show that the associated deformation mode is a privileged mode also when considering more complicated macroscopic deformations. This means that the stiffness of the material associated to this deformation mode (which we will call shear stiffness) is very low when compared to the others. The macroscopic deformation associated to shear is basically due to the change of the angle between yarns at the mesoscopic scale. The behavior of the reinforcement subjected to shear in the plane, results to be highly nonlinear. Some studies based on the technique of the image correlation [DUM03a, DUM03b] have shown that, in an initial phase of the test, the two families of yarns rotate in a relative way (like rigid bodies connected by internal pivots) and hence the shear force associated to this deformation is relatively low. When the shear angle variation between yarns becomes larger than 40° (and lower than 50°) a stiffening in the shear behavior is observed and the mechanism of deformation drastically changes. In this phase the relative motions described above are replaced by a contact between the yarns (and their relative lateral compaction), so to this fact corresponds to an increased stiffness.

Two simple tests permit the study of the behavior of the composite reinforcement subjected to shear in the plane: the *picture frame test* and the *bias extension test*. Due to the important effect that such macroscopic deformation mode has on the deformation of specimens subjected to more complex loading conditions it is essential to set up experimental procedures which are able to give precise informations in this sense.

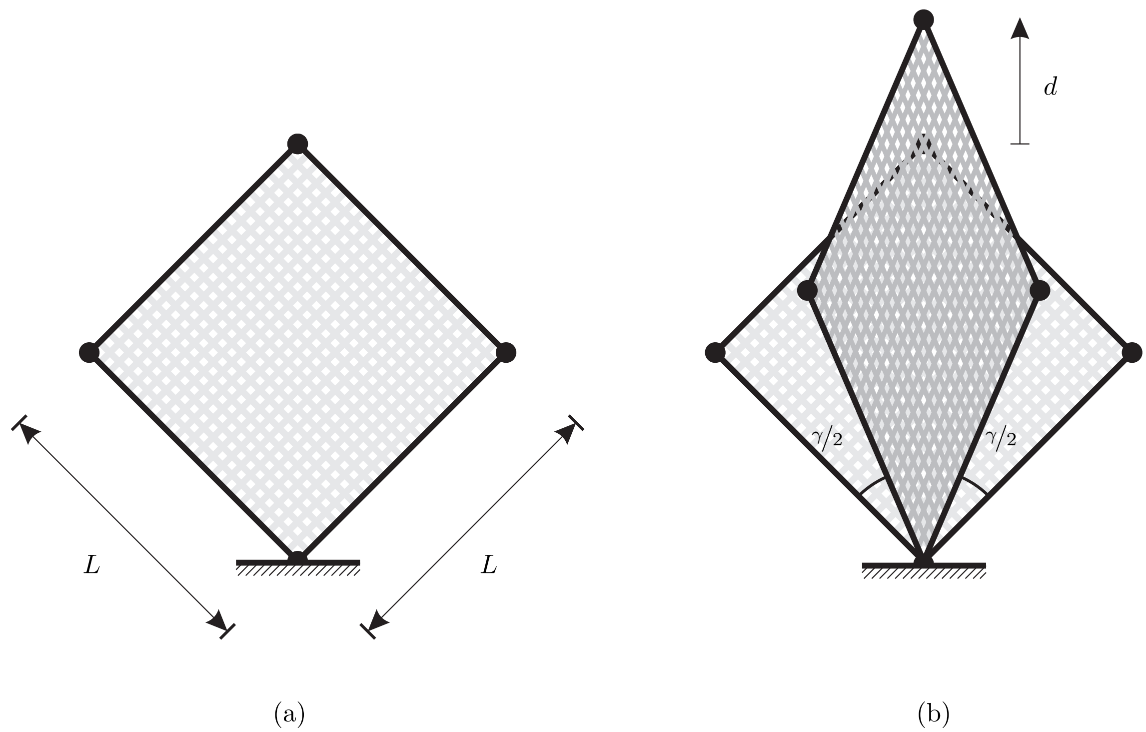

Figure 1.5: Kinematic of the picture frame test. (a) Specimen before the deformation (b) specimen after the imposed displacement d.

1.3.2.4.1 Picture Frame Test In the picture frame test the composite reinforcement is placed into an articulated quadrilateral structure, that possesses initially a square shape. By imposing a displacement d at one node of the structure, see Fig. 1.5, the reinforcement is subjected to pure shear and a simple kinematical relation furnishes the shear angle variation γ as a function of the imposed displacement d and the length of the edge of the articulated square , say L:

$$\gamma = \frac{\pi}{2} - 2\arccos\left(\frac{2d + \sqrt{2}L}{2L}\right). \tag{1.2}$$

1.3.2.4.2 Bias Extension Test The bias extension test is performed on rectangular samples of composite reinforcements, with the height (in the loading direction) relatively greater (at least twice) than the width, and the yarns initially oriented at ±45-degrees with respect to the loading direction. The specimen is clamped at two ends, one of which is maintained fixed and the second one is displaced of a given amount. The relative displacement of the two ends of the specimen provokes angle variations between the warp and weft: the creation of three different regions A, B and C, in which the shear angle between fibers remains almost constant after deformation, can be detected (see Fig. 1.6). In particular, the fibers in regions C remain undeformed, i.e. the angle between fibers remains at 45° also after deformation. On the other hand, the angle between yarns becomes much smaller than 45° in regions A and B, but it keeps almost constant in each of them. In particular if in the zone A the angle is γ it will be of $\gamma/2$ in the zone B . Also in this case, a simple kinematical relation furnishes the shear angle variation as function of the imposed displacement and of the geometry of the specimen:

$$\gamma = \frac{\pi}{2} - 2\arccos\left(\frac{\sqrt{2}}{2}\left(1 + \frac{d}{L_0 - w_0}\right)\right). \tag{1.3}$$

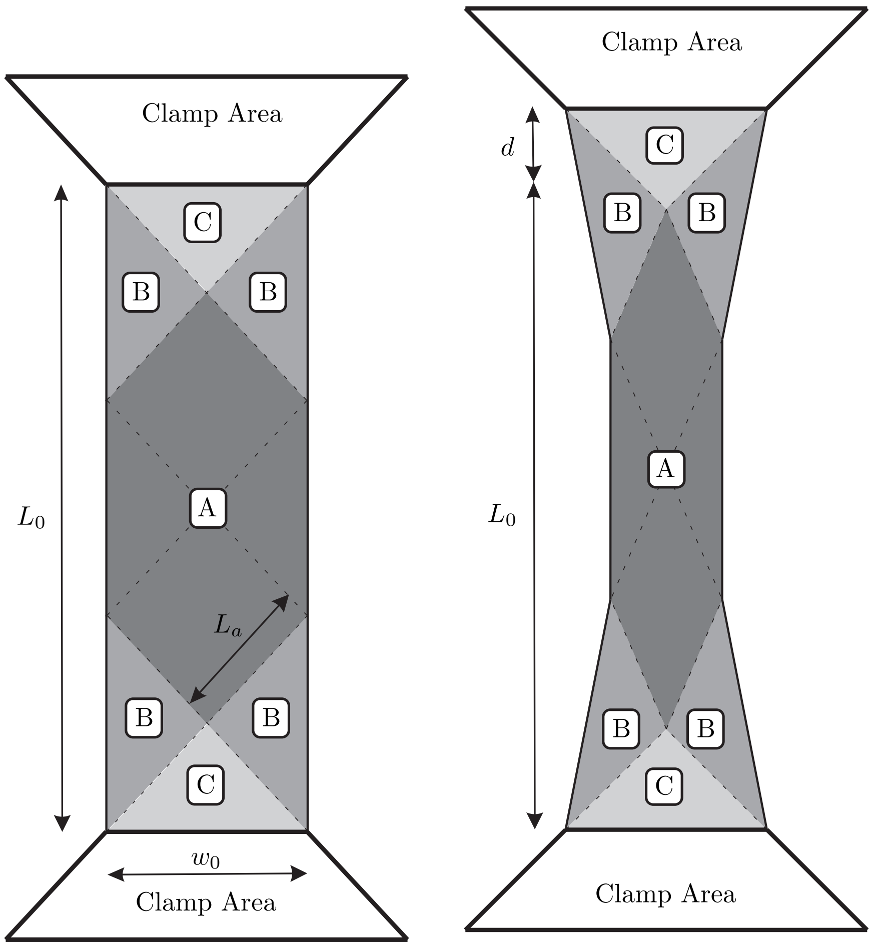

Figure 1.6: Kinematic of the bias extension test.

It is worth noting that the kinematical relations (1.2) and (1.3) are deduced by implicitly using the assumption that the yarns are inextensible so that only pantographic motions are activated at the scale of the yarns which allow to univocally relate the angle variation to the geometry of the specimen and the imposed displacement. As we will show in the remainder of this manuscript, other deformation mechanisms actually intervenes in the bias extension test which are related to the bending of the yarns at the mesoscopic scale. Such mesoscopic bending actually creates transition layers between the regions A, B and C which allow to shift from one value of the angle to the other. It is for this reason that the bias extension test, when simulated in the framework of second gradient theories, can be useful additional informations about the bending stiffness of the yarns.

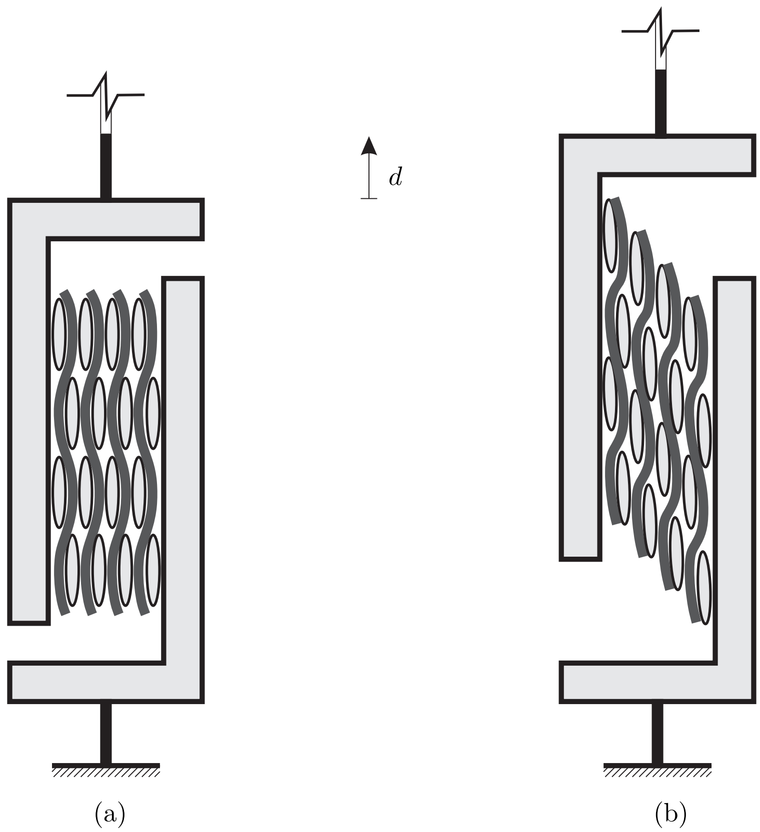

Figure 1.7: Kinematic of the transversal shear test. (a) Specimen before the deformation (b) specimen after the imposed displacement d.

1.3.2.5 Transversal Shear Test

This test is performed in order to characterize the behavior of the composite reinforcement when it is subjected to transversal shear. The machine, depicted in Fig. 1.7, imposes on the specimen (shaped as a parallelepiped) a kinematic of pure transversal shear in order to solicit the only transversal shear deformation mode. The test is usually performed twice by orienting the specimen in the direction of the warp and weft, since the material, if not perfectly balanced, may have different stiffnesses in these two directions.

Chapter 2

Continuum Mechanics Preliminaries: First Gradient Theory

In this chapter the fundamental concepts and methods of the first gradient theory are recalled. First, the basic kinematical relations and the measures of strain are presented. Then, the concept of internal contact actions (stress) are introduced. At the end of chapter, representation theorems for the functional dependence of the strain energy density with respect to the invariants of deformation are detailed, both for isotropic and anisotropic media. Some classical constitutive laws for isotropic materials are also presented. Finally, the strong form of the equations of motion for a classical Cauchy continuum are derived by means of a variational principle. It is worth noting that all these aspects are "classical" and a more extensive and systematical presentation of these arguments can be found in e.g. in [CIA88, HOL00b, SIL97].

Contents

2.1 Finite Kinematics

A continuum body $\mathcal{B}$ is a set of material points that are in bijective correspondence, at each instant of time, with the geometrical points of a region of the Euclidean Space, denoted as $\mathbb{R}^3$. The abstraction of continuum body is, clearly, an approximation since the real structure of the materials is discontinuous, but it is necessary for performing the classical mathematical operation (e.g. differentiation, etc...) and commonly accepted since the mathematical models developed under this assumption are suitable for the description of many experimental evidences.

Under the infinite possible configurations of the body, we call *reference configuration* B_0 and *current configuration* B, the configurations of the body at time $t = 0$ and $t \in \mathbb{R}^+$, respectively. The two configurations are equivalently called Lagrangian and Eulerian configuration and the material points are labeled as $\mathbf{X}$ and $\mathbf{x}$, respectively. The generic nonlinear transformation that maps the reference configuration into the current one defined as

$$\mathbf{x} = \boldsymbol{\chi}(\mathbf{X}, t) \tag{2.1}$$

is called *placement.* A fundamental hypothesis is that $\boldsymbol{\chi}(\mathbf{X}, t)$ is one-to-one in $\mathbf{X}$ in such a way that compenetration of matter is excluded. Moreover, the placement map is usually assumed to be a C^1 diffeomorphism, in order to be able to perform the space derivatives of this fundamental kinematical field. In addition, we require that

$$\det(\nabla\boldsymbol{\chi}) > 0 \tag{2.2}$$

in which $\nabla(\cdot)$ stands for the gradient with respect to the Lagrangian variable $\mathbf{X}$.

The vector field

$$\mathbf{u}(\mathbf{X}, t) = \boldsymbol{\chi}(\mathbf{X}, t) - \mathbf{X} \tag{2.3}$$

is called *displacement field.*

2.1.1 Deformation Gradient

The second order tensor

$$\mathbf{F} = \nabla\boldsymbol{\chi}, \qquad F_{ij} = \frac{\partial \chi_i}{\partial X_j} \tag{2.4}$$

is called the *deformation gradient.* This tensor has nine independent components and it characterizes the motion in the neighbor of a material point. In view of Eq. (2.3) and Eq. (2.4) we can also write[1]

$$\mathbf{F} = \mathbf{I} + \nabla\mathbf{u}, \qquad F_{ij} = \delta_{ij} + \frac{\partial u_i}{\partial X_j} \tag{2.5}$$

in which by $\mathbf{I}$ is denoted the 3×3 identity matrix and by δ_{ij} the Kronecker delta.

2.1.2 Line, Area and Volume Element Transformation

With the definition of the deformation gradient it is possible to define the deformation of line, area and volume elements from the reference to the current configuration. So, an infinitesimal line element $d\mathbf{X}$ in the reference configuration is transformed into its image in the current configuration through the formula

[1] Here and in the sequel, we present when possible formulas both in absolute notation and in its counterpart with Levi-Civita index notation. In the body of the manuscript one notation will be preferred to the other for the sake of consistency when no confusion can arise.

$$d\mathbf{x} = \mathbf{F} \cdot d\mathbf{X}, \quad dx_i = F_{ij} dX_j, \tag{2.6}$$

where from now on we indicate by a central dot a simple contraction between two tensors of any order greater than one.

Analogously, Piola transformation establishes a relation between an infinitesimal Lagrangian area $d\mathbf{S}$ and its Eulerian image $d\mathbf{s}$ (see e.g. [CIA88, HOL00b])

$$d\mathbf{s} = \underbrace{\det(\mathbf{F})\,\mathbf{F}^{-T}}_{=:\mathrm{cof}(\mathbf{F})} \cdot d\mathbf{S} = \mathrm{cof}(\mathbf{F}) \cdot d\mathbf{S}. \tag{2.7}$$

In the previous formula $d\mathbf{S} := \mathbf{N}dS$, $d\mathbf{s} := \mathbf{n}ds$, with $\mathbf{N}$, $\mathbf{n}$ unit normal vectors with respect to the two elements of area dS and ds.

Finally, the deformation of a volume element dV in the reference configuration is obtained by the well known change of variables formula

$$dv = \det(\mathbf{F})\, dV. \tag{2.8}$$

2.1.3 Deformation Measures

In this section we introduce some deformation measures which are usually encountered in continuum mechanics and which will be useful in the following for the formulation of suitable first and second gradient constitutive theories. We want to stress the fact that the introduction of such deformation measures in not unique. We will present different deformation measures which can be used in various contexts with the aim of describing at best the available experimental evidences. For example, a logarithmic deformation measure is introduced [NEF14a, NEF14b] with the main scope of showing that such a measure can sometimes be more realistic than others to describe the deformation of some materials like e.g. rubber.

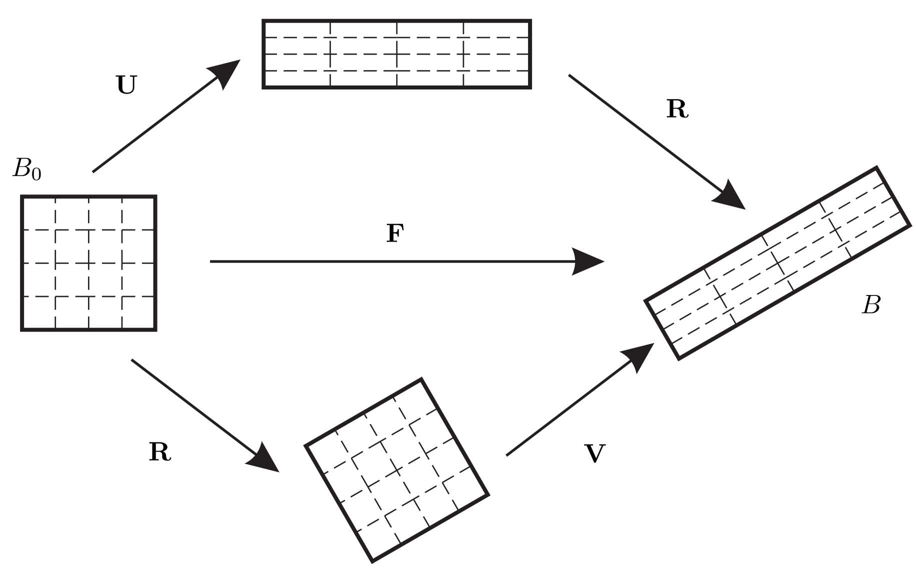

Figure 2.1: Geometric representation of the polar decomposition.

2.1.3.1 Polar Decomposition

The deformation gradient can be decomposed in a multiplicative form through the *polar decomposition*, and one can obtain:

$$\mathbf{F} = \mathbf{R} \cdot \mathbf{U} = \mathbf{V} \cdot \mathbf{R} \tag{2.9}$$

which is called right and left polar decomposition. In Eq. (2.9) $\mathbf{R}$ is an orthogonal tensor (i.e. $\mathbf{R}^T = \mathbf{R}^{-1}$ and $\det(\mathbf{R}) = 1$) and it represents a rotation, and $\mathbf{U}$ and $\mathbf{V}$ are symmetric and definite positive tensors. These two tensors are called right and left stretch tensor respectively and are linked via the rotation tensor through the formula

$$\mathbf{V} = \mathbf{R} \cdot \mathbf{U} \cdot \mathbf{R}^T. \tag{2.10}$$

The right and left polar decomposition have a direct geometric interpretation that is depicted in Fig. 2.1 (which is 2D only to ensure a rapid interpretation): the deformation of a body, under the action of a constant $\mathbf{F}$, can be obtained first by stretching it by means of $\mathbf{U}$ and later by the application of the rotation $\mathbf{R}$; equivalently, the same result can be obtained first by the application of the rotation $\mathbf{R}$ and later by applying the stretch $\mathbf{V}$.

Two important tensors, related to the right and left stretch tensors, are the right ($\mathbf{C}$) and left ($\mathbf{B}$) Cauchy-Green tensor (this latter sometimes referred to as Finger tensor). Such tensors are defined as

$$\begin{aligned}
\mathbf{C} &= \mathbf{F}^T \cdot \mathbf{F} = (\mathbf{R} \cdot \mathbf{U})^T \cdot \mathbf{R} \cdot \mathbf{U} = \mathbf{U}^T \cdot \mathbf{R}^T \cdot \mathbf{R} \cdot \mathbf{U} = \mathbf{U}^T \cdot \mathbf{U} = \mathbf{U}^2, \qquad & C_{ij} = F_{hi} F_{hj} = \frac{\partial \chi_h}{\partial X_i} \frac{\partial \chi_h}{\partial X_j} \\
\mathbf{B} &= \mathbf{F} \cdot \mathbf{F}^T = \mathbf{V} \cdot \mathbf{R} \cdot (\mathbf{V} \cdot \mathbf{R})^T = \mathbf{V} \cdot \mathbf{R} \cdot \mathbf{R}^T \cdot \mathbf{V}^T = \mathbf{V} \cdot \mathbf{V}^T = \mathbf{V}^2, \qquad & B_{ij} = F_{ih} F_{jh} = \frac{\partial \chi_i}{\partial X_h} \frac{\partial \chi_j}{\partial X_h}
\end{aligned} \tag{2.11}$$

and are linked via the formula

$$\mathbf{B} = \mathbf{R} \cdot \mathbf{C} \cdot \mathbf{R}^T. \tag{2.12}$$

2.1.3.2 Different Types of Strain Measure

Suitable strain measures useful for applications are the Green-Lagrange strain tensor

$$\boldsymbol{\varepsilon} = \frac{1}{2} (\mathbf{C} - \mathbf{I}), \qquad \varepsilon_{ij} = \frac{1}{2} (C_{ij} - \delta_{ij}) \tag{2.13}$$

and the Almansi strain tensor

$$\mathbf{e} = \frac{1}{2} \left(\mathbf{I} - \mathbf{B}^{-1}\right), \qquad e_{ij} = \frac{1}{2} \left(\delta_{ij} - B_{ij}^{-1}\right) \tag{2.14}$$

that both become identically zero when the motion of the body is rigid.

It is worth noting that this is not the only way for the quantification of strain. As a matter of fact, a family of Lagrangian strains is defined by (see [SET64, HIL70])

$$\boldsymbol{\varepsilon}^{(m)} = \begin{cases} \frac{1}{m} (\mathbf{U}^m - \mathbf{I}) & m \neq 0 \\ \ln [\mathbf{U}] & m = 0 \end{cases} \tag{2.15}$$

in which $\ln[\cdot]$ stands for the tensor logarithm and $m \in \mathbb{R}$. Analogously a family of Eulerian strains can be introduced as

$$\mathbf{e}^{(m)} = \begin{cases} \frac{1}{m} (\mathbf{V}^m - \mathbf{I}) & m \neq 0 \\ \ln [\mathbf{V}] & m = 0. \end{cases} \tag{2.16}$$

The two family of strain are linked via the formula

$$\mathbf{e}^{(m)} = \mathbf{R} \cdot \boldsymbol{\varepsilon}^{(m)} \cdot \mathbf{R}^T. \tag{2.17}$$

Using the spectral decomposition theorem Eq. 2.15 can be rewritten as

$$\boldsymbol{\varepsilon}^{(m)} = \sum_{i=1}^{3} g(\lambda_i)\, \mathbf{g}_i \otimes \mathbf{g}_i \tag{2.18}$$

in which $\otimes$ stand for the classic dyadic product, $g(\lambda_i)$ are the principal strains, expressed by the formula

$$g(\lambda_i) = \begin{cases} \frac{1}{m}\left(\lambda_i^m - 1\right) & m \neq 0 \\ \ln(\lambda_i) & m = 0. \end{cases} \tag{2.19}$$

λ_i are the principal stretches and $\mathbf{g}_i$ the principal directions.

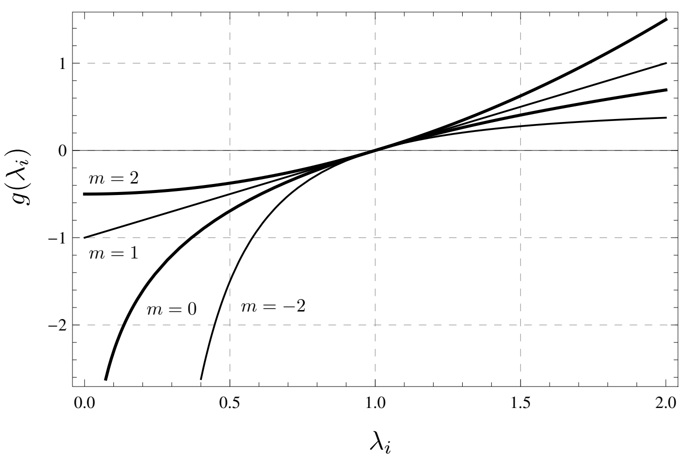

Figure 2.2: Principal strain as function of the principal stretch.

In Fig. 2.2 the principal strain as a function of principal stretch is presented, for different (integer) value of m, namely Green-Lagrange ($m = 2$), Biot ($m = 1$), Hencky ($m = 0$) and Almansi ($m = -2$). We stress the fact that all the strain measure vanish when the principal stretch are equal to one (i.e. when the deformation is locally a rigid rotation).

2.2 Internal Contact Actions

In this section we recall the concept of the internal actions (stress) and we discuss briefly the property of the traction vectors and stress tensors. Finally, different stress tensors are introduced, namely Cauchy, Piola-Kirchhoff (first and second) and Kirchoff.

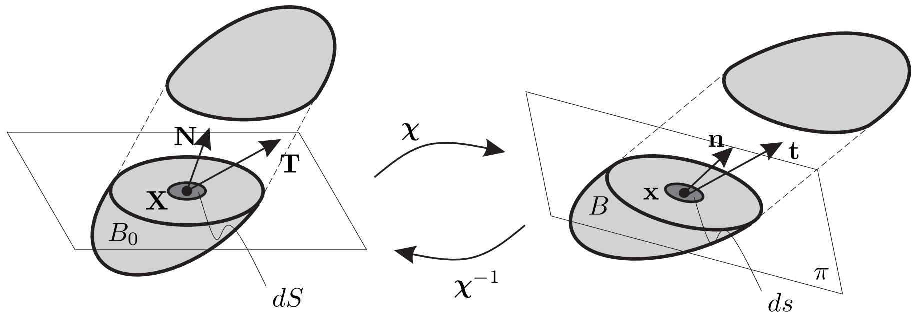

Figure 2.3: Traction vector in the current and reference configurations.

2.2.1 Cauchy Stress

The external forces that can act on a body may be classified as surface or body forces. The surface forces represent the contact actions exerted by the environment on the body (e.g. the pressure exerted by the wind on a surface); the body forces represent the "action-at-a-distance" that the environment exert on the body (e.g. the gravitational force). Under this external action (but not only) the body is solicited and this solicitation causes the onset of internal actions which finally give rise to the deformation of the body.

Let us consider a body that occupy the region $B_0 \subset \mathbb{R}^3$ with boundary ∂B_0 in the reference configuration, loaded by some external forces on a part of it that lead the body in the current configuration B with boundary ∂B, as indicated in Fig. 2.3. We postulate that this external solicitation causes the onset of internal actions per unit area. Under this postulation, if we cut the current configuration of the body by a plane π with normal $\mathbf{n}$, passing through a given point $\mathbf{x} \in \pi \cap B$ at a given time $t \in \mathbb{R}^+$, and if we consider a small neighbor ds of $\mathbf{x} \in \pi \cap B$, the two parts of the body exchange through this small region internal contact actions with resultant force $d\mathbf{f}$ (resultant couples $d\mathbf{m}$ are not consider because it can be proved that they cannot be sustainable by a first gradient medium) . By our assumption, we require that for every point $\mathbf{x} \in \pi \cap B$ and for the surface element ds with normal $\mathbf{n}$

$$d\mathbf{f} = \mathbf{t} ds. \tag{2.20}$$

The vector $\mathbf{t} = \mathbf{t}(\mathbf{x}, t, \mathbf{n})$ is called *Cauchy traction vector* and represents the force per unit area exerted on a surface element ds with normal $\mathbf{n}$. We stress the fact that this vector is defined in the current configuration, then it is the "real" internal action acting on the body. As stated above, the Cauchy traction vector depend, at given time $t \in \mathbb{R}^+$, on the position $\mathbf{x}$ and on the normal $\mathbf{n}$; an important result that links the traction vector to the normal $\mathbf{n}$ in a fixed point $\mathbf{x}$ and at a given time $t \in \mathbb{R}^+$, is the Cauchy's stress theorem. This theorem states that there exists a unique second order tensor $\boldsymbol{\sigma} = \boldsymbol{\sigma}(\mathbf{x}, t)$ such that

$$\mathbf{t}(\mathbf{x}, t, \mathbf{n}) = \boldsymbol{\sigma}(\mathbf{x}, t) \cdot \mathbf{n}, \qquad t_i = \sigma_{ij} n_j. \tag{2.21}$$

The tensor $\boldsymbol{\sigma} = \boldsymbol{\sigma}(\mathbf{x}, t)$ is called *Cauchy stress tensor* and it can be proved that it is a symmetric tensor (by imposing the balance of moments).

2.2.2 First Piola-Kirchhoff Stress

In spite of what stated above, one can define a traction vector defined on the initial configuration and is are such that

$$d\mathbf{f} = \mathbf{T} dS. \tag{2.22}$$

This traction vector, that acts on an infinitesimal surface dS of the point $\mathbf{X} = \chi^{-1}(\mathbf{x}, t)$ with normal $\mathbf{N}$, is the *first Piola-Kirchhoff traction vector.* It represents the internal contact action referred to the reference configuration. The Cauchy theorem is also valid for the first Piola-Kirchhoff traction vector, then

$$\mathbf{T}(\mathbf{X}, t, \mathbf{N}) = \mathbf{P}(\mathbf{X}, t) \cdot \mathbf{N}, \qquad T_i = P_{ij} N_j. \tag{2.23}$$

in which the second order tensor $\mathbf{P}$ is called first *Piola-Kirchhoff stress tensor.* The first Piola-Kirchhoff stress tensor, in spite of the Cauchy stress tensor, is not symmetric.

2.2.3 Kirchhoff Stress

Another stress tensor can be defined through the Cauchy stress tensor $\boldsymbol{\sigma}$ and the volume ratio $\det(\mathbf{F})$

$$\boldsymbol{\tau} = \det(\mathbf{F})\, \boldsymbol{\sigma}, \qquad \tau_{ij} = \det(\mathbf{F})\, \sigma_{ij} \tag{2.24}$$

in which the tensor $\boldsymbol{\tau}$ is referred as *Kirchhoff stress tensor.*

2.2.4 Second Piola-Kirchhoff Stress

The second *Piola-Kirchoff stress tensor* $\mathbf{S}$ is defined as the pulled-back of the Kirchoff stress tensor $\boldsymbol{\tau}$. This tensor is a symmetric tensor (proof omitted) that not have a physical interpretation. It is defined as

$$\mathbf{S} = \mathbf{F}^{-1} \cdot \boldsymbol{\tau} \cdot \mathbf{F}^{-T}, \qquad S_{ij} = F_{ih}^{-1} \tau_{hk} F_{jk}^{-1}. \tag{2.25}$$

2.2.5 Relations between Stress Tensors

The following relationships between the stress tensors defined above can be checked

$$\begin{aligned}
\mathbf{P} &= \det(\mathbf{F})\, \boldsymbol{\sigma} \cdot \mathbf{F}^{-T}, & P_{ij} &= \det(\mathbf{F})\, \sigma_{ih} F_{jh}^{-1} \\
\mathbf{S} &= \mathbf{F}^{-1} \cdot \mathbf{P}, & S_{ij} &= F_{jh}^{-1} P_{hj} \\
\mathbf{S} &= \det(\mathbf{F})\, \mathbf{F}^{-1} \cdot \boldsymbol{\sigma} \cdot \mathbf{F}^{-T}, & S_{ij} &= \det(\mathbf{F})\, F_{ih}^{-1} \sigma_{hk} F_{jk}^{-1}.
\end{aligned} \tag{2.26}$$

2.3 Hyperelastic Constitutive Laws

In this section we introduce the concept of hyperelastic material and we present some well known representation theorems for isotropic, transversely isotropic and orthotropic materials. Such representation theorems specify the functional dependence of the strain energy density on given sets of invariants of the Cauchy-Green deformation tensor. The results provided by such theorems are really useful for the effective construction of explicit constitutive laws which fit at best the available experimental evidences on the materials that one wants to model.

At the end of this section, we give some examples of explicit constitutive laws for isotropic materials which are of large use in mechanics. Such isotropic laws can be very effective to model the mechanical behavior of simple materials which can indeed be considered isotropic, but are not sufficient to model the complex materials which are the fibrous composite reinforcements. Such explicit isotropic constitutive laws are given here as an example to get familiar with standard results. We leave to the remainder of this manuscript (see Chap. 5 and 6) the introduction of suitable explicit orthotropic constitutive laws which will be able to correctly model fibrous composite reinforcement.

2.3.1 General aspects

A material is said to be *hyperelastic* or *Green-elastic material* if there exist a scalar function W, called *Helmhotz free energy function* starting from which one can derive the stress-strain relationships . In the case in which $W = W(\mathbf{F})$ depend only on $\mathbf{F}$, the Helmholtz function is referred to as *strain-energy* function or *stored-energy function*. In the above description, the homogeneity of the medium has been assumed, then the function W depends only on $\mathbf{F}$. A more richer description could require that the function W depends also on the position of the material point in the medium, which is the case for materials which are macroscopically heterogeneous. In this manuscript we limit ourselves to consider strain energy densities which are homogeneous at the macroscopic scale and we will introduce the possibility of microscopic heterogeneity by means of second gradient or micromorphic models (see Chap. 5 and 6).

With the aim of defining a suitable and consistent constitutive law for considered materials, the strain-energy function must satisfy the fundamental requirement itemized below

- The function W must be differentiable with respect to $\mathbf{F}$;
- The function must vanish in the the reference configuration (*normalization condition*), so that $W(\mathbf{I}) = 0$;
- The function W increases with the deformation, so that $W(\mathbf{F}) > 0$;
- The function W must satisfy the *growth condition*

$$\begin{cases} W(\mathbf{F}) \to \infty & \text{as} \quad \det(\mathbf{F}) \to \infty \\ W(\mathbf{F}) \to \infty & \text{as} \quad \det(\mathbf{F}) \to 0^+ \end{cases} \tag{2.27}$$

this condition possesses a physical meaning: an infinite energy is needed for expanding a continuous body in an infinite range or compressing it in a point with vanishing volume.

- The function must respect the principle of frame indifference (objectivity): the energy does not change under a change of Galilean observer

$$W(\mathbf{F}) = W(\mathbf{QF}) \tag{2.28}$$

for all orthogonal tensor $\mathbf{Q}$.

- The energy must respect the symmetry group of the material

$$W(\mathbf{F}) = W(\mathbf{FQ}) \tag{2.29}$$

for every $\mathbf{Q} \in \mathcal{G} \subset \mathrm{SO}(3)$, in which $\mathcal{G}$ is the symmetry group of the material.

It is important to note that the the condition of objectivity expressed by (2.28) is automatically satisfied if one choses the right Cauchy-Green tensor as argument of W (i.e. $W = W(\mathbf{C})$) .

2.3.2 Representation Theorem for Isotropic Materials

A material is said to be isotropic if its response, in terms of stress-strain relation, is the same in all possible direction (see e.g. [CIA88, RAU09]). The symmetry group for such material is represented by all rotations and all reflections (i.e. $\mathcal{G} = O(3)$). Then, the well known representation theorem for the isotropic strain energy function states that the function W does not depend arbitrarily and entirely on $\mathbf{C}$ but only on three scalar invariants of such tensor. In other words

$$W = W^{\text{iso}}(i_1, i_2, i_3) \tag{2.30}$$

where i_1, i_2 and i_3 are defined as

$$i_1 = \mathrm{tr}\left(\mathbf{C}\right), \qquad i_2 = \mathrm{tr}\left(\mathrm{cof}\left(\mathbf{C}\right)\right), \qquad i_3 = \det\left(\mathbf{C}\right). \tag{2.31}$$

By using the Eq. (2.30), one can write the second Piola-Kirchoff stress tensor as

$$\mathbf{S} = 2\frac{\partial W^{\mathrm{iso}}}{\partial \mathbf{C}} = 2\left[\left(\frac{\partial W^{\mathrm{iso}}}{\partial i_1} + i_1\frac{\partial W^{\mathrm{iso}}}{\partial i_2}\right)\mathbf{I} - \frac{\partial W^{\mathrm{iso}}}{\partial i_2}\mathbf{C} + i_3\frac{\partial W^{\mathrm{iso}}}{\partial i_3}\mathbf{C}^{-1}\right]. \tag{2.32}$$

2.3.3 Representation Theorem for Transversally-Isotropic Materials

A material is said to be transversally isotropic when it has the same properties in one plane and other properties in the direction normal to this plane, that we label as $\mathbf{d}_1$ (see e.g. [RAU09]). In this materials

- a rotation around the direction $\mathbf{d}_1$
- a rotation with axis orthogonal to $\mathbf{d}_1$ and with angle π

before applying a homogeneous deformation should not change the strain energy.

Then, the representation theorem for transversally isotropic materials states that the energy depends on five scalar invariants (see e.g. [RAU09]), so that

$$W = W^{\mathrm{tran}}\left(i_1, i_2, i_3, i_4, i_5\right) \tag{2.33}$$

where i_4 and i_5 are defined as

$$i_4 = \mathbf{d}_1 \cdot \mathbf{C} \cdot \mathbf{d}_1, \qquad i_5 = \mathbf{d}_1 \cdot \mathbf{C}^2 \cdot \mathbf{d}_1. \tag{2.34}$$

This two additional invariant (with respect the isotropic case), describe the local stretch in the direction of the preferential direction $\mathbf{d}_1$ and changes of angles mixed to changes of length respectively.

Then, as for the isotropic case, by using (2.33) one can write the second Piola-Kirchoff stress tensor as

$$\begin{aligned}\mathbf{S} = 2\frac{\partial W^{\mathrm{tran}}}{\partial \mathbf{C}} =& 2\left[\left(\frac{\partial W^{\mathrm{tran}}}{\partial i_1} + i_1\frac{\partial W^{\mathrm{tran}}}{\partial i_2}\right)\mathbf{I} - \frac{\partial W^{\mathrm{tran}}}{\partial i_2}\mathbf{C} + i_3\frac{\partial W^{\mathrm{tran}}}{\partial i_3}\mathbf{C}^{-1}\right.\\ &\left.+\frac{\partial W^{\mathrm{tran}}}{\partial i_4}\mathbf{d}_1\otimes\mathbf{d}_1 + \frac{\partial W^{\mathrm{tran}}}{\partial i_5}\left(\mathbf{d}_1\otimes\left(\mathbf{C}\cdot\mathbf{d}_1\right) + \left(\mathbf{C}\cdot\mathbf{d}_1\right)\otimes\mathbf{d}_1\right)\right].\end{aligned} \tag{2.35}$$

2.3.4 Representation Theorem for Orthotropic Materials

If the material possesses two privileged directions, that we label as $\mathbf{d}_1$ and $\mathbf{d}_2$, in its reference configuration then it is called orthotropic. For such materials it is natural to require that a rotation around $\mathbf{d}_1$ or $\mathbf{d}_2$ with angle π before the application of an homogeneous deformation, should not change the strain energy.

As discussed more extensively in the Chap. 5, the more diffused version of the representation theorem for the strain energy potential for orthotropic media states that seven invariants can be used to write the functional dependence of the strain energy density. However, it can be proved that, indeed, only six independent scalar invariants are sufficient to completely describe the behavior of an orthotropic material (see e.g. [RAU09]). So, the functional dependence of the energy with respect to a suitable set of scalar invariants of $\mathbf{C}$, can be written as

$$W = W^{\mathrm{orth}}\left(i_1, i_4, i_6, |i_8|, |i_9|, |i_{10}|, \mathrm{sgn}\left(i_8 i_9 i_{10}\right)\right) \tag{2.36}$$

in which

$$i_6 = \mathbf{d}_2 \cdot \mathbf{C} \cdot \mathbf{d}_2, \qquad i_8 = \mathbf{d}_1 \cdot \mathbf{C} \cdot \mathbf{d}_2, \qquad i_9 = \mathbf{d}_1 \cdot \mathbf{C} \cdot \mathbf{d}_3, \qquad i_{10} = \mathbf{d}_2 \cdot \mathbf{C} \cdot \mathbf{d}_3. \tag{2.37}$$

where $\mathbf{d}_3 := \mathbf{d}_1 \wedge \mathbf{d}_2$ and $\mathrm{sgn}\,(\cdot)$ stands for the sign function[2]. It is worth noting that i_6 represents a stretch in the direction $\mathbf{d}_2$, while i_8, i_9 and i_{10} represent changes of angles mixed to changes of length between the directions $(\mathbf{d}_1, \mathbf{d}_2)$, $(\mathbf{d}_1, \mathbf{d}_3)$ and $(\mathbf{d}_2, \mathbf{d}_3)$ respectively. Then, by using (2.36), the second Piola-Kirchhoff reads

$$\begin{aligned}\mathbf{S} = 2\frac{\partial W^{\mathrm{orth}}}{\partial \mathbf{C}} =& 2\frac{\partial W^{\mathrm{orth}}}{\partial i_1}\mathbf{I} + 2\frac{\partial W^{\mathrm{orth}}}{\partial i_4}\mathbf{d}_1 \otimes \mathbf{d}_1 + 2\frac{\partial W^{\mathrm{orth}}}{\partial i_6}\mathbf{d}_2 \otimes \mathbf{d}_2 + \mathrm{sgn}\,(i_8)\,\frac{\partial W^{\mathrm{orth}}}{\partial\,|i_8|}\,(\mathbf{d}_1 \otimes \mathbf{d}_2 + \mathbf{d}_2 \otimes \mathbf{d}_1) \\ &+ \mathrm{sgn}\,(i_9)\,\frac{\partial W^{\mathrm{orth}}}{\partial\,|i_9|}\,(\mathbf{d}_1 \otimes \mathbf{d}_3 + \mathbf{d}_3 \otimes \mathbf{d}_1) + \mathrm{sgn}\,(i_{10})\,\frac{\partial W^{\mathrm{orth}}}{\partial\,|i_{10}|}\,(\mathbf{d}_2 \otimes \mathbf{d}_3 + \mathbf{d}_3 \otimes \mathbf{d}_2)\,.\end{aligned} \tag{2.38}$$

2.3.5 Hyperelastic incompressible materials

There exists a wide class of materials that are able to sustain large strains without notable changing volume [OGD84, HOL00b]. Such kind of materials are nearly incompressible materials and in this section we recall the principal aspects with respect to their modeling. In a more precise way, a material is incompressible if it respects the constraint

$$\det(\mathbf{F}) = 1 \tag{2.39}$$

under a generic motion. This constraint may be taken into account by defining a suitable strain energy function

$$W = W(\mathbf{F}) - p\,(\det(\mathbf{F}) - 1) \tag{2.40}$$

in which the scalar function p is a Lagrangian multiplier added in order to take into account the incompressibility condition. The quantity p can be identified as hydrostatic pressure and can be determined only by solving the equilibrium equations equipped with suitable boundary conditions [HOL00b]. It is worth noting that the incompressibility condition may be defined in an equivalent way imposing e.g. $\det(\mathbf{C}) = 1$.

In the case of isotropic incompressible material [HOL00b] a suitable energy function is given by

$$W = W(i_1, i_2) - \frac{1}{2}p\,(i_3 - 1) \tag{2.41}$$

in which the functional dependency of W is reduced to only two scalar invariant (i.e. i_1 and i_2). For a material described by a strain energy function of the type given in Eq. (2.41), the second Piola-Kirchhoff stress tensor reads

$$\mathbf{S} = -p\mathbf{C}^{-1} + 2\left[\left(\frac{\partial W}{\partial i_1} + i_1\frac{\partial W}{\partial i_2}\right)\mathbf{I} - \frac{\partial W}{\partial i_2}\mathbf{C}\right]. \tag{2.42}$$

[2]The sign function for $x \in \mathbb{R}$ is defined as

$$\mathrm{sgn}\,(x) := \begin{cases} -1 & \text{if } x < 0 \\ 0 & \text{if } x = 0\,. \\ +1 & \text{if } x > 0 \end{cases}$$

2.3.6 Some Energies for Isotropic Materials

The simpler hyperelastic model for isotropic materials is the Saint Venant-Kirchhoff model. The strain energy function for this model reads

$$W(\boldsymbol{\varepsilon}) = \frac{\lambda}{2}\mathrm{tr}(\boldsymbol{\varepsilon})^2 + \mu \mathrm{tr}(\boldsymbol{\varepsilon}^2) \tag{2.43}$$

in which λ and μ are the Lamé constants of the material. It is worth noting that the strain energy function of Eq. (2.43) may be expressed in terms of the right Cauchy-Green tensor $\mathbf{C}$ instead of the Green-Lagrange tensor $\boldsymbol{\varepsilon}$ (see e.g. [CIA88]).

Another useful model is the Rivlin model [RIV48], in which the strain energy function is expressed as a polynomial series. For incompressible materials it reads

$$W = \sum_{i=0,j=0}^{n} C_{ij}(i_1 - 3)^i (i_2 - 3)^j \tag{2.44}$$

in which $C_{00} = 0$ (normalization condition), and for compressible material

$$W = \sum_{i=0,j=0}^{n} C_{ij}(i_1 - 3)^i (i_2 - 3)^j + \sum_{k=1}^{m} D_k (\det(\mathbf{F}) - 1)^{2k} \tag{2.45}$$

From the energy defined by Eq. (2.44), one can obtain different known models in the literature

- Neo-Hooke model

$$W = C_{10}(i_1 - 3) \tag{2.46}$$

- Mooney-Rivlin model

$$W = C_{10}(i_1 - 3) + C_{01}(i_2 - 3) \tag{2.47}$$

- Yeoh model

$$W = C_{10}(i_1 - 3) + C_{20}(i_1 - 3)^2 + C_{30}(i_1 - 3)^3 \tag{2.48}$$

Finally, a model suitable for describing the behavior of incompressible (rubber-like) material is the Ogden model [OGD84, HOL00b], in which the strain energy is defined as

$$W = \sum_{k=1}^{n} \frac{\mu_n}{\alpha_k}(\lambda_1^{\alpha_k} + \lambda_2^{\alpha_k} + \lambda_3^{\alpha_k} - 3) \tag{2.49}$$

where λ_i, $i = 1, \ldots, 3$ are the principal stretches.

All the strain energy densities defined in this section are adapted to describe the behavior of some specific isotropic materials and each of such energies is more or less adapted to fit experimental evidences on real materials. Indeed, the choice of the constitutive expression to be used to model a given material must be based on the correct fitting of the available experimental data. In such sense, the constitutive choice of the energy can be seen as the "engineering effort" to model at best the behavior of the considered system. Nevertheless, one is not always guaranteed that an arbitrary choice of the constitutive relation for deformation energy always gives rise to a well posed problem.

A huge amount of work is available in the literature to establish some conditions which ensure existence and sometimes uniqueness of the solution for differential problems stemming from deformation energies. The convexity of the strain energy function with respect to $\mathbf{F}$ would render the mathematical analysis of the associated minimization problem very simple (see e.g. [CIA88]). Nevertheless, such requirement is too strict to lead to the choice of energies which are realistic enough to model materials which rather complicated behaviors (see e.g. [CIA88]). It is for this reason that weaker requirements (policonvexity, rank-one convexity) have also been introduced for the strain energy function which can still guarantee well-posedness of the associated differential problem (see e.g. [CIA88]). It is sometimes hard to look for an energy which satisfies such requirements and which fits well the experimental data. In such cases, one could try to rely on some theorems which state that if a suitable second gradient energy is added to a generic first gradient energy, then the resulting problem can be considered to be well posed. In the remainder of this manuscript we will adopt this latter strategy to reach the compromise of modeling at best the available physical phenomena and, at the same time, having good possibilities of dealing with a well-posed problem.

2.4 Variational Deduction of the Equations of Motions

The action functional for a first gradient continuum is defined as

$$\mathcal{A} = \int_0^T \int_{B_0} W(\boldsymbol{\varepsilon}) \tag{2.50}$$

where W is the Lagrangian strain energy density defined per unit volume which possesses the features itemized in the previous section and $\boldsymbol{\varepsilon}$ is the Green-Lagrange strain tensor defined by Eq. (2.13). In order to calculate the equations of motion for the considered continua, one must compute the first variation (denoted as $\delta\mathcal{A}$) of the action functional and impose it to be equal to zero. This equations consist in bulk equation and duality condition, which must be satisfied in the domain of the continuum body and on its boundary respectively. So, by assuming suitable kinematical regularity for the field expressed by the placement function $\boldsymbol{\chi}$, one can write the first variation $\delta\mathcal{A}$ as

$$\delta\mathcal{A} = \int_0^T \int_{B_0} \left(\frac{\partial W}{\partial \boldsymbol{\varepsilon}} \,|\delta\boldsymbol{\varepsilon} \right) \tag{2.51}$$

where the symbol $|$ stands for the scalar product between two tensor of the same order[3]. For notational convenience, we set

$$\mathbf{S} = \frac{\partial W}{\partial \boldsymbol{\varepsilon}} = \mathbf{S}^T, \qquad S_{ij} = \frac{\partial W}{\partial \varepsilon_{ij}} = S_{ji} \quad . \tag{2.52}$$

Since the tensor $\mathbf{H}$ is symmetric, by recalling the Eq. (2.13), one can easily check that

$$\mathbf{S}\,|\delta\boldsymbol{\varepsilon} = \mathbf{S}\,\middle|\left(\mathbf{F}^T \cdot \delta\mathbf{F}\right), \qquad S_{ij}\delta\varepsilon_{ij} = S_{ij}F_{ki}\delta F_{kj}. \tag{2.53}$$

Then, integrating by part Eq. (2.51) and remembering that $F_{kj} = \chi_{k,j}$, one obtains

$$\delta\mathcal{A} = -\int_0^T \int_{B_0} \left(S_{ij}F_{ki}\right)_{,j} \delta\chi_k + \int_0^T \int_{B_0} \left(S_{ij}F_{ki}\delta\chi_k\right)_{,j} \tag{2.54}$$

and using the divergence theorem

$$\delta\mathcal{A} = -\int_0^T \int_{B_0} \left(S_{ij}F_{ki}\right)_{,j} \delta\chi_k + \int_0^T \int_{\partial B_0} S_{ij}F_{ki}n_j\delta\chi_k \quad . \tag{2.55}$$

From this last expression for $\delta\mathcal{A}$, recalling that $\delta\boldsymbol{\chi} = \delta\mathbf{u}$ and assuming that the test functions are arbitrary in the volume, it can be checked that the condition $\delta\mathcal{A} = 0$ implies the bulk equation

$$\mathrm{Div}\left(\mathbf{F} \cdot \frac{\partial W}{\partial \boldsymbol{\varepsilon}}\right) = 0 \tag{2.56}$$

[3]Let for example $\mathbf{A}$ and $\mathbf{B}$ two four order tensors of component A_{ijhk} and B_{ijhk}, respectively. Their scalar product is defined as $\mathbf{A}\,|\mathbf{B} = A_{ijhk}\,B_{ijhk}$.

and the duality conditions

$$\mathbf{t} \cdot \delta \mathbf{u} = 0. \tag{2.57}$$

in which the quantity $\mathbf{t}$ is linked at the strain energy function through the relation

$$\mathbf{t} := \left(\mathbf{F} \cdot \frac{\partial W}{\partial \varepsilon} \right) \cdot \mathbf{n} \quad . \tag{2.58}$$

Here no external action has been considered but its inclusion in the theory is straightforward, especially if it can be derived from a potential energy.

Chapter 3

Continuum Mechanics Preliminaries: Micro-structured Continua

It is known that every material is heterogeneous if one looks at sufficiently small scales. It is hence often interesting to introduce models accounting for the presence of the microstructure and which are suitable for describing the real material behavior. The first gradient theory, presented in the previous chapter, is not able to take into account some macroscopic manifestations of particular microstructures and then in this chapter we want to highlight the existing so called continuum micro-structured theory.

The introduction of generalized continuum theories dates back to Piola [PIO46, PIO14] who was the first to use second and N-th gradient continuum theories to account for microstructure-related long-range interactions. Then other authors continued to develop generalized continuum theories (see Germain [GER73a] for second gradient theories, Mindlin and Eringen [MIN64, ERI64a, ERI64b, ERI01] for micromorphic theories, Cosserat [COS09] for particular generalized theories only accounting for rotation of the microstructure) giving rise to a flourishing research activity. In addition to these references, more recent and interesting results can be found e.g. in [FOR06, NEF06a, NEF06b, NEF07].

In the first part of this chapter, following [ERI01], we present the basic kinematics of the micro-structured continua in the framework of nonlinear regime. Then, we present the linear theory of micro-structured materials proposed by [MIN64]. Motivated by the large number of material constants which are present in Mindlin's micromorphic model, we present a particular simplified version of it which is valid for the isotropic, linearized case, following the spirit of [NEF13]. Finally, starting from this last simplified version of micromorphic model, we show how, by introducing suitable constraints, it is possible to obtain second gradient theories from micromorphic ones. Moreover, we propose another particular micromorphic model called "relaxed micromorphic model" introduced in [NEF13], which has been proven to be the simplest possible micromorphic model which needs to be considered in the linear, isotropic case, to guarantee well-posedness of the associated Euler-Lagrange equations. In order to get familiar with the procedure of obtaining a particular generalized theory by constraining a more general one with suitable constraints, we also show how a Cosserat continuum theory can be obtained by constraining the relaxed micromorphic model. Finally, to the sake of completeness, we also show how the equations of motion in strong form can be obtained for a micromorphic continuum by using variational arguments.

The tools which are presented in this chapter are well established in the literature and the constitutive choices made here for presenting them consists of very simple energy densities (often isotropic and linearized case). Nevertheless, the core message which we want to transmit to the reader is basically focused on the procedure of obtaining a particular generalized theory starting from a more general micromorphic one. This procedure, suitably readapted for the more complicated cases considered thereafter, will allow us, in the following, to obtain the hyperelastic, orthotropic, second gradient model which is needed for modeling fibrous composite reinforcements as a particular limit case of a more general micromorphic model. As it will be better pointed out in the chapter concerning the constitutive second gradient modeling of fibrous composite reinforcements, the tool which will be used to impose the needed constraints in the considered micromorphic model will be that of using suitable Lagrange multipliers. In this chapter, we refrain to present the theory of Lagrange multipliers which is indeed well established in the literature (see e.g. [FER13]) and we limit ourselves to make some considerations about the behavior of the considered micromorphic model when considering suitable limit cases.

Contents

3.1 Kinematics

In the classical Cauchy continua, as we have seen in the previous chapter, a continuum body is seen as a set of material points which interact by means of simplified internal contact actions. This type of mathematical idealization, which is suitable to give a global description of numerous experimental evidences, however, is not always able to take into account the microstructure of the materials which is evident when one look at a given characteristic length-scale. Then, in order to take into account the effect of such microstructure on the overall mechanical behavior of considered micro-structured materials, we present in this section (and in general in this chapter), what is called theory of micromorphic continua. Also in this theory a continuum body is regarded as a set of deformable material points, but the embedded microstructure is accounted for by the introduction of suitable additional kinematical fields. In particular, the deformability of the material points, as proposed in [ERI64a, ERI01], is taken into account by replacing the classical deformable particle by a geometric point P and a set of vectors $\mathbf{\Xi}_\alpha$, $\alpha = 1, \ldots, N$, which account for its inner structures. So, both the geometric point P and the vectors $\mathbf{\Xi}_\alpha$ posses their own motion. A continuuum of this type is called microcontinuum of grade N, but in this manuscript we focus the attention only on the case $N = 1$.

3.1.1 Motions

As in the previous chapter, we call B_0 and B the Lagrangian and the Eulerian configuration of the body. The deformable material point $P(\mathbf{X}, \mathbf{\Xi})$, in the reference configuration, is characterized by its centroid C (indeed, as in classical Cauchy theory a material point is seen as a small elementary volume of the considered continuum) and by the vector $\mathbf{\Xi}$ attached to it (see Fig. 3.1). The centroid is labeled as $\mathbf{X}$ (respectively $\mathbf{x}$) in the reference (current) configuration; similarly the vector attached to it is labeled as $\mathbf{\Xi}$ (respectively $\boldsymbol{\xi}$).

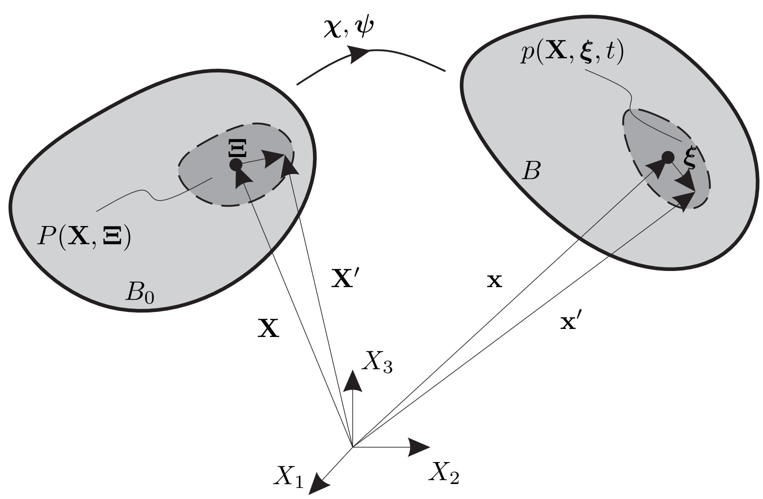

Figure 3.1: Lagrangian and Eulerian configurations of the micromorphic continuum.

The classical placement function, that in this case map the centroid of the material point from the reference configuration to the current configuration

$$\mathbf{x} = \boldsymbol{\chi}(\mathbf{X}, t) \tag{3.1}$$

must be complement by the *microplacement*

$$\boldsymbol{\xi} = \hat{\boldsymbol{\xi}}(\mathbf{X}, \mathbf{\Xi}, t) \tag{3.2}$$

which maps the vector attached to the centroid from the reference configuration into the current one.

Since the deformable material particle is considered small with respect the macroscopic scale of the body, then a linear approximation is generally assumed for the microplacement

$$\boldsymbol{\xi} = \boldsymbol{\psi}(\mathbf{X}, t) \cdot \boldsymbol{\Xi}, \qquad \xi = \psi_{ij}\Xi_j \tag{3.3}$$

where $\boldsymbol{\psi}(\mathbf{X}, t)$ is a second order tensor often called *microdeformation tensor.*

Following [ERI01], a material body is called *micromorphic continuum of grade one* if its motion is described by (3.1) and (3.3), which are of class C^1 with respect to the variable $\mathbf{X}$ and t and uniquely invertible

$$\begin{aligned} \mathbf{X} &= \boldsymbol{\chi}^{-1}(\mathbf{X}, t) \\ \boldsymbol{\Xi} &= \boldsymbol{\psi}^{-1}(\mathbf{X}, t) \cdot \boldsymbol{\xi}. \end{aligned} \tag{3.4}$$

Similarly to what done in the previous chapter for the first gradient theory, we require that

$$\det(\nabla\boldsymbol{\chi}) > 0 \tag{3.5}$$

and in addition

$$\det(\boldsymbol{\psi}) = 1/\det\left(\boldsymbol{\psi}^{-1}\right) > 0. \tag{3.6}$$

The two conditions expressed by the Eq. (3.5) and (3.6) ensure the physical assumption of continuity, indestructibility and impenetrability of matter. In addition, the three independent directors Φ_i are transformed into three independent directors ϕ_i

$$\begin{aligned} \phi_j &= \psi_{ij}(\mathbf{X}, t)\, a_i, \\ \Phi_j &= \psi_{ij}^{-1}(\mathbf{X}, t)\, A_i \end{aligned} \tag{3.7}$$

in which A_i and a_i $(i = 1, 2, 3)$ are the components of suitable Cartesian unit vectors in the reference and current configuration, respectively. Then, it is worth noting that a material point possesses, in addition to the three usual translations, *three deformable directors* which represent the additional degrees of freedom that are able to take into account the deformation of the microstructure.

3.1.2 Polar Decomposition for the Microdeformation Tensor

The polar decomposition presented in the previous chapter for the deformation gradient still holds, but in a similar way one can perform the polar decomposition for the microdeformation tensor

$$\boldsymbol{\psi} = \bar{\mathbf{R}} \cdot \bar{\mathbf{U}} = \bar{\mathbf{V}} \cdot \bar{\mathbf{R}} \tag{3.8}$$

where $\bar{\mathbf{R}}$ is an orthogonal tensor (i.e. $\bar{\mathbf{R}}^{-1} = \bar{\mathbf{R}}^T$ and $\det\left(\bar{\mathbf{R}}\right) = 1$) called *microrotation tensor* and $\bar{\mathbf{U}}$ and $\bar{\mathbf{V}}$ are symmetric and definite positive matrices called *right* and *left microstrech tensor*, respectively.

3.1.3 Definition of Different Type of Continua

By imposing particular constraints on the microdeformation tensor one can define particular class of micro-structured continua. Here, following [ERI01], we recall, as an example, the definition of two of the most famous types of microstructured continua. A systematical presentation of different classes of micro-structured continua can be found in [FOR06].

3.1.3.0.1 Microstretch Continua A microstretch continuum is a micromorphic continuum constrained to undergo microrotation and microstretch (expansion and contraction) without microshearing.

3.1.3.0.2 Micropolar Continua A micropolar continuum is a micromorphic continuum in which the director are orthogonal and rigid, so that the microdeformation tensor consists only in a microrotation.

Such particular cases of constrained generalized continua can all be rigorously obtained by imposing precise kinematical constraints on the introduced set of kinematical parameters. We refrain here to extensively show here how such model are obtained from a general micromorphic model, but we will show analogous procedures in the remainder of this chapter to obtain a second gradient theory from a general micromorphic one and a Cosserat theory from a relaxed micromorphic one.

Then, one can summarize the situation in this way

- A micromorphic continuum is a classical continuum that possesses additional degrees of freedom represented by deformable directors;
- A micromorphic continuum in which the directors are stretchable but not shear-deformable is called microstretch continuum;
- A micromorphic continuum in which the directors are rigid is called micropolar.

3.2 Micro-strucure in Linear Elasticity: Mindilin Theory

Once the kinematical framework which is needed for describing the mechanical behavior of microstructured materials via a continuum micromorphic theory is introduced, then one needs to deal with the problem of the conception of suitable constitutive laws which are able to account for the behavior which is peculiar of each microstructured material. The problem of choosing constitutive laws which are representative of real material behaviors is not trivial and passes through the introduction of suitable deformation measures. We will present in the following chapters constitutive laws which are suitable for the description of the mechanical behavior of orthotropic micro-structured materials at finite strains which are suitable for the study of the mechanical behavior of fibrous composite reinforcements. Nevertheless, to the sake of conciseness and in order to focus on the main objective of this chapter which is to introduce micromorphic theories and to show how they can be suitably constrained to obtain more particular generalized theories, we limit ourselves to introduce here some argumentations based on the constitutive modeling of materials under the assumption of small strains. To this aim, it is of interest the presentation of the linear theory of micro-stuctured continua that has been introduced by Mindlin in 1964 [MIN64]. The interest of this presentation lies in the fact that

- the linear model possesses a paradigmatic structure that can be useful for a simpler comprehension of the nonlinear one since the mathematical complexity introduced by nonlinearities is avoided;
- the linearized case allows to familiarize with the process of obtaining particular generalized continuum theories by constraining more general micromorphic theories
- the linear model is suitable for the description of a wide range of physical phenomena.

3.2.1 Kinematics and Lagrangian Deformation Measure

The kinematics of the model introduced by Mindlin in [MIN64] is the same presented in the previous paragraph. Then, the classical placement map $\boldsymbol{\chi}(\mathbf{X}, t)$ is complemented by a second order tensor field $\mathbf{P}(\mathbf{X}, t)$, which accounts for the deformation associated with the microstructure of the medium. So, the degrees of freedom of the system becomes 12, in spite of the 3 classical degrees of freedom present in Cauchy continua.

The Lagrangian strain measures introduced by Mindlin are of the type[1]

$$\begin{aligned}
&\boldsymbol{E} = \frac{1}{2}\left(\nabla\mathbf{u} + \nabla\mathbf{u}^T\right), && E_{ij} = \frac{1}{2}\left(u_{i,j} + u_{j,i}\right), && \text{macro strain}\\
&\boldsymbol{\gamma} = \nabla\mathbf{u} - \mathbf{P}, && \gamma_{ij} = u_{i,j} - P_{ij}, && \text{relative microdeformation}\\
&\boldsymbol{\kappa} = \nabla\mathbf{P}, && \kappa_{ijk} = P_{ij,k}, && \text{gradient of microdeformation}
\end{aligned} \tag{3.9}$$

in which $\mathbf{u} = \boldsymbol{\chi} - \mathbf{X}$ is the classical macroscopic displacement field. The tensor $\mathbf{E}$ is the classical linearized macro deformation strain tensor, the tensor $\boldsymbol{\gamma}$ accounts for the relative micro-macro deformation and, finally, $\boldsymbol{\kappa}$ is the gradient of the microdeformation.

3.2.2 Kinetic and Potential Energies

Let us denote by ϱ and η the macroscopic and microscopic mass densities defined per unit of macro volume, then the kinetic energy-density defined by Mindlin is of the type

$$T = \frac{1}{2}\varrho\left\|\mathbf{u}_{,t}\right\|^2 + \frac{1}{2}\eta\left\|\boldsymbol{\psi}_{,t}\right\|^2, \qquad T = \frac{1}{2}\varrho\, u_{i,t}\, u_{i,t} + \frac{1}{2}\eta\, P_{ij,t}\, P_{ij,t} \tag{3.10}$$

in which $\|\cdot\|$ stands for the norm induced by the scalar product[2] in $\mathbb{R}^3$ and in $\mathbb{R}^{3\times3}$, respectively. Since the second order tensor $\mathbf{P}$ is dimensionless the coefficient η has a dimension of a bulk density times a square of a length. Then, if ϱ' is the true density of the microstructure one can write the microscopic mass densities as

$$\eta = l^2\varrho', \tag{3.11}$$

where l is a characteristic length which can be directly associated to the characteristic size of the microscopic inclusions embedded in the considered micro-structured material (see[MIN64]). It is important to note that in the definition of the kinetic energy we have considered a micro-structured material that possesses only one characteristics length. A more general form of the energy, accounting for a wealthy of characteristic lengths l_{ij} and hence for more complicated microstructures, in considered in Mindilin [MIN64] and is of the type

$$T = \frac{1}{2}\varrho\, u_{i,t}\, u_{i,t} + \frac{1}{2}\eta_{ij}\, P_{ki,t}\, P_{kj,t}, \tag{3.12}$$

where $\eta_{ij} = l_{ij}^2\varrho'$.

The general form of the strain energy density is a function of the 42 kinematical variables E_{ij}, γ_{ij} and κ_{ijk}

$$W = W(\mathbf{E}, \boldsymbol{\gamma}, \boldsymbol{\kappa}) = W(E_{ij}, \gamma_{ij}, \kappa_{ijk}) \tag{3.13}$$

and it is defined for unit of macro volume.

[1] We consider here a microdeformation tensor $\mathbf{P}$ which is the transposed of the the microdeformation tensor $\boldsymbol{\psi}$ introduced by Mindlin. This choise is related to the used convention about the differentiation of considered tensor fields.

[2] Let $\mathbf{a}, \mathbf{b} \in \mathbb{R}^3$ two vectors and $\mathbf{A}, \mathbf{B} \in \mathbb{R}^3 \times \mathbb{R}^3$ two second order tensors. We denote here and in the sequel the scalar product in $\mathbb{R}^3$ and in $\mathbb{R}^{3\times3}$ as $\langle\mathbf{a}, \mathbf{b}\rangle_{\mathbb{R}^3} = a_i b_i$ and $\langle\mathbf{A}, \mathbf{B}\rangle_{\mathbb{R}^{3\times3}} = \mathbf{A}\,|\mathbf{B} = A_{ij}B_{ij}$.

3.2.3 Variational Deduction of the Equations of Motion in Strong Form

Let $T \in \mathbb{R}^+$ and B_0 the reference (Lagrangian) configuration of the considered continuum. The equations of motion for a linear micromorphic continuum will be derived through the *Hamilton Principle* which states *that the motion of a dynamical system subjected to conservative loads make minimum the Hamiltonian functional*

$$\mathcal{H} = \int_0^T (\mathcal{T} - \mathcal{W} + \mathcal{W}_{\text{ext}}) \tag{3.14}$$

with respect to all kinematically admissible motions that lead the system from the initial position to the final one in the same interval of time $[0, T]$. In the Hamiltonian functional expressed by Eq. (3.14), the symbols $\mathcal{T}$ and $\mathcal{W}$ stands respectively for the total kinetic and elastic potential energies which expressions are defined by

$$\begin{aligned}\mathcal{T} &= \int_{B_0} T\\ \mathcal{W} &= \int_{B_0} W\end{aligned} \tag{3.15}$$

where T and W have been defined in (3.10) and (3.13) respectively and $\mathcal{W}_{\text{ext}}$ represents the potential of the external loads.

The minimization condition for the action functional (3.14) can be written as

$$\delta\mathcal{H} = \int_0^T (\delta\mathcal{T} - \delta\mathcal{W} + \delta\mathcal{W}_{\text{ext}}) = 0 \tag{3.16}$$

from which one can derive the equations of motion as done below. The variation of the kinetic terms expressed by Eq. (3.10) can be written as

$$\int_0^T \delta\mathcal{T} = \int_0^T \int_{B_0} \delta T = -\int_0^T \int_{B_0} (\varrho u_{i,t}\delta u_{i,t} + \eta P_{ij,t}\delta P_{ij,t}) \tag{3.17}$$

that integrated by parts with respect to the time variable t becomes

$$\int_0^T \delta\mathcal{T} = \int_0^T \int_{B_0} \delta T = -\int_0^T \int_{B_0} (\varrho u_{i,tt}\delta u_i + \eta P_{ij,tt}\delta P_{ij}) \tag{3.18}$$

in which the conditions $\delta u_i|_{t=0} = \delta u_i|_{t=T} = 0$ and $\delta P_{ij}|_{t=0} = \delta P_{ij}|_{t=T} = 0$ has been accounted for. Analogously, for the elastic potential energy, which is given by Eq. (3.13), one can write

$$\int_0^T \delta\mathcal{W} = \int_0^T \int_{B_0} \delta W = \int_0^T \int_{B_0} \left(\frac{\partial W}{\partial \mathbf{E}}\,|\delta\mathbf{E} + \frac{\partial W}{\partial \boldsymbol{\gamma}}\,|\delta\boldsymbol{\gamma} + \frac{\partial W}{\partial \boldsymbol{\kappa}}\,|\delta\boldsymbol{\kappa}\right) \tag{3.19}$$

For notational convenience, we will set

$$\begin{aligned}\boldsymbol{\sigma} &= \frac{\partial W}{\partial \mathbf{E}} = \boldsymbol{\sigma}^T, & \sigma_{ij} &= \frac{\partial W}{\partial E_{ij}} = \sigma_{ji},\\ \boldsymbol{\tau} &= \frac{\partial W}{\partial \boldsymbol{\gamma}}, & \tau_{ij} &= \frac{\partial W}{\partial \gamma_{ij}},\\ \boldsymbol{\mu} &= \frac{\partial W}{\partial \boldsymbol{\kappa}}, & \mu_{ijk} &= \frac{\partial W}{\partial \kappa_{ijk}} = \mu_{jik}.\end{aligned} \tag{3.20}$$

Recalling the definition of $\mathbf{E}$ from the first line of Eq. (3.9) and using the fact that $\boldsymbol{\sigma}$ is symmetric, it is easy to check that

$$\boldsymbol{\sigma}\,|\delta\mathbf{E} = \boldsymbol{\sigma}\,|\delta\nabla\mathbf{u}\,, \qquad \sigma_{ij}\delta E_{ij} = \sigma_{ij}\delta u_{i,j}. \tag{3.21}$$

With the notations given in Eq. (3.20) using Eq. (3.21) and the definition of $\boldsymbol{\gamma}$ (3.9), one can check that Eq. (3.19) becomes

$$\int_0^T \delta\mathcal{W} = \int_0^T \int_{B_0} \delta W = \int_0^T \int_{B_0} \left(\sigma_{ij}\delta u_{i,j} + \tau_{ij}\left(\delta u_{i,j} - \delta P_{ij}\right) + \mu_{ijk}\delta P_{ij,k}\right), \tag{3.22}$$

which integrated by parts reads

$$\begin{aligned}\int_0^T \delta\mathcal{W} = \int_0^T \int_{B_0} \delta W = \int_0^T \int_{B_0} \Big\{&\left[\left(\sigma_{ij} + \tau_{ij}\right)\delta u_i\right]_{,j} - \left(\sigma_{ij} + \tau_{ij}\right)_{,j}\delta u_i \\ &- \left(\tau_{ij} + \mu_{ijk,k}\right)\delta P_{ij} + \left(\mu_{ijk}\delta P_{ij}\right)_{,k}\Big\}.\end{aligned} \tag{3.23}$$

By using the divergence theorem, Eq. (3.23) is transformed into

$$\begin{aligned}\int_0^T \delta\mathcal{W} = \int_0^T \int_{B_0} \delta W = -\int_{B_0} &\left(\sigma_{ij} + \tau_{ij}\right)_{,j}\delta u_i - \int_{B_0} \left(\mu_{ijk,k} + \tau_{ij}\right)\delta P_{ij} \\ &+ \int_{\partial B_0} n_j\left(\sigma_{ij} + \tau_{ij}\right)\delta u_i + \int_{\partial B_0} \mu_{ijk} n_k \delta P_{ij},\end{aligned} \tag{3.24}$$

in which n_j (or n_k) are the components of the unit normal vector $\mathbf{n}$ to the boundary surface ∂B_0.

Following Mindlin [MIN64] we assume that the variation of the energy due to the external loads takes the form

$$\int_0^T \delta\mathcal{W}_{\text{ext}} = \int_0^T \int_{B_0} \delta W_{\text{ext}} = \int_{B_0} b_i^{\text{ext}}\delta u_i + \int_{B_0} \Phi_{ij}^{\text{ext}}\delta P_{ij} + \int_{\partial B_0} t_i^{\text{ext}}\delta u_i + \int_{\partial B_0} T_{ij}^{\text{ext}}\delta P_{ij}, \tag{3.25}$$

in which b_i^{ext} is the external body force per unit volume, t_i^{ext} is the external surface force per unit area, Φ_{ij}^{ext} is the external double force per unit volume and T_{ij}^{ext} is the external double force per unit area (see [MIN64] for further details) .

So, by substituting Eqs. (3.18), (3.24) and (3.25) in Eq. (3.16) one finally obtains

$$\begin{aligned}\int_0^T \int_{B_0} &\left[\left(\sigma_{ij} + \tau_{ij}\right)_{,j} + b_i^{\text{ext}} - \varrho u_{i,tt}\right]\delta u_i + \int_0^T \int_{B_0} \left[\mu_{ijk,k} + \tau_{ij} + \Phi_{ij}^{\text{ext}} - \eta P_{ij,tt}\right]\delta P_{ij} \\ &+ \int_0^T \int_{\partial B_0} \left[t_i^{\text{ext}} - n_j\left(\sigma_{ij} + \tau_{ij}\right)\right]\delta u_i + \int_0^T \int_{\partial B_0} \left[T_{ij}^{\text{ext}} - \mu_{ijk} n_k\right]\delta P_{ij} = 0\end{aligned} \tag{3.26}$$

from which, by assuming arbitrary variations of the introduced kinematical fields δu_i and δP_{ij}, one obtains the bulk equations with associated natural boundary conditions in terms of components

$$\begin{aligned}\left(\sigma_{ij} + \tau_{ij}\right)_{,j} + b_i^{\text{ext}} &= \varrho u_{i,tt} \\ \mu_{ijk,k} + \frac{\partial W}{\partial \gamma_{ij}} + \Phi_{ij}^{\text{ext}} &= \eta P_{ij,tt} \\ n_j\left(\sigma_{ij} + \tau_{ij}\right) &= t_i^{\text{ext}} \\ \mu_{ijk} n_k &= T_i^{\text{ext}}\end{aligned} \tag{3.27}$$

or in compact form

$$\begin{aligned}\text{Div}\left(\boldsymbol{\sigma} + \boldsymbol{\tau}\right) + \mathbf{b}^{\text{ext}} &= \varrho \mathbf{u}_{,tt} \\ \text{Div}\left(\boldsymbol{\mu}\right) + \boldsymbol{\tau} + \boldsymbol{\Phi}^{\text{ext}} &= \eta \mathbf{P}_{,tt} \\ \left(\boldsymbol{\sigma} + \boldsymbol{\tau}\right)\cdot\mathbf{n} &= \mathbf{t}^{\text{ext}} \\ \boldsymbol{\mu}\cdot\mathbf{n} &= \mathbf{T}^{\text{ext}}\end{aligned}. \tag{3.28}$$

The tensors $\boldsymbol{\sigma}$, $\boldsymbol{\tau}$ and $\boldsymbol{\mu}$ represent the Cauchy stress, the relative stress and the double stress, respectively. It is worth noting that differently from first and second gradient theories in which the only kinematical field is the displacement field, here the kinematical variables are the displacement field $\mathbf{u}$ and the components of the microstructural tensor $\mathbf{P}$. So, the scalar equations of motion are augmented in a number that equates the one of the new kinematical variables.

3.2.4 Constitutive Equations

The general form of the potential energy presented in Mindlin [MIN64] is an homogeneous quadratic function of the 42 variables E_{ij}, γ_{ij} and κ_{ijk}, and it is of the type[3]

$$\begin{aligned} W = &\frac{1}{2} c_{ijkl}\, E_{ij}\, E_{kl} + \frac{1}{2} b_{ijkl}\, \gamma_{ij}\, \gamma_{kl} + \frac{1}{2} a_{ijklmn}\, \kappa_{ijk}\, \kappa_{lmn} \\ &+ d_{ijklm}\, \gamma_{ij}\, \kappa_{klm} + f_{ijklm}\, \kappa_{ijk}\, E_{lm} + g_{ijkl}\, \gamma_{ij}\, E_{kl}. \end{aligned} \tag{3.29}$$

In Eq. (3.29) there are 1764 scalar coefficients but only 903 of them are independent due to the symmetries of the introduced strain and micro-strain tensors. The isotropy of the material reduces again the number of independent constant at 18(see [MIN64]), so the potential energy expressed by the Eq. (3.29) reduces to

$$\begin{aligned} W = &\frac{1}{2}\lambda\, E_{ii}\, E_{jj} + \mu\, E_{ij}\, E_{ij} + \frac{1}{2} b_1\, \gamma_{ii}\, \gamma_{jj} + \frac{1}{2} b_2\, \gamma_{ij}\, \gamma_{ij} + \frac{1}{2} b_3\, \gamma_{ij}\, \gamma_{ji} \\ &+ g_1\, \gamma_{ii}\, E_{jj} + g_2\, (\gamma_{ij} + \gamma_{ji})\, E_{ij} + a_1\, \kappa_{iik}\, \kappa_{kjj} + a_2\, \kappa_{iik}\, \kappa_{jkj} \\ &+ \frac{1}{2} a_3\, \kappa_{iik}\, \kappa_{jjk} + \frac{1}{2} a_4\, \kappa_{ijj}\, \kappa_{ikk} + a_5\, \kappa_{ijj}\, \kappa_{kik} + \frac{1}{2} a_8\, \kappa_{iji}\, \kappa_{kjk} \\ &+ \frac{1}{2} a_{10}\, \kappa_{ijk}\, \kappa_{ijk} + a_{11}\, \kappa_{ijk}\, \kappa_{jki} + \frac{1}{2} a_{13}\, \kappa_{ijk}\, \kappa_{ikj} + \frac{1}{2} a_{14}\, \kappa_{ijk}\, \kappa_{jik} \\ &+ \frac{1}{2} a_{15}\, \kappa_{ijk}\, \kappa_{kji}. \end{aligned} \tag{3.30}$$

Such expression of the strain energy density is rather simplified with respect to the general one introduced in Eq. (3.29). Nevertheless the number of constitutive parameters is still elevated, so that we follow [NEF13] and introduce an ulteriorly simplified micromorphic strain energy density which reflects, at least qualitatively, all the features of the classical micromorphic model of Mindlin, but drastically reducing the number of constitutive parameters from 18 to 6.

$$\begin{aligned} W = &\mu_e \left\| \mathrm{sym}\left(\nabla \mathbf{u} - \mathbf{P}\right) \right\|^2 + \frac{\lambda_e}{2} \left(\mathrm{tr}\left(\nabla \mathbf{u} - \mathbf{P}\right)\right)^2 + \mu_h \left\| \mathrm{sym}\left(\mathbf{P}\right) \right\|^2 + \frac{\lambda_h}{2} \left(\mathrm{tr}\left(\mathbf{P}\right)\right)^2 \\ &+ \mu_c \left\| \mathrm{skew}\left(\nabla \mathbf{u} - \mathbf{P}\right) \right\|^2 + \frac{\alpha_g}{2} \left\| \nabla \mathbf{P} \right\|^2 . \end{aligned} \tag{3.31}$$

Suitable identification of the coefficients proposed here in terms of the ones introduced by Mindlin can be found in [MAD13].

3.3 Relaxed Micromorphic Continuum and Constrained Micromorphic Models

In this section we introduce the relaxed micromorphic energy proposed in [NEF13] which is the simpler micromorphic energy which can be introduced in order to prove existence and uniqueness of

[3]We recall once again that the microdeformation tensor $\mathbf{P}$ used in this manuscript is connected to the tensor $\boldsymbol{\psi}$ used by Mindlin via the formula $P_{ij} = \psi_{ji}$ so that the tensor $\boldsymbol{\kappa}$ introduced here has its two first indices inverted with respect to the one used by Mindlin. This implies that, in order to correctly identify the constitutive coefficients introduced here with those used by Mindlin, one must account for these slight differences.

the associated Euler-Lagrange equations. Moreover, we will show how, imposing suitable constraints, it is possible to obtain particular generalized models (like second gradient and Cosserat models) from the classical micromorphic model and the relaxed micromorphic model respectively.

3.3.1 Notation

In order to make reading easier we declare here the notation adopted in the following paragraphs. This notation is the same adopted in [NEF13], in order to avoid confusions in the reader.

Let $\mathbf{a} \in \mathbb{R}^3$ a vector and $\mathbf{A} \in \mathbb{R}^3 \times \mathbb{R}^3$ a second order tensor. We define the standard divergence and curl operators for vectors and second order tensors as

$$\begin{aligned} \mathrm{Div}\,(\mathbf{a}) &= a_{i,j}, & (\mathrm{Curl}\,(\mathbf{a}))_i &= \mathbf{a}_{a,b}\epsilon_{iab} \\ (\mathrm{Div}\,(\mathbf{A}))_i &= A_{ij,j}, & (\mathrm{Curl}\,(\mathbf{A}))_{ij} &= \mathbf{A}_{ia,b}\epsilon_{jab} \end{aligned} \tag{3.32}$$

where $\boldsymbol{\epsilon}$ is the Levi-Civita tensor. The gradient operator for vectors and tensors is the same adopted in the previous paragraphs.

In addition, we denote the symmetric, skew-symmetric, spheric, and deviatoric part of a tensor, respectively, as

$$\begin{aligned} \mathrm{sym}\,(\mathbf{A}) &= \frac{1}{2}\left(\mathbf{A} + \mathbf{A}^T\right), & \mathrm{skew}\,(\mathbf{A}) &= \frac{1}{2}\left(\mathbf{A} - \mathbf{A}^T\right), \\ \mathrm{sph}\,(\mathbf{A}) &= \frac{1}{3}\mathrm{tr}\,(\mathbf{A})\,\mathbf{I}, & \mathrm{dev}\,(\mathbf{A}) &= \mathbf{A} - \mathrm{sph}\,(\mathbf{A}), \end{aligned} \tag{3.33}$$

or equivalently

$$\begin{aligned} (\mathrm{sym}\,(\mathbf{A}))_{ij} &= \frac{1}{2}\left(A_{ij} + A_{ji}\right), & (\mathrm{skew}\,(\mathbf{A}))_{ij} &= \frac{1}{2}\left(A_{ij} - A_{ji}\right), \\ (\mathrm{sph}\,(\mathbf{A}))_{ij} &= \frac{1}{3}A_{kk}\delta_{ij}, & (\mathrm{dev}\,(\mathbf{A}))_{ij} &= A_{ij} - (\mathrm{sph}\,(\mathbf{A}))_{ij}, \end{aligned} \tag{3.34}$$

where δ_{ij} is the Kronecker delta and $\mathbf{I}$ is the identity matrix.

3.3.2 The relaxed Micromorphic Energies

The kinetic energies in the relaxed micromorphic model is of the same type of one presented by the Eq. (3.10). Instead, the authors in [NEF13] proposed the following strain energy density

$$\begin{aligned} W = {} & \mu_e \left\|\mathrm{sym}\,(\nabla\mathbf{u} - \mathbf{P})\right\|^2 + \frac{\lambda_e}{2}\left(\mathrm{tr}\,(\nabla\mathbf{u} - \mathbf{P})\right)^2 + \mu_h \left\|\mathrm{sym}\,(\mathbf{P})\right\|^2 + \frac{\lambda_h}{2}\left(\mathrm{tr}\,(\mathbf{P})\right)^2 + \\ & + \mu_c \left\|\mathrm{skew}\,(\nabla\mathbf{u} - \mathbf{P})\right\|^2 + \frac{\alpha_c}{2}\left\|\mathrm{Curl}\,(\mathbf{P})\right\|^2, \end{aligned} \tag{3.35}$$

in which all the introduced constitutive coefficients are assumed to be constant. It is important to note, as highlighted by the authors in [NEF13], that in Eq. (3.35) appears an energy term involving the curl of the microdeformation tensor $\mathbf{P}$, instead of its gradient as done in the classical models (see Eq. (3.31)). This choice allows, among others, for the description of frequency band-gaps (see [MAD13] for details) which are observed when considering wave propagation in phononic crystals and lattice structures. The interesting aspect of this constitutive choice is that the structure of the proposed strain energy density is the simplest possible which is needed to prove well-posedness of the associated Euler-Lagrange equations by means of arguments related to Legendre-Hadamard ellipticity of the Energy itself (see [NEF13]). Positive definiteness of the potential energy implies the following simple relations on the introduced parameters [NEF13]

$$\mu_e > 0, \qquad \mu_c > 0, \qquad 3\lambda_e + 2\mu_e > 0, \qquad \mu_h > 0, \qquad 3\lambda_h + 2\mu_h > 0, \qquad \alpha_c > 0. \tag{3.36}$$

One of the most appealing features of the energy proposed by the authors in [NEF13], is the reduced number of elastic parameters which are needed to fully determine the mechanical behavior of a micromorphic continuum. Indeed, as showed by the same authors [NEF13], each parameter can be easily related to specific micro- and macro-deformation modes.

3.3.3 A second gradient model obtained as a limit case of a classical micromorphic model

As said above, the strain energy function expressed by Eq. (3.31) is the simpler one that reflects (at least qualitatively) the classical micromorphic model of Mindlin. In this section we want to show that such classical micromorphic model contains in itself a second gradient model when one consider a suitable limit case. More precisely, if one let simultaneously $\mu_e \to \infty$ and $\mu_c \to \infty$ in Eq. (3.31), since the energy must be bounded, this implies that

$$\begin{aligned} \operatorname{sym}(\mathbf{P}) &\to \operatorname{sym}(\nabla \mathbf{u}), \\ \operatorname{skew}(\mathbf{P}) &\to \operatorname{skew}(\nabla \mathbf{u}), \end{aligned} \tag{3.37}$$

so, we finally have that

$$\mathbf{P} \to \nabla \mathbf{u} \tag{3.38}$$

and the strain energy function expressed by thus becomes

$$W \to W_{2\mathrm{G}}(\nabla \mathbf{u}, \nabla\nabla \mathbf{u}) = \mu_h \left\| \operatorname{sym}(\nabla \mathbf{u}) \right\|^2 + \frac{\lambda_h}{2} \left(\operatorname{tr}(\nabla \mathbf{u}) \right)^2 + \frac{\alpha_g}{2} \left\| \nabla\nabla \mathbf{u} \right\|^2 \tag{3.39}$$

which is a function of the first and second gradient of the placement.

We have hence proven by simple arguments that if one is able to impose suitable constraints on the extra degrees of freedom which are peculiar of a micromorphic theory then more particular theories can be easily derived as particular cases. This type of procedure will be applied in the remainder of this manuscript in order to numerically implement a second gradient theory as the limit case of a micromorphic one.

3.3.4 A Cosserat model obtained as a limit case of a relaxed micromorphic model

In a similar way, one can obtain another well-known model starting from the relaxed micromorphic energy introduced above in Eq. (3.35). In particular, by letting $\mu_h \to \infty$, since the energy must be bounded, one equivalently obtain

$$\operatorname{sym}(\mathbf{P}) \to \mathbf{0}, \tag{3.40}$$

and then

$$\operatorname{tr}(\mathbf{P}) \to \mathbf{0}. \tag{3.41}$$

These two last equations imply that the relaxed energy (3.35) degenerates into the Cosserat one

$$\begin{aligned} W \to W_{\mathrm{Cosserat}}(\nabla \mathbf{u}, \operatorname{skew}(\mathbf{P})) = {} & \mu_e \left\| \operatorname{sym}(\nabla \mathbf{u}) \right\|^2 + \frac{\lambda_e}{2} \left(\operatorname{tr}(\nabla \mathbf{u}) \right)^2 \\ & + \mu_c \left\| \operatorname{skew}(\nabla \mathbf{u} - \mathbf{P}) \right\|^2 + \frac{\alpha_c}{2} \left\| \operatorname{Curl}(\operatorname{skew}(\mathbf{P})) \right\|^2 . \end{aligned} \tag{3.42}$$

As a general remark, we want to stress, once again, the fact that a rigorous but simple procedure based on suitable constraining of micromorphic theories can lead to some other more particular generalized theories as limit cases. The operative way in which such constraints can imposed may be different: one can, for example, think to let some elastic parameters to infinity, as done here, or can use the well-known method of Lagrange multipliers (see e.g. [FER13]). In the following chapters, when introducing a second gradient model for fibrous composite reinforcements, as the limit case of a suitable micromorphic model, we will choose to use the method of Lagrange multipliers to impose the desired constraints. This choice is related to the fact that we found more convenient this last strategy to implement the constraints in the numerical code.

Chapter 4

Continuum Mechanics Preliminaries: Second Gradient Theory

In this chapter we recall some well-established facts about second gradient theories. In particular, we introduce the definition of second gradient continuum and we find the general equations of motion in strong form for a hyperelastic, second gradient material. The main scope of this chapter is to show that second gradient theories can indeed be obtained both as constrained micromorphic theories but also by means of direct variational principles based on a standard kinematics which accounts for the displacement field alone.

In summary, we want to underline the fact that two possible strategies are possible to deal with second gradient continua

- Directly use a constrained kinematics uniquely based on the macroscopic displacement field and then consider higher gradients of the displacement in the strain energy density (this is the strategy described in this chapter).
- Start from a richer kinematics (as done for micromorphic media) and then impose suitable constraints on the extra kinematical descriptors in order to obtain the desired second gradient model as as a limit case (see what done in Chap. 5).

Which of the two strategies has to be used to deal with the application of a second gradient theory is a matter of convenience. In this manuscript we report all the available possibilities to the sake of a complete description of generalized continuum theories. As it will be seen in the following, we will privilege the second strategy in order to deal with the application of second gradient theories to fibrous composite reinforcements. This choice was dictated by two advantages:

i) micromorphic theories are more suitable for an easier physical interpretation of internal and external internal actions related to microstructure and

ii) micromorphic theories are more convenient to be treated from a numerical point of view since the differential system of associated Euler-Lagrange equations is of lower order with respect to second gradient case.

Notwithstanding the previous considerations, we want to stress the fact that the correct continuum framework which we found to be well-adapted for describing the mechanical behavior of fibrous composite reinforcements is the one of second gradient theories.

Contents

4.1 Nonlinear Second Gradient Models

The kinematics that has to be introduce when one wants to deal with second gradient continua is the same introduced in the first chapter for the first gradient theory. Then, this kinematics is described by the usual placement function $\boldsymbol{\chi}(\mathbf{X},t)$ which associates at any material point that occupies the position $\mathbf{X}$ in the reference configuration B_0 its current position $\mathbf{x}$ in the current one. The characteristic which makes a second gradient theory different from a first gradient one is the fact that the strain energy density is a function not only of the Green-Lagrange strain tensor $\boldsymbol{\varepsilon}$ but also of its gradient $\nabla\boldsymbol{\varepsilon}$ (that is a third order tensor). In formulas, one have

$$W = W(\boldsymbol{\varepsilon}, \nabla\boldsymbol{\varepsilon}). \tag{4.1}$$

In the following subsection we derive the equations of motion for a second gradient continuum in which the strain energy function is defined by Eq. (4.1) also considering the possible presence of surfaces of discontinuity inside the considered medium (e.g. the considered domain is constituted by two different materials).

4.1.1 Variational Deduction of the Equations of Motion

Let $T \in \mathbb{R}^+$ and B_0 be the reference (Lagrangian) configuration of a body. The action functional for the considered second gradient continuum is defined as

$$\mathcal{A} = \int_0^T \int_{B_0} W(\boldsymbol{\varepsilon}, \nabla\boldsymbol{\varepsilon}), \tag{4.2}$$

in which W is the Lagrangian strain energy density defined per unit volume, $\boldsymbol{\varepsilon}$ is the Green-Lagrange strain tensor defined as

$$\boldsymbol{\varepsilon} = \frac{1}{2}\left(\mathbf{F}^T\mathbf{F} - \mathbf{I}\right), \qquad \varepsilon_{ij} = \frac{1}{2}(F_{ik}F_{kj} - \delta_{ij}) \tag{4.3}$$

where δ_{ij} stands for the Kronecker delta and $\mathbf{F}$ denotes the gradient of the placement function (i.e. $\mathbf{F} = \nabla\boldsymbol{\chi}$).

In order to calculate the the stationary points of the action functional, one must compute its first variation (denoted as $\delta\mathcal{A}$) and impose it to be equal to zero. This allows to determine the Euler-Lagrange equations and the associated duality conditions, which represent the equilibrium equations that must be satisfied in the bulk and at any (eventual) surface of discontinuity. So, by assuming that the kinematical field expressed by the placement function $\boldsymbol{\chi}$ is suitably regular, one can write the first variation of the action functional as

$$\delta\mathcal{A} = \int_0^T \int_{B_0} \left(\frac{\partial W}{\partial\boldsymbol{\varepsilon}} \,|\delta\boldsymbol{\varepsilon} + \frac{\partial W}{\partial\nabla\boldsymbol{\varepsilon}} \,|\delta\nabla\boldsymbol{\varepsilon}\right) \tag{4.4}$$

For notational convenience, we set

$$\begin{aligned} \mathbf{S} &= \frac{\partial W}{\partial\boldsymbol{\varepsilon}}, & S_{ij} &= \frac{\partial W}{\partial\varepsilon_{ij}}, \\ \mathbb{S} &= \frac{\partial W}{\partial\nabla\boldsymbol{\varepsilon}}, & \mathbb{S}_{ijk} &= \frac{\partial W}{\partial\varepsilon_{ij,k}}, \end{aligned} \tag{4.5}$$

that, naturally, are a second order and a third order tensor, respectively. The tensor $\mathbf{H}$ is symmetric and the tensor $\mathbb{H}$ is symmetric with respect to its first two indices, so, with these two symmetry properties and by recalling Eq. (4.3), it can be checked that

$$\begin{aligned} \mathbf{S}\,|\delta\boldsymbol{\varepsilon} &= \mathbf{S}\,\middle|\left(\mathbf{F}^T\cdot\delta\mathbf{F}\right), & S_{ij}\delta\varepsilon_{ij} &= S_{ij}F_{ki}\delta F_{kj}, \\ \mathbb{S}\,|\delta\nabla\boldsymbol{\varepsilon} &= \mathbb{S}\,\middle|\nabla\left(\delta\mathbf{F}^T\cdot\mathbf{F}\right), & \mathbb{S}_{ijk}\delta\varepsilon_{ij,k} &= \mathbb{S}_{ijk}\left(\delta F_{hi}F_{hj}\right)_{,k}. \end{aligned} \tag{4.6}$$

Integrating by part Eq. (4.4) a suitable number of times and remembering that $\mathbf{F} = \nabla\boldsymbol{\chi}$, one obtains

$$\begin{aligned}\delta\mathcal{A} = &-\int_0^T\int_{B_0}\left[\left(S_{ij}-\mathbb{S}_{ijp,p}\right)F_{ki}\right]_{,j}\delta\chi_k + \int_0^T\int_{B_0}\left[\left(S_{ij}-\mathbb{S}_{ijp,p}\right)F_{ki}\delta\chi_k\right]_{,j}\\ &+\int_0^T\int_{B_0}\left[\mathbb{S}_{ijp}F_{kj}\delta F_{ki}\right]_{,p}\end{aligned} \tag{4.7}$$

By using the divergence theorem and by considering test functions with compact support K included in B_0 that have non-empty intersection Σ_K with a (possible) discontinuity surface Σ (see [DEL09a] for more details), the previous equation implies

$$\begin{aligned}\delta\mathcal{A} = &-\int_0^T\int_{K}\left[\left(S_{ij}-\mathbb{S}_{ijp,p}\right)F_{ki}\right]_{,j}\delta\chi_k + \int_0^T\int_{\Sigma_K}[\![\left(S_{ij}-\mathbb{S}_{ijp,p}\right)F_{ki}n_j\delta\chi_k]\!]\\ &+\int_0^T\int_{\Sigma_K}[\![\mathbb{S}_{ijp}F_{kj}n_p\delta\chi_{k,i}]\!]\end{aligned} \tag{4.8}$$

in which n_j is the component of the unit normal vector $\mathbf{n}$ to the surface Σ_K and the symbol $[\![a]\!] := a^+ - a^-$ stands for the jump of any field a on a surface (here) or, with a slight abuse of notation, also on an edge (after). The last term in Eq. (4.8) involve the quantity $\nabla\delta\boldsymbol{\chi}$ which can be decomposed by projecting it in the normal and in the tangential direction of the surface as

$$\nabla\delta\boldsymbol{\chi} = \nabla\delta\boldsymbol{\chi}\cdot(\mathbf{n}\otimes\mathbf{n}) + \nabla\delta\boldsymbol{\chi}\cdot(\mathbf{I}-\mathbf{n}\otimes\mathbf{n}) = \left(\delta\boldsymbol{\chi}\right)_n\otimes\mathbf{n} + \nabla^{\Sigma}\delta\boldsymbol{\chi} \tag{4.9}$$

in which the symbol $(a)_n := \nabla(a)\cdot\mathbf{n}$ stands for the normal derivative of any field a, while the symbol $\nabla^{\Sigma}a$ stands for its surface gradient. In what follows, in order to distinguish the surface gradient from other differentiations defined on the whole domain, we will use Greek letters. In particular, we set $\left(\nabla^{\Sigma}a\right)_\alpha =: a_{,\alpha}$. So, by using this decomposition, Eq. (4.8) becomes

$$\begin{aligned}\delta\mathcal{A} = &-\int_0^T\int_{K}\left[\left(S_{ij}-\mathbb{S}_{ijp,p}\right)F_{ki}\right]_{,j}\delta\chi_k + \int_0^T\int_{\Sigma_K}[\![\left(S_{ij}-\mathbb{S}_{ijp,p}\right)F_{ki}n_j\delta\chi_k]\!]\\ &+\int_0^T\int_{\Sigma_K}[\![\mathbb{S}_{ijp}F_{kj}n_in_p\left(\left(\delta\boldsymbol{\chi}\right)_n\right)_k]\!] + \int_0^T\int_{\Sigma_K}[\![\mathbb{S}_{\alpha jp}F_{kj}n_p\delta\chi_{k,\alpha}]\!]\,.\end{aligned} \tag{4.10}$$

Integrating by parts of the last term of Eq. (4.8) and using the surface divergence theorem, one finally obtains

$$\begin{aligned}\delta\mathcal{A} = &-\int_0^T\int_{K}\left[\left(S_{ij}-\mathbb{S}_{ijp,p}\right)F_{ki}\right]_{,j}\delta\chi_k + \int_0^T\int_{\Sigma_K}[\![\left(S_{ij}-\mathbb{S}_{ijp,p}\right)F_{ki}n_j\delta\chi_k]\!]\\ &-\int_0^T\int_{\Sigma_K}\left[\!\!\left[\left(\mathbb{S}_{\alpha jp}F_{kj}n_p\right)_{,\alpha}\delta\chi_k\right]\!\!\right] + \int_0^T\int_{\Sigma_K}[\![\mathbb{S}_{ijp}F_{kj}n_in_p\left(\left(\delta\boldsymbol{\chi}\right)_n\right)_k]\!]\\ &+\sum_{i=1}^{N}\int_0^T\int_{\mathcal{E}_i}[\![\mathbb{S}_{\alpha jp}F_{kj}n_p\delta\chi_k\nu_\alpha]\!]\end{aligned} \tag{4.11}$$

in which $\mathcal{E}_i,\quad i=1,\ldots,N$ are the edges of the surface Σ_K and ν_α is the component of the normal $\boldsymbol{\nu}$ to the border of Σ_K.

From this last expression for $\delta\mathcal{A}$, recalling that $\mathbb{H}$ is symmetric with respect to its first two indices, that $\delta\boldsymbol{\chi} = \delta\mathbf{u}$ and assuming that the test functions are arbitrary in the volume but not necessarily on the (eventual) discontinuity surface, it can be checked that the condition $\delta\mathcal{A}$ implies the bulk equation

$$\mathrm{Div}\left[\mathbf{F}\cdot\left(\frac{\partial W}{\partial\boldsymbol{\varepsilon}} - \mathrm{Div}\left(\frac{\partial W}{\partial\nabla\boldsymbol{\varepsilon}}\right)\right)\right] = 0 \tag{4.12}$$

and the duality conditions

$$\begin{aligned} [\![\mathbf{t} \cdot \delta \mathbf{u}]\!] &= 0, \\ [\![\boldsymbol{\tau} \cdot (\delta \mathbf{u})_n]\!] &= 0, \\ [\![\mathbf{f} \cdot \delta \mathbf{u}]\!] &= 0. \end{aligned} \tag{4.13}$$

The first two duality conditions of the Eq. (4.13) are valid on any (eventual) discontinuity surface $\Sigma \subset B_0$ and the last one on its (eventual) edges $\mathcal{E}_i, \quad i = 1, \ldots, N$. The quantities that appear in Eq. (4.13) are linked to the strain energy function by means of the following relationships

$$\begin{aligned} \mathbf{t} &:= \left[\mathbf{F} \cdot \left(\frac{\partial W}{\partial \boldsymbol{\varepsilon}} - \operatorname{Div}\left(\frac{\partial W}{\partial \nabla \boldsymbol{\varepsilon}}\right)\right)\right] \cdot \mathbf{n} - \operatorname{Div}^{\Sigma}\left(\mathbf{F} \cdot \frac{\partial W}{\partial \nabla \boldsymbol{\varepsilon}} \cdot \mathbf{n}\right), \\ \boldsymbol{\tau} &:= \left(\mathbf{F} \cdot \frac{\partial W}{\partial \nabla \boldsymbol{\varepsilon}} \cdot \mathbf{n}\right) \cdot \mathbf{n}, \\ \mathbf{f} &:= \left(\mathbf{F} \cdot \frac{\partial W}{\partial \nabla \boldsymbol{\varepsilon}} \cdot \mathbf{n}\right) \cdot \boldsymbol{\nu}, \end{aligned} \tag{4.14}$$

in which $\operatorname{Div}^{\Sigma}(\cdot)$ stands for the surface divergence operator.The vector t represents the so-called "generalized force" which, contrarily to what happens in classical Cauchy theory, explicitly depends on the "shape" of Σ. Moreover, following the notation introduced by Germain [GER73a], the vector $\boldsymbol{\tau}$ is the so-called "double-force", i.e. a special type of non-local contact action which expends power on the normal derivative of velocity. Finally, $\mathbf{f}$ represents a contact action per unit line which can be exchanged by two sub-bodies of the considered body across the edges (if any) of the Cauchy cut.

Here no external actions have been considered but their inclusion in the theory is straightforward, especially if they can be derived from a potential energy.

4.2 Constitutive Equations for Second Gradient, Isotropic Continua

In this section, we introduce some constitutive relations for isotropic second gradient continua. These equations can be used to describe the material behavior of microstructured materials, such as fibrous composite reinforcements, which can take advantage of a second gradient description. The introduced constitutive equations take into account geometrical non-linearities (since the deformation measure is the Green-Lagrange strain tensor) but not material non-linearities.

In [DEL09] dell'Isola et al., propose a generalization of the Hooke's law for second gradient materials and establish a relation between the generalized stress (named above as $\mathbf{S}$ and $\mathbb{S}$) and the strain and strain gradient ($\boldsymbol{\varepsilon}$ and $\nabla\boldsymbol{\varepsilon}$ respectively). The constitutive relations expressed by the Eq. (4.5) are assumed to be linear with respect to the strain measures and, then, the stored elastic energy is assumed to be a quadratic form of both its arguments. In formulas

$$W(\boldsymbol{\varepsilon}, \nabla\boldsymbol{\varepsilon}) = \frac{1}{2}\left(C_{ijkl}\, \varepsilon_{ij}\, \varepsilon_{kl} + 2K_{ijklp}\, \varepsilon_{ij,k}\, \varepsilon_{lp} + G_{ijklpq}\, \varepsilon_{ij,k}\, \varepsilon_{lp,q}\right) \tag{4.15}$$

where $\mathbf{C}$, $\mathbf{K}$ and $\mathbf{G}$ are fourth-, fifth- and sixth-order tensors respectively, which satisfy the following symmetry conditions

$$\begin{aligned} C_{ijkl} &= C_{klij}, \\ K_{ijklp} &= K_{lpijk}, \\ G_{ijklpq} &= G_{lpqijk}. \end{aligned} \tag{4.16}$$

Moreover, in [DEL09] it is shown that the symmetry of the Green-Lagrange strain tensor induce on the tensors introduced above, other additional symmetries

$$\begin{aligned} C_{ijkl} &= C_{ijlk} = C_{jikl}, \\ K_{ijklp} &= K_{jiklp} = K_{ijkpl}, \\ G_{ijklpq} &= G_{jiklpq} = G_{ijkplq}. \end{aligned} \tag{4.17}$$

So, with the definition of the energy (4.15) and using Eq. (4.5), the relation between generalized stress and strain, becomes

$$\begin{aligned} S_{ij} &= C_{ijkl}\,\varepsilon_{kl} + K_{klpij}\,\varepsilon_{kl,p}, \\ \mathbb{S}_{ijk} &= K_{ijklp}\,\varepsilon_{lp} + G_{ijklpq}\,\varepsilon_{lp,q}. \end{aligned} \tag{4.18}$$

By requiring that the energy satisfies frame indifference by means of the relation

$$W\left(\varepsilon_{ij}, \varepsilon_{ij,k}\right) = W\left(Q_{hi}\,\varepsilon_{ij}\,Q_{mj}, Q_{hi}\,\varepsilon_{hm,n}\,Q_{mj}\,Q_{nk}\right), \tag{4.19}$$

for all orthogonal tensors $\mathbf{Q}$, in addition to the conditions (4.16) and (4.17), the authors obtain the generalized Hooke's law for isotropic second gradient materials in the form

$$\begin{aligned} C_{ijkl} &= \lambda\,\delta_{ij}\,\delta_{kl} + \mu\left(\delta_{ik}\,\delta_{jl} + \delta_{il}\,\delta_{jk}\right), \\ K_{ijklp} &= 0, \\ G_{ijklpq} &= c_2\left(\delta_{ij}\,\delta_{kl}\,\delta_{pq} + \delta_{ij}\,\delta_{kp}\,\delta_{lq} + \delta_{ik}\,\delta_{jq}\,\delta_{lp} + \delta_{iq}\,\delta_{jk}\,\delta_{lp}\right) + c_3\,\delta_{ij}\,\delta_{kq}\,\delta_{lp} \\ &\quad + c_5\left(\delta_{ik}\,\delta_{jl}\,\delta_{pq} + \delta_{ik}\,\delta_{jp}\,\delta_{lq} + \delta_{ij}\,\delta_{jk}\,\delta_{pq} + \delta_{ip}\,\delta_{jk}\,\delta_{lq}\right) + c_{11}\left(\delta_{il}\,\delta_{jp}\,\delta_{kq} + \delta_{ip}\,\delta_{jl}\,\delta_{kq}\right) \\ &\quad + c_{15}\left(\delta_{il}\,\delta_{jq}\,\delta_{kp} + \delta_{ip}\,\delta_{jq}\,\delta_{kl} + \delta_{iq}\,\delta_{jl}\,\delta_{kp} + \delta_{iq}\,\delta_{jp}\,\delta_{kl}\right) \end{aligned} \tag{4.20}$$

These equations provide the most general linear elastic constitutive relations for isotropic materials. Such relations generalize standard Hooke's law to second gradient materials. The analysis presented in [DEL09] shows that a complete isotropic second gradient constitutive theory must include five more elastic parameters in addition to the classical Lamé constants λ and μ. Such parameters account for internal lengths which are peculiar of the microstructure of the considered materials. Their value can be estimated, for any given material, e.g. by means of comparison with experimental evidence by inverse approach. This is what we will do when dealing with fibrous composite reinforcements. In particular, we will present a particularized second gradient theory, we will perform numerical simulations simulating some standard experiments and we will compare the obtained results with available experimental data. This comparison will allow the estimate of some second gradient elastic parameters for the considered materials. We will see that such parameters are, for the considered material, related to the microstructural bending stiffness of the yarns constituting the composite reinforcement.

With Eq. (4.20) the energy function in Eq. (4.15) particularizes into

$$\begin{aligned} W\left(\boldsymbol{\varepsilon}, \nabla\boldsymbol{\varepsilon}\right) = {} & \frac{1}{2}\lambda\,\varepsilon_{ii}\,\varepsilon_{ii} + \mu\,\varepsilon_{ij}\,\varepsilon_{ij} + 2c_2\,\varepsilon_{ii,j}\,\varepsilon_{jk,k} + \frac{1}{2}c_3\,\varepsilon_{ii,k}\,\varepsilon_{jj,k} + 2c_5\,\varepsilon_{ij,i}\,\varepsilon_{jk,k} \\ & + c_{11}\,\varepsilon_{ij,k}\,\varepsilon_{ij,k} + 2c_{15}\,\varepsilon_{ki,j}\,\varepsilon_{ij,k}. \end{aligned} \tag{4.21}$$

4.2.1 Positive definiteness of stored elastic energy

Always in [DEL09], the authors determine the conditions under which the strain energy function is a strictly convex function of strain and strain gradient. Thus, some relations between constitutive parameters λ, μ, c_2, c_3, c_5, c_{11} and c_{15} are establish and read

$$
\begin{aligned}
& c_{11} > 0, \\
& c_{11} > -2c_{15}, \\
& c_{15} < c_{11}, \\
& 5c_3 > 2c_{15} - 4c_{11}, \\
& c_5 > \frac{c_3\left(3c_{11} + c_{15}\right) + 2\left(c_{11}^2 - 5c_2^2 - 6c_{15}c_2 - 2c_{15}^2 + c_{11}\left(2c_2 + c_{15}\right)\right)}{4c_{15} - 10c_3 - 8c_{11}}.
\end{aligned}
\tag{4.22}
$$

Such relationships should be complemented and compared with the equivalent ones deriving imposing the convexity of the energy with respect to $\nabla\mathbf{F}$. Indeed, as shown in [DEL14] convexity with respect to this latter quantity is a suitable property in order to have a well posed problem.

Chapter 5

Modeling the onset of shear boundary layers in 2D fibrous composite reinforcements by second gradient theory

2D second gradient modeling of fibrous composites

It has been known since the pioneering works by Piola, Cosserat, Mindlin, Toupin, Eringen, Green, Rivlin and Germain that many micro-structural effects in mechanical systems can be still modeled by means of continuum theories. When needed, the displacement field must be complemented by additional kinematical descriptors, called sometimes microstructural fields. In this chapter a technologically important class of fibrous composite reinforcements is considered and their mechanical behavior is described at finite strains by means of a second gradient, hyperelastic, orthotropic continuum theory which is obtained as the limit case of a micromorphic theory. Following Mindlin and Eringen, we consider a micromorphic continuum theory based on an enriched kinematics constituted by the displacement field $\mathbf{u}$ and a second order tensor field $\boldsymbol{\psi}$ describing microscopic deformations. The governing equations in weak form are used to perform numerical simulations in which a bias extension test is reproduced. We show that second gradient energy terms allow for an effective prediction of the onset of internal shear boundary layers which are transition zones between two different shear deformation modes. The existence of these boundary layers cannot be described by a simple first gradient model and its features are related to second gradient material coefficients. The obtained numerical results, together with the available experimental evidences, allow us to estimate the order of magnitude of the introduced second gradient coefficients by inverse approach. This justifies the need of a novel measurement campaign aimed to estimate the value of the introduced second gradient parameters for a wide class of fibrous materials.

Contents

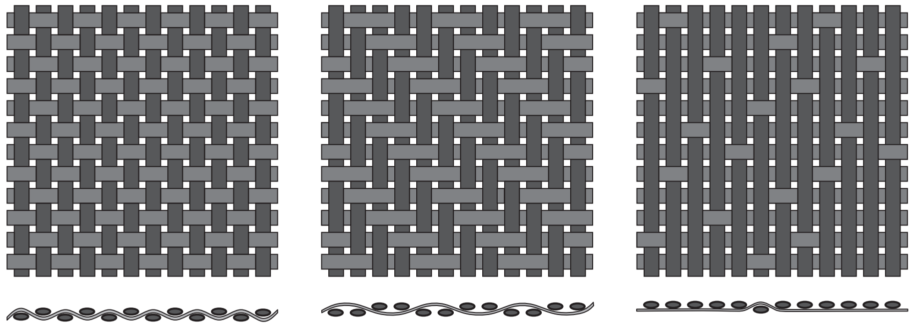

Figure 5.1: Schemes of weaving for fibrous composite reinforcements.

5.1 Introduction

In the engineering effort of designing new materials, a constant demand is directed towards the search for better performances and new functionalities. A class of materials which is gaining more and more attention is that of so-called complex materials, e.g. materials exhibiting different mechanical responses at different scales due to different scales of heterogeneity. Indeed, the overall mechanical behavior of such materials is macroscopically influenced by the underlying microstructure especially in presence of particular loading and/or boundary conditions. Therefore, understanding the mechanics of meso- and micro-structured materials is becoming a major issue in engineering.

Such materials may exhibit superior mechanical properties with respect to more commonly used engineering materials, also providing some advantages as easy formability processes. We focus in this chapter on a class of engineering materials which are known as woven fibrous composite reinforcements (see Chap. 1 for additional details) . These materials, as already remarked in chapter 1, are constituted by woven tows which are themselves made up of thousand of fibers. Different weaving schemes can be used giving rise to different types of composite reinforcements (see Fig.5.1), but in each of considered case one can assume that sharp changes in mechanical properties may occur inside the unit cell. Indeed, for the considered materials, the tensile stiffness of tows can be considered to be of many order of magnitudes higher than the shear stiffness related to angle variations between yarns. The hierarchical heterogeneity of composite reinforcements is illustrated in Fig. 5.2, in which three different scales can be recognized: the macroscopic scale (left), the mesoscopic scale (center) and the microscopic scale (right).

All materials are actually heterogeneous if one considers sufficiently small scales, but the woven composites reinforcements show their heterogeneity at scales which are significant from an engineering point of view. It is also clear that woven materials also macroscopically show strong anisotropy, since their mechanical response significantly varies if the load is applied in the direction of the fibers or in some other direction. As it will be better pointed out in the following, the introduced continuum model for composite reinforcements belongs to the class of initially orthotropic continua, i.e. continua which have two privileged directions in their undeformed configuration.

The fibrous composite preforms can be shaped and their final shape is maintained by injection and curing of a thermoset resin or by the use of a thermoplastic polymer (see chapter 1 for additional details). The final composite material commonly used in aerospace engineering is hence constituted by the fibrous composite reinforcement and the organic matrix. We are interested here only in describing the mechanical behavior of the fibrous composite reinforcements since this knowledge is fundamental for the process of formability of the final composite. Following [CHA11a, CHA12] we find convenient to model the quoted fibrous reinforcements as continuous media. This hypothesis can be considered to be realistic if no relative displacement between superimposed fibers occurs. In other words, we are assuming that two superimposed fibers can rotate around their contact point,

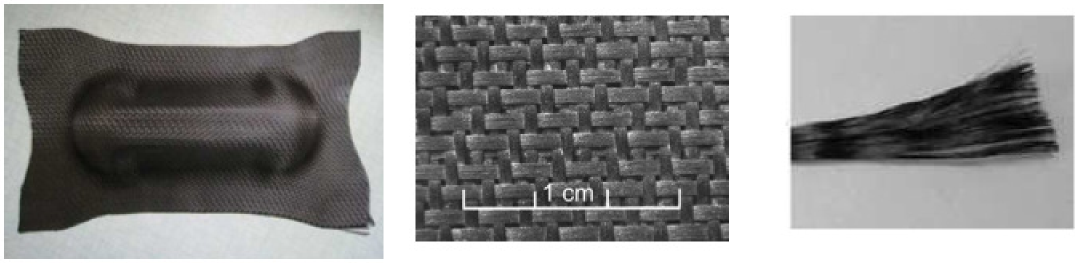

Figure 5.2: The different scales of textile composite reinforcements.

while no slipping takes place. This hypothesis is generally verified during experimental analyses, even at finite strains. In fact, when straight lines are drawn on the textile reinforcement, these lines become curved after forming but they remain continuous (see e.g. [BOI95]). As it will be better pointed out in the remainder of this chapter, the anisotropy of the considered reinforcements will be taken into account by introducing suitable hyperelastic, orthotropic constitutive laws which are able to characterize the behavior of considered materials also at large strains.

Nevertheless, a first gradient continuum orthotropic model is not able to take into account all the possible effects that the microstructure of considered materials have on their macroscopic deformation. More precisely, some particular loading conditions, associated to particular types of boundary conditions may cause some microstructure-related deformation modes which are not fully taken into account in first gradient continuum theories. This is the case, for example, when observing some regions inside the materials in which high gradients of deformation occur, concentrated in those relatively narrow regions which we will call boundary layers.

Actually, the onset of shear boundary layers can be observed in some experimental tests which are used to characterize the mechanical properties of fibrous composite reinforcements. Indeed, internal boundary layers do arise in the so-called bias extension test, the phenomenology of which we duly describe in section 5.4. One way to deal with the description of such boundary layers, while remaining in the framework of a macroscopic theory, is to consider so-called "generalized continuum theories". Such generalized theories allow for the introduction of a class of internal actions which is wider than the one which is accounted for by classical first gradient Cauchy continuum theory. These more general contact actions excite additional deformation modes which can be seen to be directly related with the properties of the microstructure of considered materials.

Indeed, it has been known since the pioneering works by Piola [PIO46], Cosserat [COS09], Midlin [MIN64], Toupin [TOU64], Eringen [ERI01], Green and Rivlin [GRE64] and Germain [GER73a, GER73b] that many microstructure-related effects in mechanical systems can be still modeled by means of continuum theories. It is known since then that, when needed, the placement function must be complemented by additional kinematical descriptors, called sometimes micro-structural fields. More recently, these generalized continuum theories have been widely developed to describe the mechanical behavior of many complex systems, such as e.g. porous media [SCI07, DEL00, SCI08, MAD08], capillary fluids [CAS72, DEG81, DEL95a, DEL96, DEL95b], exotic media obtained by homogenization of heterogeneous media [ALI03, SEP11, PID97]. Interesting applications on wave propagation in such generalized media has also gained attention in the recent years for the possible application of this kind of materials to passive control of vibrations and stealth technology (see e.g. [DEL12a, MAD12b, PLA13, ROS13]).

In this chapter, the class of fibrous composite preforms described before is considered and their macroscopic mechanical behavior (i.e. at a scale relatively larger than the yarn) is described by means of a second gradient, hyperelastic continuum theory. The quoted hyperelastic, second gradient theory is obtained as the limit case of a micromorphic theory, following what done in [BLE67, MIN64] for the linear-elastic case. The governing equations in weak form are used as a basis for the formulation of suitable numerical codes, which allow to perform simulations reproducing the so-called bias extension test. We show that second gradient energy terms allow for an effective prediction of the onset of internal shear boundary layers which can be defined as those transition zones between two different regions exhibiting different shear deformation modes. The existence and thickness of these boundary layers cannot be described by a first gradient model and its overall features are related to the particular second gradient model introduced here. The obtained numerical results seem to be in a good agreement with the already available experimental evidence and fully justify the need of a novel measurement campaign.

5.2 Micromorphic media and second gradient continua

We describe the deformation of the considered continuum by introducing a Lagrangian configuration $B_0 \subset \mathbb{R}^3$ and a suitably regular kinematical field $\boldsymbol{\chi}(\mathbf{X}, t)$ which associates to any material point $\mathbf{X} \in B_0$ its current position $\mathbf{x}$ at time t. The image of the function $\boldsymbol{\chi}$ gives, at any instant t the current shape of the body $B(t)$: this time-varying domain is usually referred to as the Eulerian configuration of the medium and, indeed, it represents the system during its deformation. Since we will use it in the following, we also introduce the displacement field $\mathbf{u}(\mathbf{X}, t) := \boldsymbol{\chi}(\mathbf{X}, t) - \mathbf{X}$, the tensor $\mathbf{F} := \nabla\boldsymbol{\chi}$ and the Right Cauchy-Green deformation tensor $\mathbf{C} := \mathbf{F}^T \cdot \mathbf{F}$ (SEE E.G. Chap. 2). The kinematics of the continuum is then enriched by adding a second order tensor field $\boldsymbol{\psi}(\mathbf{X}, t)$ which accounts for deformations associated to the microstructure of the continuum. Indeed, as it was explained e. g. by Mindlin [MIN64] and Cosserat [COS09], the addition of supplementary kinematical fields can be of help to describe the deformation of the microstructure of the considered material independently of its average continuum deformation. If, on the one hand, Cosserat's models are able to complement the classical continuum deformations with extra rotations of considered microstructure, on the other hand, micromorphic models also allow to consider micro-stretches and micro-shear deformations. In particular, the introduced micromorphic tensor $\boldsymbol{\psi}(\mathbf{X}, t)$ allows to account for all these microscopic deformation in a very general fashion. If some constraints are introduced on the tensor $\boldsymbol{\psi}$, the micromorphic model can then be particularized so as to obtain Cosserat or second gradient models as limit cases (SEE E.G. Chap. 3). In what follows, the current state of the considered medium is, in general, identified by 12 independent kinematical fields: 3 components of the displacement field and 9 components of the micro-deformation field. Such a theory of a continuum with microstructure has been derived in [MIN64] for the linear-elastic case and re-proposed e.g. in [ERI64a, ERI64b, FOR06, FOR09] for the case of non-linear elasticity. For the sake of clearness, using similar notations to [MIN64] and [BLE67], ALSO USED IN 3, we introduce the following kinematical quantities which are all functions of the basic kinematical fields introduced before

$$
\begin{aligned}
\varepsilon_{ij} &= \left(C_{ij} - \delta_{ij}\right)/2, && \text{the macro-strain,} \\
\gamma_{ij} &= \varepsilon_{ij} - \psi_{ij}, && \text{the relative(micro/macro) deformation,} \\
\kappa_{ijk} &= \psi_{ij,k}, && \text{the gradient of micro-deformation,}
\end{aligned}
\tag{5.1}
$$

where clearly C_{ij} and ψ_{ij} represent the components of the second order tensors $\mathbf{C}$ and $\boldsymbol{\psi}$ respectively. If one, for example, imposes the relative deformation to be zero (i.e. $\psi_{ij} \to \varepsilon_{ij}$), then $\kappa_{ijk} \to \varepsilon_{ij,k}$ and one recovers the standard second gradient theory presented in [GER73a, GER73b]. As it will be more clearly explained in the following, the external actions which can be introduced in the framework of a micromorphic continuum theory are more easily understandable than those intervening in second gradient theories since they have a more direct physical meaning. Since second gradient theory can be readily obtained as limit case of the micromorphic theory, one can then derive the second gradient contact actions in terms of the micromorphic ones following the procedure used in [BLE67]. We present in the following the weak formulation of a constrained micromorphic theory which will actually give rise to a particular second gradient theory. This constrained micromorphic theory is the one which we directly implement in the numerical simulations presented in this chapter.

5.2.1 Equations in weak form for a constrained micromorphic continuum

We assume that we can write the power of internal actions as the first variation of a suitable action functional $\mathcal{A}$ as follows

$$\mathcal{P}^{\text{int}} = \delta\mathcal{A} = \delta \int_{B_0} \left[W\left(\varepsilon_{ij},\ \gamma_{ij},\ \kappa_{ijk}\right) + \sum_{\alpha=1}^{n} \lambda_\alpha\, f_\alpha(\varepsilon_{ij},\ \gamma_{ij},\ \kappa_{ijk}) \right] d\mathbf{X}, \tag{5.2}$$

where W and f are real scalar-valued functions of the introduced deformation measures and, in particular, $W\left(\varepsilon_{ij},\ \gamma_{ij},\ \kappa_{ijk}\right)$ is the bulk micromorphic strain energy density, λ_α are Lagrange multipliers and f_α are particular constraints the particular form of which will be better specified later on. As it will be better explained in the sequel, this expression of the power of internal forces is the one which is necessary to describe a micromorphic continuum which is subjected to the n constraints $f_\alpha(\varepsilon_{ij},\ \gamma_{ij},\ \kappa_{ijk}) = 0$.

Considering that the independent kinematical fields appearing in (5.2) are indeed ε_{ij}, ψ_{ij} and κ_{ijk}, it can be recovered that the power of internal actions can be rewritten by computing the first variation of the action functional as

$$\begin{aligned}\mathcal{P}^{\text{int}} = \delta\mathcal{A} = \int_{B_0} \left(\frac{\partial W}{\partial \varepsilon_{ij}} + \sum_{\alpha=1}^{n} \lambda_\alpha \frac{\partial f_\alpha}{\partial \varepsilon_{ij}} \right) \delta\varepsilon_{ij} + \left(\frac{\partial W}{\partial \psi_{ij}} + \sum_{\alpha=1}^{n} \lambda_\alpha \frac{\partial f_\alpha}{\partial \psi_{ij}} \right) \delta\psi_{ij} \\ + \left(\frac{\partial W}{\partial \kappa_{ijk}} + \sum_{\alpha=1}^{n} \lambda_\alpha \frac{\partial f_\alpha}{\partial \kappa_{ijk}} \right) \delta\kappa_{ijk} + \sum_{\alpha=1}^{n} f_\alpha \delta\lambda_\alpha,\end{aligned} \tag{5.3}$$

where from now on we drop the symbol $d\mathbf{X}$ inside the integral sign and we adopt the Einstein notation of sum over repeated indices if no confusion can arise.

As for the expression of the power of external forces, we assume that they take the following general form (see also [MIN64, BLE67])

$$\mathcal{P}^{\text{ext}} = \int_{B_0} b_i^{\text{ext}} \delta u_i + \int_{B_0} \Phi_{ij}^{\text{ext}} \delta\psi_{ij} + \int_{\partial B_0} t_i^{\text{ext}} \delta u_i + \int_{\partial B_0} T_{ij}^{\text{ext}}\, \delta\psi_{ij} \tag{5.4}$$

where b_i^{ext} are volume forces, Φ_{ij}^{ext} are so called double forces per unit volume, t_i^{ext} are forces per unit area and T_{ij}^{ext} are double forces per unit area. The physical meaning of aforementioned external actions is immediate: b_i^{ext} and t_i^{ext} work on the displacement of the centroid of each Representative Elementary Volume, while Φ_{ij}^{ext} and T_{ij}^{ext} work on micro-deformations inside the considered REV. If one forces $\psi_{ij} \to \varepsilon_{ij}$, i.e. imposes the constraint $\psi_{ij} - \varepsilon_{ij} = 0$, then a more complicated form of the contact actions than those appearing in (5.4) can be derived by integration by parts. In this way, it is possible to recover the standard form for external actions of second gradient materials which work on displacement and on the normal derivatives of displacement (see e.g. [GER73a, MAD12a, SCI08, MAD08, DEL95c, DEL97, DEL12b]). Considering the surface power densities $t_i^{\text{ext}} \delta u_i$ and $T_{ij}^{\text{ext}} \delta\psi_{ij}$ appearing in expression (5.4) for the power of external actions, one can imagine to act on the boundary of considered body both by assigning the forces and/or double forces (natural boundary conditions) or by assigning the displacements and/or micro-deformation (kinematical boundary conditions).

The mechanical governing equations in weak form can be directly expressed by imposing the validity of the principle of virtual powers

$$\mathcal{P}^{\text{int}} = \mathcal{P}^{\text{ext}}, \tag{5.5}$$

where $\mathcal{P}^{\text{int}}$ and $\mathcal{P}^{\text{ext}}$ are respectively given in Eq. (5.3) and (5.4). We explicitly remark that, given the considered expression of the principle of virtual powers, we are assuming that the considered phenomena are sufficiently slow to neglect inertia. We do not explicitly write here the corresponding strong form of balance equations since we will directly implement a particularization of the weak form (5.5) in the finite element code used to perform numerical simulations.

5.3 Hyperelastic orthotropic model with micromorphic correction

In this section we specify the constitutive equations for the strain energy density $W(\varepsilon_{ij},\ \gamma_{ij},\ \kappa_{ijk})$ which we use to model the mechanical behavior of some fibrous composite reinforcements in the finite strain regime. We will equivalently use the deformation measure $\mathbf{C} = 2\boldsymbol{\varepsilon} + \mathbf{I}$ instead of $\boldsymbol{\varepsilon}$ to specify the form for the energy, i.e. $W(\varepsilon_{ij},\ \gamma_{ij},\ \kappa_{ijk}) = \tilde{W}(C_{ij},\ \gamma_{ij},\ \kappa_{ijk})$. In particular, we will assume that

$$\tilde{W}(C_{ij},\ \gamma_{ij},\ \kappa_{ijk}) = W_{\mathrm{I}}(C_{ij}) + W_{\mathrm{II}}(\kappa_{ijk}). \tag{5.6}$$

In this formula W_{I} is the first gradient strain energy and W_{II} is the energy associated to the macro-inhomogeneity of micro-deformation. We do not explicitly consider a coupling energy depending on γ_{ij}, but some coupling effects will be accounted for by introducing particular constraints $f_\alpha(\varepsilon_{ij},\ \gamma_{ij},\ \kappa_{ijk}) = 0$ in the power of internal actions by using Lagrange multipliers, as specified in Eq.(5.2).

5.3.1 Representation theorem for hyperelastic orthotropic materials

Various hyperelastic constitutive equations for an isotropic strain energy density $W^{\mathrm{iso}}(\mathbf{C})$ have been proposed in the literature which are suitable to describe the mechanical behavior of isotropic materials even at finite strains (see e.g. [OGD84, STE02]). Generalized constitutive laws are also available for linear elastic isotropic second gradient media (see [DEL09]). These constitutive equations for isotropic materials are classically derived starting from a well-known representation theorem for the strain energy potential which states that only three independent scalar invariants of the Cauchy-Green tensor $\mathbf{C}$ are sufficient to correctly represent the functional dependence of W^{iso} on $\mathbf{C}$. In other words, for an isotropic material, it is sufficient to consider that $W^{\mathrm{iso}}(\mathbf{C}) = W(i_1, i_2, i_3)$, where $i_1,\ i_2,\ i_3$ are the three scalar invariants of $\mathbf{C}$ classically defined as

$$i_1 = \mathrm{tr}(\mathbf{C}), \quad i_2 = \mathrm{tr}\left(\det(\mathbf{C})\ \mathbf{C}^{-\mathbf{T}}\right), \quad i_3 = \det(\mathbf{C}). \tag{5.7}$$

These three invariants respectively describe local deformations associated to changes of length, changes of area and changes of volume: superposition of these three deformation modes are sufficient to reproduce the global deformation of an isotropic medium. Constitutive equations for transversely isotropic materials are also well assessed in the literature (see e.g. [ITS04, BOE87, BOE78, OGD03, CHA11a, ITS00]) and their derivation relies on the classical representation theorem according to which five independent invariants of the tensor $\mathbf{C}$ are needed to characterize the behavior of such materials: $W^{\mathrm{tran}}(\mathbf{C}) = W(i_1, i_2, i_3, i_4, i_5)$. If one denotes by $\mathbf{d}_1$ the unitary vector along the preferred direction inside the transversely isotropic material in its reference (Lagrangian) configuration, then the two additional invariants appearing in the representation of W^{tran} are defined as

$$i_4 = \mathbf{d}_1 \cdot \mathbf{C} \cdot \mathbf{d}_1, \quad i_5 = \mathbf{d}_1 \cdot \mathbf{C}^2 \cdot \mathbf{d}_1. \tag{5.8}$$

These two invariants respectively describe local stretch in the direction of the preferential direction $\mathbf{d}_1$ and changes of angles mixed to changes of length.

As far as orthotropic materials are considered, clear and exploitable constitutive hyperelastic equations are harder to be found in the literature. Plenty of authors try to generalize the representation theorems valid for isotropic and transversely isotropic media, but often there is apparently not agreement between the different versions proposed for such a theorem. The more diffused version of the representation theorem for the strain energy potential for orthotropic media states that seven invariants can be used to write the functional dependence of the strain energy density (see e.g. [HOL00b, SPE84, OGD03]). More precisely, denoting by $\mathbf{d}_1$ and $\mathbf{d}_2$ two orthogonal unitary vectors along the preferred directions in the considered orthotropic material, the functional dependence of the orthotropic energy on $\mathbf{C}$ can be expressed in the form $W^{\mathrm{orth}} = W(i_1, i_2, i_3, i_4, i_5, i_6, i_7)$, where the additional two invariants are defined as

$$i_6 = \mathbf{d}_2 \cdot \mathbf{C} \cdot \mathbf{d}_2, \quad i_7 = \mathbf{d}_2 \cdot \mathbf{C}^2 \cdot \mathbf{d}_2, \tag{5.9}$$

Nevertheless, it can be proved that, indeed, only six independent scalar invariants are sufficient to completely describe the behavior of an orthotropic material (see the elegant proof given in [RAU09]), so that, even if it is effectively possible to write the strain energy as function of seven scalar invariants, it must be kept in mind that not all of them are truly independent functions of $\mathbf{C}$. In particular, following [RAU09], one can think to introduce the following set of six invariants to represent the functional dependence of W on $\mathbf{C}$:

$$i_O := \{i_1, i_4, i_6, i_8, i_9, i_{10}\}, \tag{5.10}$$

where all the invariants not previously defined are given by

$$i_8 = \mathbf{d}_1 \cdot \mathbf{C} \cdot \mathbf{d}_2, \quad i_9 = \mathbf{d}_1 \cdot \mathbf{C} \cdot \mathbf{d}_3, \quad i_{10} = \mathbf{d}_2 \cdot \mathbf{C} \cdot \mathbf{d}_3, \tag{5.11}$$

where $\mathbf{d}_3 := \mathbf{d}_1 \wedge \mathbf{d}_2$. All the invariants belonging to the set i_O correspond to simple deformation modes. In particular, in addition to the invariants already discussed before, one can remark that i_6 represents stretching in the direction $\mathbf{d}_2$, while i_8, i_9 and i_{10} represent changes of angles between the directions $(\mathbf{d}_1, \mathbf{d}_2)$, $(\mathbf{d}_1, \mathbf{d}_3)$ and $(\mathbf{d}_2, \mathbf{d}_3)$ respectively. It can be shown (see [RAU09]) that all previously introduced invariants can be written as functions of the six invariants in i_O as

$$\begin{aligned}
i_2 &= i_4 i_6 + (i_4 + i_6)\,(i_1 - (i_4 + i_6)) - i_8^2 - i_9^2 - i_{10}^2, \\
i_3 &= \left(i_4 i_6 - i_8^2\right)(i_1 - (i_4 + i_6)) + 2\; i_8 i_9 i_{10} - i_6 i_9^2 - i_4 i_{10}^2, \\
i_5 &= i_4^2 + i_8^2 + i_9^2, \\
i_7 &= i_6^2 + i_8^2 + i_{10}^2.
\end{aligned} \tag{5.12}$$

The fact of correctly identifying the maximum number of scalar invariants which are all independent functions of $\mathbf{C}$ is of fundamental importance when one wants to write the constitutive hyperelastic laws starting from the considered strain energy potential. Indeed, a hyperelastic energy is, by construction, differentiable with respect to the strain tensor $\mathbf{C}$ and, considered that all the invariants in i_O are independent functions of $\mathbf{C}$, one can obtain the second Piola-Kirchhoff stress tensor for orthotropic materials as

$$\mathbf{S} := \frac{\partial W^{\mathrm{orth}}}{\partial \boldsymbol{\varepsilon}} = 2\frac{\partial W^{\mathrm{orth}}}{\partial \mathbf{C}} = 2\sum_{k\in i_O} \frac{\partial W^{\mathrm{orth}}}{\partial i_k}\,\frac{\partial i_k}{\partial \mathbf{C}}, \tag{5.13}$$

$$W^{\mathrm{orth}}(\mathbf{C}) := W(i_1, i_4, i_6, i_8, i_9, i_{10}) \tag{5.14}$$

In [RAU09] it is also explicitly proved that a strain energy $\bar{W}(i_1, i_2, i_3, i_4, i_5, i_6, i_7)$ which is function of the seven classical invariants can also be obtained starting from the strain energy W^{orth} defined in (5.14). If we consider the functional dependence of W^{orth} on the six invariants in i_O given in (5.14) we must take into account the results found in [RAU09] where it is proven that $W(i_1, i_4, i_6, i_8, i_9, i_{10}) = \bar{W}\left(i_1, i_4, i_6, |i_8|, |i_9|, |i_{10}|, \mathrm{sgn}(i_8 i_9 i_{10})\right)$. Using this expression for the energy and replacing it in (5.13), then it is possible to prove that the constitutive law for the second Piola Kirchhoff stress tensor is given by

$$\begin{aligned}
\mathbf{S} = {} & 2\frac{\partial \bar{W}}{\partial i_1}\mathbf{I} + 2\frac{\partial \bar{W}}{\partial i_4}\mathbf{d}_1 \otimes \mathbf{d}_1 + 2\frac{\partial \bar{W}}{\partial i_6}\mathbf{d}_2 \otimes \mathbf{d}_2 + \mathrm{sgn}(i_8)\frac{\partial \bar{W}}{\partial |i_8|}(\mathbf{d}_1 \otimes \mathbf{d}_2 + \mathbf{d}_2 \otimes \mathbf{d}_1) \\
& + \mathrm{sgn}(i_9)\frac{\partial \bar{W}}{\partial |i_9|}(\mathbf{d}_1 \otimes \mathbf{d}_3 + \mathbf{d}_3 \otimes \mathbf{d}_1) + \mathrm{sgn}(i_{10})\frac{\partial \bar{W}}{\partial |i_{10}|}(\mathbf{d}_2 \otimes \mathbf{d}_3 + \mathbf{d}_3 \otimes \mathbf{d}_2).
\end{aligned} \tag{5.15}$$

This orthotropic constitutive law can be used to model the macroscopic behavior at finite strains of 3D interlocks of fibrous composite reinforcements. Fully reliable models which are able to describe the mechanical behavior of 3D composite preforms are not completely developed up to now both for the interlock reinforcements (see e.g. [CHA12]) and for the complete composite (reinforcements plus organic matrix) (see e.g. [DUM87]). For this reason, the mechanical characterization of such materials is nowadays a major scientific and technological issue. The mechanical behavior of composite preforms with rigid organic matrix (see e.g. [DUM87, OSH06, MAK10, MIK09]) is quite different from the behavior of the sole fibrous reinforcements (see e.g. [CHA12]). In [CHA12] a hyperelastic approach is presented which allows to capture the main features of 3D interlocks at finite strain. On the other hand, in [CHA12] it is also underlined that Cauchy continuum theory may not be sufficient to model a class of complex contact interactions which are related to local stiffness of the yarns and which macroscopically affect the overall deformation of interlocks. Such microstructure-related contact interactions may be taken into account by using generalized continuum theories, such as higher order or micromorphic theories. In this chapter, we will limit ourselves to the application of a hyperelastic, orthotropic, second gradient model to the case of thin fibrous composite reinforcements at finite strains, for which the third direction can easily be thought to have negligible effect on the overall behavior of the material.

5.3.2 Phenomenological choice of the potential W_{I} for thin sheets of fibrous composite reinforcements

Explicit expressions for the strain energy potential W^{orth} as function of the invariants i_O which are suitable to describe the real behavior of orthotropic elastic materials are difficult to be found in the literature. Certain constitutive models are for instance presented in [ITS04], where some polyconvex energies for orthotropic materials are proposed to describe the deformation of rubbers in uniaxial tests. Explicit anisotropic hyperelastic potentials for soft biological tissues are also proposed in [HOL00a] and reconsidered in [SCH05, BAL06] in which their polyconvex approximations are derived. Other examples of polyconvex energies for anisotropic solids are given in [STE03].

Polyconvex energies are energies automatically satisfying the Legendre-Hadamard (L-H) ellipticity condition which, in turns, guarantees material stability of considered potentials. Reliable constitutive models for the description of the real behavior of fibrous composite reinforcements at finite strains are even more difficult to be found in the literature and can be for instance recovered in [AIM09, CHA11a]. In the present chapter, we will introduce a first gradient anisotropic hyperelastic potential of the type proposed in [CHA11a, CHA12] to model the overall behavior of considered fibrous materials and we will add a second gradient term to account for the onset of some boundary layers which are observed experimentally but which cannot be described by means of a first gradient theory. We do not attempt in this manuscript to test L-H ellipticity of the chosen first gradient potential $W_{\mathrm{I}}(C_{ij})$, our major concern being that one of recovering the experimental deformed shape of some particular fibrous composite preforms. We are nevertheless aware that the used first gradient potential might not be L-H elliptic on some precise directions along which one could hence obtain material instability. We postpone these investigations to subsequent works in which we will also put in evidence how the addition of some second gradient terms in the energy potential can indeed guarantee mathematical existence of the solution.

To the sake of consistency, we recall here some steps which have been followed to derive the constitutive hyperelastic expression for the potential $W_{\mathrm{I}}(\mathbf{C})$ proposed in [CHA11a, CHA12]. We recall that the two privileged directions in the reference (or Lagrangian) configuration are identified by means of two vectors $\mathbf{d}_1$ and $\mathbf{d}_2$ which are assumed to be orthogonal and to have unitary length. For the considered fibrous composite reinforcements the two privileged directions clearly coincide with the fiber directions $\mathbf{d}_1$ and $\mathbf{d}_2$ (called warp and weft) in the undeformed configuration. For the case studied in this chapter, we focus on the modeling of specimens of fibrous composite reinforcements which are very thin in the direction $\mathbf{d}_3 = \mathbf{d}_1 \wedge \mathbf{d}_2$ and we will treat the case of thick composite reinforcements in subsequent works. The fact of considering very thin sheets of fibrous composite preforms allows us to assume that the strain energy potential is constant with respect to the invariants i_9 and i_{10}, so that the calculation to get the stress tensor $\mathbf{S}$ starting from (5.13) results to be simplified since the last two terms are automatically vanishing. We hence propose the following additive decomposition which separately accounts for the potential associated to isotropic deformation, to elongation of fibers in the two privileged directions (warp and weft) and to the variation of the shear angle among two fibers respectively

$$W_{\mathrm{I}}(\mathbf{C}) = W^{\mathrm{NH}}(\mathbf{C}) + W^{1}_{\mathrm{elong}}(\mathbf{C}) + W^{2}_{\mathrm{elong}}(\mathbf{C}) + W_{\mathrm{shear}}(\mathbf{C}). \tag{5.16}$$

The isotropic energy potential W^{NH} can be assumed to take the classical Neo-Hooke form

$$W^{\mathrm{NH}}(i_1, i_4, i_6, i_8, i_9, i_{10}) = \mu\left[(i_1 - 3) - ln\left(i_3(i_1, i_4, i_6, i_8, i_9, i_{10})\right)\right], \tag{5.17}$$

where the explicit expression of i_3 as function of the other invariants is given in the previous subsection. We remark that, in the case studied in the following, the isotropic deformations can be considered to be very small compared to the anisotropic ones, so that the stiffness coefficient μ will be considered to be very small with respect to the anisotropic material constants. As for the anisotropic energies appearing in (5.16), we now specify their explicit dependence on the invariants i_4, i_6 and i_8 following what done in [CHA12]. To do so, we first introduce the three scalar functions

$$I^{1}_{\mathrm{elong}}(i_4) = ln\left(\sqrt{i_4}\right), \qquad I^{2}_{\mathrm{elong}}(i_6) = ln\left(\sqrt{i_6}\right), \qquad I_{\mathrm{shear}}(i_4, i_6, i_8) = \frac{i_8}{\sqrt{i_4 i_6}}, \tag{5.18}$$

which clearly represent elongation measures in the two principal directions of fibers and variation of the angle between fibers. It can be checked that the function I_{shear} is indeed related to the angle variation ϕ from the reference angle between the fibers by the formula $I_{\mathrm{shear}} = \sin(\phi)$ (see e.g.[CHA11a, CHA12]). We then recall the explicit form of the three introduced potentials which has been shown to be suitable for describing physically reasonable material behavior for thin fibrous composite reinforcements (see [CHA11a, CHA12]):

$$\begin{aligned}
W^{1}_{\mathrm{elong}}(i_1) &= \begin{cases} \frac{1}{2}\mathrm{K}^{0}_{\mathrm{elong}}\left(I^{1}_{\mathrm{elong}}\right)^2 & \text{if } I^{1}_{\mathrm{elong}} \le I^{0}_{\mathrm{elong}} \\ \frac{1}{2}\mathrm{K}^{1}_{\mathrm{elong}}\left(I^{1}_{\mathrm{elong}} - I^{0}_{\mathrm{elong}}\right)^2 + \frac{1}{2}\mathrm{K}^{0}_{\mathrm{elong}} I^{1}_{\mathrm{elong}} I^{0}_{\mathrm{elong}} & \text{if } I^{1}_{\mathrm{elong}} > I^{0}_{\mathrm{elong}}, \end{cases} \\
W^{2}_{\mathrm{elong}}(i_2) &= \begin{cases} \frac{1}{2}\mathrm{K}^{0}_{\mathrm{elong}}\left(I^{2}_{\mathrm{elong}}\right)^2 & \text{if } I^{2}_{\mathrm{elong}} \le I^{0}_{\mathrm{elong}} \\ \frac{1}{2}\mathrm{K}^{1}_{\mathrm{elong}}\left(I^{2}_{\mathrm{elong}} - I^{0}_{\mathrm{elong}}\right)^2 + \frac{1}{2}\mathrm{K}^{0}_{\mathrm{elong}} I^{2}_{\mathrm{elong}} I^{0}_{\mathrm{elong}} & \text{if } I^{2}_{\mathrm{elong}} > I^{0}_{\mathrm{elong}}, \end{cases} \\
W_{\mathrm{shear}}(i_4, i_6, |i_8|) &= \begin{cases} \mathrm{K}^{12}_{\mathrm{shear}}\left(|I_{\mathrm{shear}}|\right)^2 & \text{if } |I_{\mathrm{shear}}| \le I^{0}_{\mathrm{shear}} \\ \mathrm{K}^{21}_{\mathrm{shear}}\left(1 - |I_{\mathrm{shear}}|\right)^{-p} + W^{0}_{\mathrm{shear}} & \text{if } |I_{\mathrm{shear}}| > I^{0}_{\mathrm{shear}}. \end{cases}
\end{aligned} \tag{5.19}$$

In the three proposed potentials one can notice the existence of threshold values of the three introduced scalar functions, namely I^{0}_{elong} for I^{1}_{elong} and I^{2}_{elong} and I^{0}_{shear} for I_{shear}. The threshold value for the elongation strain measures I^{0}_{elong} is due to the fact that, for small stretch of the fibers, the weft and warp yarns are undulated due to weaving. When the fibers are completely stretched, they start showing their complete tension stiffness which can indeed reach extremely high values if one considers e.g. carbon fibers. Also for the shear deformation measure a threshold value is identified (related to lateral contact between the yarns due to shearing) which discriminates between two different behaviors.

As already explained in detail, the first gradient energy given by Eqs. (5.16), (5.19) has been introduced on a phenomenological basis. The strong non-linearities and some loss of regularity of such energy make the well-posedness of elastic problems related to it difficult to prove. Actually, some new mathematical results seem to be needed in order to regularize the considered form of the energy potential. In the literature, these regularization has been proposed by the use of judicious numerical techniques: in [HAM13a, HAM13b] the functional space where looking for solutions is constrained by suitably choosing the mesh for employed finite elements. This is done in [HAM13a, HAM13b] in conformity with the indications given by the models developed e.g. in [SPE84]. Another possible method for regularizing hill-posed problems, as the one which seems to be confronted here, is to introduce an *ad hoc* regularizing parameters involving higher order derivatives or fictitious additional kinematical parameters. However, until a physical interpretation for such parameters is not reached, one cannot consider that the ill-posedness is removed: indeed, as it is obvious, there is not a unique limit of the solution when these parameters vanish. An elegant example of successful regularization, obtained by introducing in the mathematical modeling some physically relevant corrections, is given e.g. in [LAS88] where some important dissipation phenomena in strain softening are accounted for by means of suitably chosen regularizing parameters. It has to be remarked that the first remedy proposed by [HAM13a, HAM13b] determines the correct limit to be obtained when regularizing parameters vanish. In the subsequent subsection we propose a first attempt to find a regularized energy which is based on the physical concept of longer range mechanical interactions among non-adjacent unit cells of considered fibrous composite reinforcements. A validation of the regularized model proposed here is obtained by comparing the obtained numerical results with those presented in [HAM13a, HAM13b].

Mathematically speaking, micromorphic models produce boundary problems for partial differential equations which are "singular perturbations" of the boundary problems obtained in the framework of first gradient models. Therefore, the type of PDEs may change when micromorphic constitutive parameters tend to zero and, as a consequence, it could be lost the possibility of describing the onset of boundary layers. Also relevant are the phenomena of loss of stability, buckling and post-buckling phenomena which may occur in considered structures: while refraining here to attempt to model e.g. the wrinkling occurring in bias test for very high imposed displacements, we want to mention that, by using methods similar to those presented in [LUO91, LUO01, LUO05], also this modeling challenge may be confronted.

5.3.3 Some physical considerations leading to regularized micromorphic strain energy potentials

In woven reinforcements for composite materials, when the external loads are applied only at the terminal extremities of the yarns, a unit cell is deformed because of its interaction with the closest ones. The basic assumption about these interactions which leads to first gradient homogenized continua is that they are negligible when the two considered cells are not the closest adjacent ones. However, simple mechanical considerations can be heuristically developed: i) for low loads, friction among yarns introduces perfect constraints at the contact points between them and, in a first approximation[1], these constraints are internal pivots which do not interrupt continuity of single yarns, ii) the actions which are deforming one unit cell are transmitted to closer cells via these internal pivots. Therefore, jumps in elongation and in shear deformation are not allowed as it can be seen from microscopic balance considerations. More detailed models considering friction between yarns can be obtained by following e.g. the methods used in [NAD03]

We postpone to further investigations the quantitative analysis needed to identify the macroscopic constitutive parameters which we are going to introduce in terms of the microscopic properties of yarns. Suitable multi-scale methods as the one introduced in [NAD06] may be generalized to be applied to the present case. Moreover, the description of the considered system at the microscopic scale may take advantage of some of the results proposed in [ATA97, HAS96, STE92, RIN08, RIN09, RIN07a, RIN11, RIN13]. Indeed, we content ourselves here with the introduction of three

[1]When yarns experience a relative displacement of the contact points the macroscopic modeling may become very difficult to be obtained from microscopic considerations: an eventual attempt should be based on the methods used in [RIN13, RIN07b].

phenomenological parameters controlling the thickness of the shear and elongation boundary layers and the value of the introduced deformation gradients.

The micromorphic hyperelastic model which we propose here is based on a phenomenological approach: the addition of the micromorphic terms in the strain energy density as specified in Eq. (5.6) allows us to describe the existence of some regions inside the material in which high gradients of deformation occur (see also [AIF92, TRI86] for the use of gradient theories to model strain localization). The onset of such boundary layers is completely accounted for by the proposed generalized hyperelastic model and will be illustrated by numerical simulations which will be subsequently compared with experimental results.

At this point, we can finally introduce the constitutive form of the micromorphic strain energy densities which will be used to describe the onset of some boundary layers which are actually observed in experimental tests on the described thin specimens of fibrous composite reinforcements. In particular, we assume that the micromorphic term appearing in Eq.(5.6) takes the particular form

$$\begin{aligned} W_{\mathrm{II}}(\boldsymbol{\kappa}) = & \frac{1}{2}\,\alpha_1\,\left(d_i^1\,\kappa_{ijk}\,d_j^2\right)\left(d_p^1\,\kappa_{pqk}\,d_q^2\right) + \frac{1}{2}\,\alpha_2\,\left(d_i^1\,\kappa_{ijk}\,d_j^1\right)\left(d_p^1\,\kappa_{pqk}\,d_q^1\right) \\ & + \frac{1}{2}\,\alpha_3\,\left(d_i^2\,\kappa_{ijk}\,d_j^2\right)\left(d_p^2\,\kappa_{pqk}\,d_q^2\right) \end{aligned} \tag{5.20}$$

where we denoted by d_i^1 and d_j^2 the components of the vectors $\mathbf{d}_1$ and $\mathbf{d}_2$ respectively. We can then rewrite the action functional defined in (5.2) as

$$\mathcal{A} = \int_{B_0} \left(W_{\mathrm{I}}(\boldsymbol{\varepsilon}) + W_{\mathrm{II}}(\boldsymbol{\kappa}) + \sum_{\alpha=1}^{3} \lambda_\alpha\, f_\alpha(\boldsymbol{\gamma}) \right), \tag{5.21}$$

where we set $n = 3$ for the number of introduced constraints which we now suppose to depend only on the relative deformation $\boldsymbol{\gamma}$. With the considered expressions of the strain energy densities $W_{\mathrm{I}}(\boldsymbol{\varepsilon})$ and $W_{\mathrm{II}}(\boldsymbol{\kappa})$ and with the considered constraints, one can recover the particularization of the power of internal forces given in (5.3) which reads

$$\begin{aligned} \mathcal{P}^{\mathrm{int}} = \delta\mathcal{A} = & \int_{B_0} \left(\left(\frac{\partial W_{\mathrm{I}}}{\partial \varepsilon_{ij}} + \sum_{\alpha=1}^{3} \lambda_\alpha \frac{\partial f_\alpha}{\partial \gamma_{hk}} \frac{\partial \gamma_{hk}}{\partial \varepsilon_{ij}} \right) \delta\varepsilon_{ij} \right) \\ & + \int_{B_0} \left(\sum_{\alpha=1}^{3} \lambda_\alpha \frac{\partial f_\alpha}{\partial \gamma_{hk}} \frac{\partial \gamma_{hk}}{\partial \psi_{ij}}\, \delta\psi_{ij} + \frac{\partial W_{\mathrm{II}}}{\partial \kappa_{ijk}}\, \delta\kappa_{ijk} + \sum_{\alpha=1}^{3} f_\alpha \delta\lambda_\alpha \right). \end{aligned} \tag{5.22}$$

We now choose the following particular form for the constraints $f_\alpha(\boldsymbol{\gamma})$

$$f_1(\boldsymbol{\gamma}) = \mathbf{d}_1 \cdot \left(\boldsymbol{\gamma} + \frac{\mathbf{I}}{2}\right) \cdot \mathbf{d}_2, \quad f_2(\boldsymbol{\gamma}) = \mathbf{d}_1 \cdot \left(\boldsymbol{\gamma} + \frac{\mathbf{I}}{2}\right) \cdot \mathbf{d}_1, \quad f_3(\boldsymbol{\gamma}) = \mathbf{d}_2 \cdot \left(\boldsymbol{\gamma} + \frac{\mathbf{I}}{2}\right) \cdot \mathbf{d}_2. \tag{5.23}$$

In other words, recalling the definition of $\boldsymbol{\gamma}$ given in (5.1), we are imposing that particular projections of the micro-deformation tensor $\boldsymbol{\psi}$ on directions $\mathbf{d}_1$ and $\mathbf{d}_2$ actually tend to angle variations between the directions $\mathbf{d}_1$ and $\mathbf{d}_2$ and to macroscopic stretches in these two privileged directions. Other possible types of constraints could be included in the proposed micromorphic model which, for example, impose inextensibility of yarns so giving rise to so-called micropolar continua (see e.g. [ERI01, PIE09, ERE05, ALT03, ERE13]). This is not the case here, since we suppose that the yarns are very stiff in elongation, but still deformable. More particularly and as it will be better seen in the following, f_1 imposes constraints on the variation of shear angle, while f_2 and f_3 impose constraints on the elongations in the two preferred directions $\mathbf{d}_1$ and $\mathbf{d}_2$. Recalling definition (5.1) for $\boldsymbol{\gamma}$, and that the vectors $\mathbf{d}_1$ and $\mathbf{d}_2$ are constant vectors, it is possible to verify that the power of internal forces can be finally written as

$$\begin{aligned}\mathcal{P}^{\text{int}} &= \int_{B_0}\left(\frac{\partial W_{\text{I}}}{\partial \varepsilon_{ij}} + \lambda_1\, d_i^1\, d_j^2 + \lambda_2\, d_i^1\, d_j^1 + \lambda_3\, d_i^2\, d_j^2\right)\delta\varepsilon_{ij} \\ &- \int_{B_0}\left(\lambda_1 d_i^1\, d_j^2 + \lambda_2\, d_i^1\, d_j^1 + \lambda_3\, d_i^2\, d_j^2\right)\delta\psi_{ij} + \int_{B_0}\left(\frac{\partial W_{\text{II}}}{\partial \kappa_{ijk}}\,\delta\kappa_{ijk} + \sum_{\alpha=1}^{3} f_\alpha \delta\lambda_\alpha\right).\end{aligned} \tag{5.24}$$

It can be checked that, imposing the principle of virtual powers $\mathcal{P}^{\text{int}} = \mathcal{P}^{\text{ext}}$, where $\mathcal{P}^{\text{int}}$ and $\mathcal{P}^{\text{ext}}$ are respectively given by equations (5.24) and (5.4), and considering arbitrary variations $\delta\lambda_i$ one explicitly gets the constraints

$$f_1(\boldsymbol{\gamma}) = 0, \qquad f_2(\boldsymbol{\gamma}) = 0, \qquad f_3(\boldsymbol{\gamma}) = 0. \tag{5.25}$$

We explicitly remark that, recalling definitions (5.1), the constraints $f_\alpha = 0$ actually relates the micro-deformation to the macroscopic deformation as follows

$$\begin{aligned}f_1(\boldsymbol{\gamma}) &= \mathbf{d}_1\cdot\left(\boldsymbol{\gamma} + \frac{\mathbf{I}}{2}\right)\cdot\mathbf{d}_2 = \frac{1}{2}\,\mathbf{d}_1\cdot(\mathbf{C} - 2\,\boldsymbol{\psi})\cdot\mathbf{d}_2 = \frac{1}{2}\left(i_8 - \psi^1\right) = 0, \\ f_2(\boldsymbol{\gamma}) &= \mathbf{d}_1\cdot\left(\boldsymbol{\gamma} + \frac{\mathbf{I}}{2}\right)\cdot\mathbf{d}_1 = \frac{1}{2}\,\mathbf{d}_1\cdot(\mathbf{C} - 2\,\boldsymbol{\psi})\cdot\mathbf{d}_1 = \frac{1}{2}\left(i_4 - \psi^2\right) = 0, \\ f_3(\boldsymbol{\gamma}) &= \frac{1}{2}\,\mathbf{m}_2\cdot\left(\boldsymbol{\gamma} + \frac{\mathbf{I}}{2}\right)\cdot\mathbf{m}_2 = \frac{1}{2}\,\mathbf{m}_2\cdot(\mathbf{C} - 2\,\boldsymbol{\psi})\cdot\mathbf{m}_2 = \frac{1}{2}\left(i_6 - \psi^3\right) = 0\end{aligned} \tag{5.26}$$

where we set $\psi^1 := 2\,\mathbf{d}_1\cdot\boldsymbol{\psi}\cdot\mathbf{d}_2$, $\psi^2 := 2\,\mathbf{d}_1\cdot\boldsymbol{\psi}\cdot\mathbf{d}_1$, $\psi^3 := 2\,\mathbf{d}_2\cdot\boldsymbol{\psi}\cdot\mathbf{d}_2$. If we now consider the constitutive expression for W_{II} given in Eq. (5.20), recalling that $\mathbf{d}_1$ and $\mathbf{d}_2$ are constant vectors and that $\kappa_{ijk} = \psi_{ij,k}$, equation (5.24) reduces to

$$\begin{aligned}\mathcal{P}^{\text{int}} &= \int_{B_0}\left(\frac{\partial W_{\text{I}}}{\partial \varepsilon_{ij}} + \lambda_1\, d_i^1\, d_j^2 + \lambda_2\, d_i^1\, d_j^1 + \lambda_3\, d_i^2\, d_j^2\right)\delta\varepsilon_{ij} \\ &- \int_{B_0}\left(\lambda_1\, d_i^1\, d_j^2 + \lambda_2\, d_i^1\, d_j^1 + \lambda_3\, d_i^2\, d_j^2\right)\delta\psi_{ij} \\ &+ \int_{B_0}\left(\frac{\alpha_1}{2}\, d_i^1\, d_j^2 \psi^1_{,k} + \frac{\alpha_2}{2}\, d_i^1\, d_j^1 \psi^2_{,k} + \frac{\alpha_3}{2}\, d_i^2\, d_j^2 \psi^3_{,k}\right)\delta\psi_{ij,k},\end{aligned} \tag{5.27}$$

together with the constraints $\psi^1 = i_8$, $\psi^2 = i_4$, $\psi^3 = i_6$. Recalling that $\mathbf{d}_1$ and $\mathbf{d}_2$ are constant vectors, we can write

$$\begin{aligned}m_i^1\, m_j^2\,\delta\psi_{ij} &= \delta(m_i^1\, m_j^2\,\psi_{ij}) = \frac{1}{2}\,\delta\psi^1, \\ m_i^1\, m_j^2\,\delta\psi_{ij,k} &= \delta\left(m_i^1\, m_j^2\,\psi_{ij,k}\right) = \delta\left(m_i^1\, m_j^2\,\psi_{ij}\right)_{,k} = \frac{1}{2}\delta(\psi^1_{,k}),\end{aligned} \tag{5.28}$$

and analogously

$$\begin{aligned}d_i^1\, d_j^1\,\delta\psi_{ij} &= \frac{1}{2}\,\delta\psi^2 \\ d_i^2\, d_j^2\,\delta\psi_{ij} &= \frac{1}{2}\,\delta\psi^3 \\ d_i^1\, d_j^1\,\delta\psi_{ij,k} &= \frac{1}{2}\delta(\psi^2_{,k}) \\ d_i^2\, d_j^2\,\delta\psi_{ij,k} &= \frac{1}{2}\delta(\psi^3_{,k})\end{aligned} \tag{5.29}$$

so that the power of internal forces, written in terms of the strain tensor $\mathbf{C}$, finally simplifies into

$$\begin{aligned}\mathcal{P}^{\text{int}} = & \int_{B_0} \left(\frac{\partial W_{\text{I}}}{\partial C_{ij}} + \tilde{\lambda}_1 \, d_i^1 \, d_j^2 + \tilde{\lambda}_2 \, d_i^1 \, d_j^1 + \tilde{\lambda}_3 \, d_i^2 \, d_j^2 \right) \delta C_{ij} - \int_{B_0} \sum_{i=1}^{3} \tilde{\lambda}_i \, \delta\psi^i \\ & + \int_{B_0} \sum_{i=1}^{3} \tilde{\alpha}_i \, \psi^i_{,k} \, \delta(\psi^i_{,k}),\end{aligned} \tag{5.30}$$

where we set $\tilde{\lambda}_i := \lambda/2$ and $\tilde{\alpha}_i := \alpha/4$. As for the power of external forces given in Eq. (5.4), we neglect body actions setting $b_i^{\text{ext}} = 0$ and $\Phi_{ij}^{\text{ext}} = 0$, and we also set $T_{ij}^{\text{ext}} = 2\tilde{\beta}_1^{\text{ext}} \, d_i^1 \, d_j^2 + 2\tilde{\beta}_2^{\text{ext}} \, d_i^1 \, d_j^1 + 2\tilde{\beta}_3^{\text{ext}} \, d_i^2 \, d_j^2$, so that the principle of virtual powers $\mathcal{P}^{\text{int}} = \mathcal{P}^{\text{ext}}$ finally implies

$$\begin{aligned}& \int_{B_0} \left(\frac{\partial W_{\text{I}}}{\partial C_{ij}} + \tilde{\lambda}_1 \, d_i^1 \, d_j^2 + \tilde{\lambda}_2 \, d_i^1 \, d_j^1 + \tilde{\lambda}_3 \, d_i^2 \, d_j^2 \right) \delta C_{ij} \\ & \qquad - \int_{B_0} \sum_{i=1}^{3} \tilde{\lambda}_i \delta\psi^i + \int_{B_0} \sum_{i=1}^{3} \tilde{\alpha}_i \, \psi^i_{,k} \, \delta(\psi^i_{,k}) = \int_{\partial B_0} t_i^{ext} \delta u_i + \int_{\partial B_0} \sum_{i=1}^{3} \tilde{\beta}_i^{ext} \, \delta\psi^i,\end{aligned} \tag{5.31}$$

together with the constraints $\psi^1 = i_8$, $\psi^2 = i_4$ and $\psi^3 = i_6$. We remark that the considered expression for the external double forces, actually allows to consider external actions which expend power on shear angle variations and on fiber elongation. In this way, one has the possibility to act on the boundary of considered material assigning force or displacement, shear double force or shear angle variation and also elongation double force or fiber elongation.

We finally want to explicitly remark that Eq. (5.31) actually represents a very particular case of second gradient theory. In fact, using the constraints $\psi^1 = i_8$, $\psi^2 = i_4$ and $\psi^3 = i_6$ one gets

$$\begin{aligned}&\delta\psi^1 = \delta i_8 = d_i^1 \, d_j^2 \, \delta C_{ij}, && \delta\psi^2 = \delta i_4 = d_i^1 \, d_j^1 \, \delta C_{ij}, && \delta\psi^3 = \delta i_6 = d_i^2 \, d_j^2 \, \delta C_{ij}, \\ &\delta(\psi^1_{,k}) = \delta(i_8)_{,k} = d_i^1 \, d_j^2 \, \delta C_{ij,k}, && \delta(\psi^2_{,k}) = \delta(i_4)_{,k} = d_i^1 \, d_j^1 \, \delta C_{ij,k}, && \delta(\psi^3_{,k}) = \delta(i_6)_{,k} = d_i^2 \, d_j^2 \, \delta C_{ij,k},\end{aligned} \tag{5.32}$$

so that Eq. (5.31) is also equivalent to

$$\begin{aligned}& \int_{B_0} \left[\frac{\partial W_{\text{I}}}{\partial C_{ij}} \, \delta C_{ij} + \left(\tilde{\alpha}_1 \, \left(d_p^1 \, d_q^2 \, C_{pq,k} \right) \, d_i^1 \, d_j^2 + \tilde{\alpha}_2 \, \left(d_p^1 \, d_q^1 \, C_{pq,k} \right) \, d_i^1 \, d_j^1 + \tilde{\alpha}_3 \, \left(d_p^2 \, d_q^2 \, C_{pq,k} \right) \, d_i^2 \, d_j^2 \right) \, \delta C_{ij,k} \right] \\ & \qquad = \int_{\partial B_0} t_i^{\text{ext}} \delta u_i + \int_{\partial B_0} \left(\tilde{\beta}_1^{\text{ext}} \, d_i^1 \, d_j^2 + \tilde{\beta}_2^{\text{ext}} \, d_i^1 \, d_j^1 + \tilde{\beta}_3^{\text{ext}} \, d_i^2 \, d_j^2 \right) \, \delta C_{ij}\end{aligned} \tag{5.33}$$

We have hence explicitly recovered a special second gradient theory starting from the proposed constrained micromorphic model. Nevertheless, in our numerical simulations, instead of using the second gradient weak form (5.33), we use the constrained micromorphic one (5.31). The advantage of using the micromorphic approach instead of directly using a second gradient theory is that the boundary conditions which can be imposed are, in the present case, more easily understandable from a physical point of view. In particular, we remark that, for example, under the constraints $\psi^1 = i_8$, the fact of imposing $\psi^1 = 0$ on the boundary means that we are imposing zero variation of the angle between the fibers. Analogously, under the constraints $\psi^2 = i_4$ and $\psi^3 = i_6$, imposing $\psi^2 = 1$ and $\psi^3 = 1$ is equivalent to prevent elongation in the preferred directions $\mathbf{d}_1$ and $\mathbf{d}_2$. We therefore end up with a model in which it is possible to impose, at the boundary of considered system, both the displacement field and the deformation fields measuring variation of the angle between fibers and elongations along the two preferred directions. The generalized theory proposed in this chapter becomes essential for describing deformation patterns in which high gradients of deformation occur in relatively narrow regions of the material. This is the case for the deformation patterns which will be described in the next section.

5.4 Phenomenology of the bias extension test

The bias extension test is a mechanical test which is very well known in the field of composite materials manufacturing (see e.g. [CAO08, HAR04, PEN13]). It is widely used to characterize the mechanical behavior of woven-fabric fibrous composite preforms undergoing large shear deformations. Such fibrous materials have attracted significant attention from both industry and academia, due to their high specific strength and stiffness as well as their excellent formability characteristics. These materials are widely being used in the aerospace industry since they provide a suitable compromise between high mechanical performances, light weight and easy shaping. The bias extension test is performed on rectangular samples of woven composite reinforcements, with the height (in the loading direction) relatively greater (at least twice) than the width, and the yarns initially oriented at $\pm$ 45-degrees with respect to the loading direction. The specimen is clamped at two ends, one of which is maintained fixed and the second one is displaced of a given amount. The relative displacement of the two ends of the specimen provokes angle variations between the warp and weft: the creation of three different regions A, B and C, in which the shear angle between fibers remains almost constant after deformation, can be detected (see Fig. 5.3). In particular, the fibers in regions C remain undeformed, i.e. the angle between fibers remains at 45° also after deformation. On the other hand, the angle between fibers becomes much smaller than 45° in regions A and B, but it keeps almost constant in each of them.

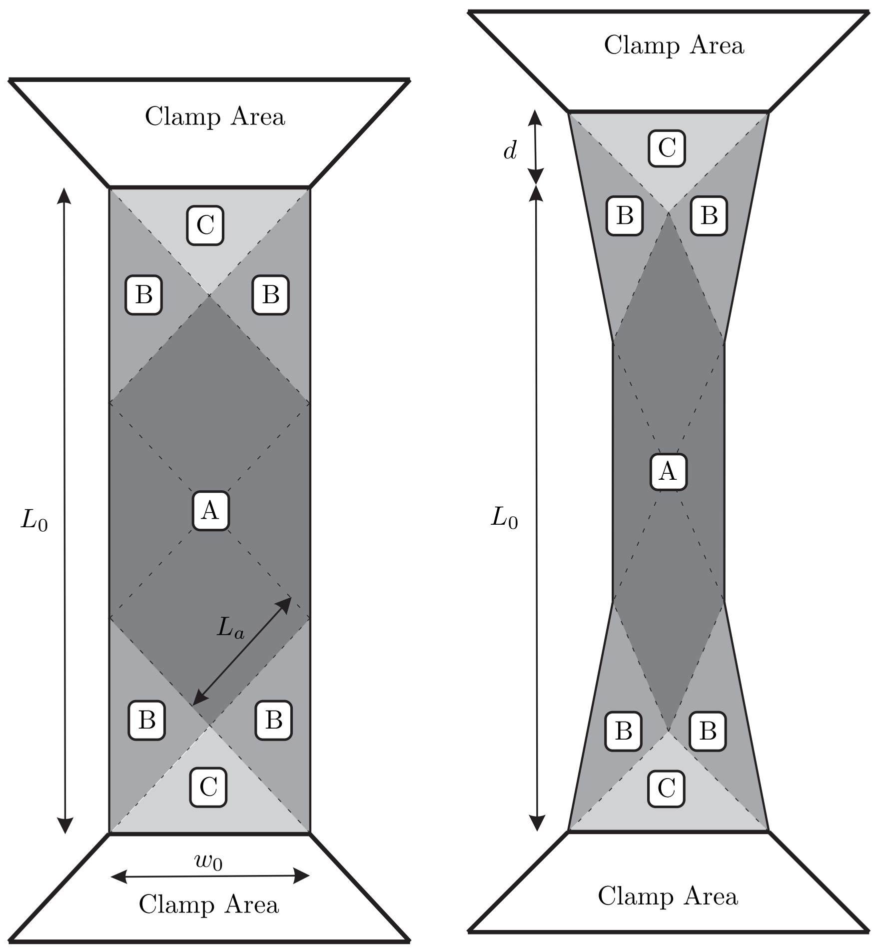

Figure 5.3: Simplified description of the deformation pattern in the bias extension test.

The main characteristics of the bias extension test are summarized in Fig. 5.3 in which both the undeformed and deformed shapes of the considered specimen are depicted. The specimen is clamped

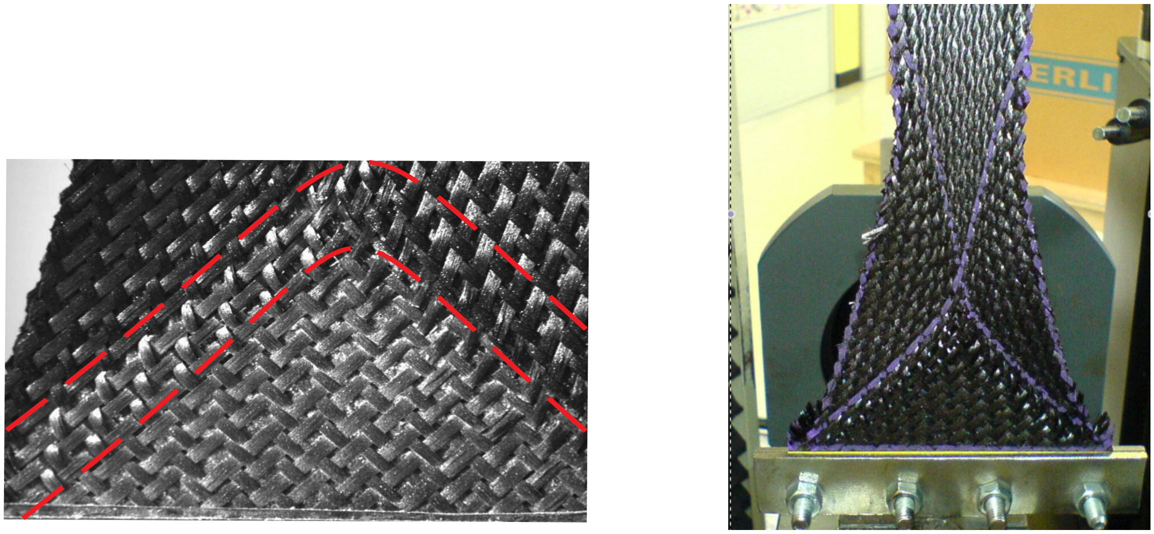

Figure 5.4: Boundary layers between two regions at constant shear (left) and curvature of the free boundary (right).

at its two ends using specific tools which impose the following boundary conditions:

- vanishing displacement at the bottom of the specimen,
- assigned displacement at the top of the specimen
- fixed angle between the fibers (45°) at both the top and the bottom of the specimen.
- vanishing elongation of the fibers at both the top and the bottom of the specimen.

It is clear that the third type of boundary condition which imposes that the angle between fibers cannot vary during deformation of the specimen is a boundary condition which, at the level of a macro model, imposes deformation and not displacement. The same is for the fourth type of boundary conditions blocking elongation of fibers. Boundary conditions of this type cannot be accounted for in a first gradient theory, while they can be naturally included in a second gradient one, as duly explained in the previous section.

Moreover, the deformation scheme described in Fig. 5.3 does not take into account some specificity of the deformations which are actually observed during a bias extension test. In particular, the following two experimental evidences are not included in the scheme presented in the quoted figure:

- the presence of transition layers between two adjacent zones with constant shear deformation
- the more or less pronounced curvature of the free boundaries of the specimen.

Indeed, both these evidences can be observed in almost any bias extension test on woven composite preforms, as it is shown in Fig. 5.4.

A set of bias tests run on specimens under identical circumstances have produced some suggestive results which were gathered in a picture of [CAO08] which we reproduce here in Fig. 5.5. In this figure the contour of the shear angle variation between yarns is depicted as the result of some optical measurements conducted at INSA-Lyon. Unfortunately, the yarns constituting the considered reinforcements have a very high extensional rigidity and, as a consequence, the thickness of the corresponding elongation boundary layers is relatively smaller. Hence, in order to obtain similar results for the elongation boundary layers, suitably targeted measurement campaigns should be conceived.

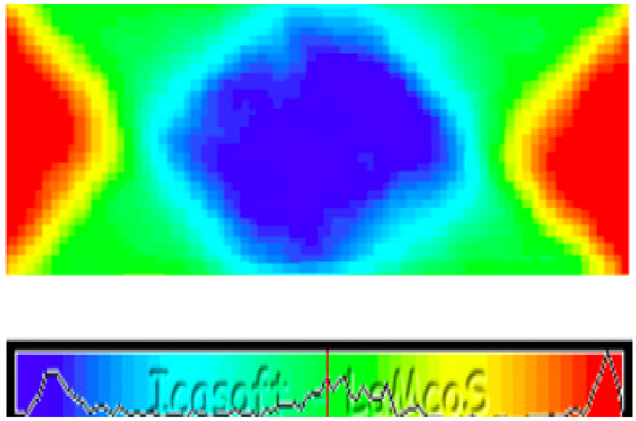

Figure 5.5: Contour of shear angle in a bias-extension test obtained from the optical measurement software Icasoft (INSA-Lyon).

Table 5.1: Constitutive first gradient coefficients used in the numerical simulations.

$\mathrm{K}^0_{\text{elong}}$	$\mathrm{K}^1_{\text{elong}}$	I^0_{elong}	$\mathrm{K}^{12}_{\text{shear}}$	$\mathrm{K}^{21}_{\text{shear}}$	p	W^0_{shear}	I^0_{shear}
[MPa]	[MPa]	[−]	[MPa]	[MPa]		[MPa]	[−]
37.85	816.33	1.45×10^{-2}	0.07575	1.69×10^{-4}	3.69	-1.69×10^{-4}	4.20×10^{-3}

The principle of virtual powers for constrained micromorphic media formulated in Eq. (5.31) allows for the description of the onset of thin boundary layers in which high gradients of shear deformation occur and which allow for a gradual transition from one value of the shear angle to the other one. The onset of these boundary layers cannot be accounted for by a first gradient theory, while it can be described by adding a dependence of the energy density on gradients of the shear deformation. Curvature effects will be also pointed out in the results obtained in the performed numerical simulations and which will be shown in the next section.

5.5 Numerical simulations

We now propose to apply the introduced second gradient model to perform numerical simulations of the bias extension test which take into account the onset of shear boundary layers. We consider a rectangular specimen of 100 mm of width of and 300 mm of height in the undeformed configuration. The fibers are at ±45° with respect to the direction of the height of the specimen in the undeformed configuration. To perform the numerical simulations we choose a fixed orthonormal basis such that, the components of the two structural vectors introduced before are $\mathbf{d}_1 = \left(\sqrt{2}/2, \sqrt{2}/2, 0\right)^T$ and $\mathbf{d}_2 = \left(\sqrt{2}/2, -\sqrt{2}/2, 0\right)^T$ and we impose at the top of the specimen a vertical displacement $d = 55$ mm. Clearly, also the deformation tensor $\mathbf{C}$ and all its introduced invariants can be accordingly written in the chosen basis. We summarize in Tab. 5.1 the values of the first gradient constitutive parameters appearing in the orthotropic hyperelastic potential (5.19) which are used to perform the numerical simulations presented in this section.

These values have been proposed in [CHA12] as the result of specific measurement campaigns.

5.5.1 First gradient limit solution

As discussed in detail by [HAM13a, HAM13b], first gradient energies, in which the physical phenomena governing the onset of boundary layers are neglected, actually produce mesh-dependent numerical simulations. To remedy to this circumstance, [SPE84] suggested some techniques whose numerical counterpart has been developed in [HAM13a, HAM13b] for considered case: following the ideas there exposed we could get numerical simulations in which boundary layers reduce to lines and deformation measures are subjected to jumps.

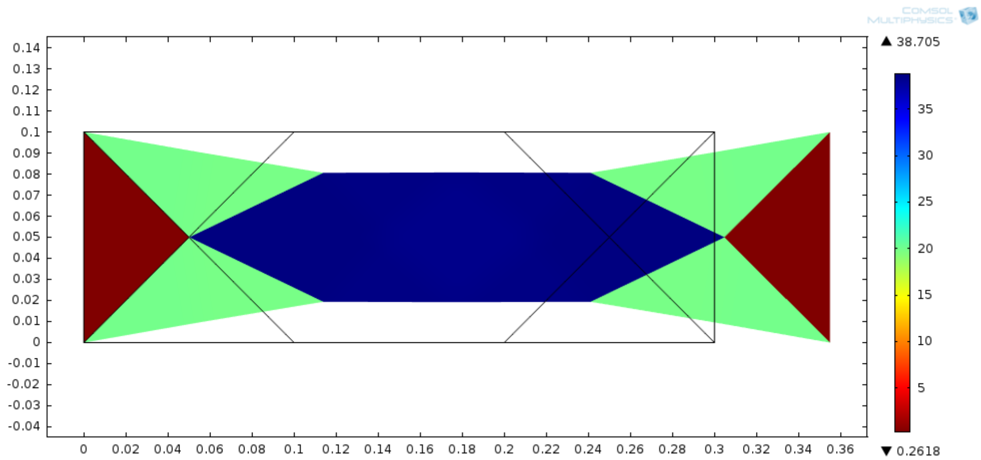

Figure 5.6: Shear angle variation ϕ for an imposed displacement $d = 55$ mm obtained with the first gradient theory. The lateral bar indicates the values of ϕ in degrees.

We show the result of one of these numerical simulations in Fig. 5.6. This picture represents the shear deformation field which is the correct limit to which regularized models must converge when higher gradient parameters tend to zero. In particular, figure 5.6 shows the shear angle variation ϕ which is obtained as solution of the first gradient equilibrium problem resulting from (5.31) by setting $\tilde{\alpha}_1 = \tilde{\alpha}_2 = \tilde{\alpha}_3 = 0$ and $\tilde{\beta}_1^{\text{ext}} = \tilde{\beta}_2^{\text{ext}} = \tilde{\beta}_3^{\text{ext}} = 0$. The boundary conditions which have been used to solve the first gradient equilibrium problem are

- Vanishing displacement on the left surface: $\delta u_i = 0,\ i = \{1, 2\}$,
- Assigned displacement on the right surface: $\delta u_1 = 55\,\text{mm},\ \delta u_2 = 0$,
- Unloaded lateral (top and bottom) surfaces (i.e. $t_i^{\text{ext}} = 0,\ i = \{1, 2\}$).

As it can be seen, the three zones A, B and C defined in Fig. 5.3 can be identified in the solution shown in Fig. 5.6: the red zones (corresponding to zones C) are such that no angle variation occurs with respect to the reference configuration ($\phi = 0$). On the other hand, the green and the blue zones respectively correspond to regions B and A and are such that two different constant angle variations ($\phi_B \approx \phi_A/2 \neq 0$) with respect to the reference configuration occur. The first gradient solution is such that a sharp interface between each pair of the three shear regions can be observed.

5.5.2 Second gradient solution and the onset of boundary layers

For what concerns the solution which we have obtained by means of the introduced second gradient model, we start by heuristically choose the values of the second gradient parameters by using an inverse method based on physical observations. However, further investigations are needed to establish a theoretical relationship between the microscopic structure of considered reinforcements and the macroscopic parameters here introduced: it is indeed well known (see e.g. [CAS72, DEG81, DEL95a, FOR10]) that the second gradient parameters are intrinsically related to a characteristic length L_c which is, in turn, associated to the micro-structural properties of considered materials. It is also known that many identification methods have been introduced to relate the macroscopic second gradient parameter to the microscopic properties of the considered medium. Some of these methods are presented in [ALI03, SEP11]. Calling L_c the measured thickness of the shear boundary layer highlighted in Fig. 5.4, we tune the value of the second gradient parameters $\tilde{\alpha}_i,\ i = \{1, 2, 3\}$ in our numerical simulations until we obtain a boundary layer having the same thickness L_c. In particular, for a characteristic length $L_c \approx 2$ cm, we obtain, by inverse approach, the following values of the shear and elongation second gradient parameters respectively

$$\tilde{\alpha}_1 = 3 \times 10^{-5}\ \text{MPa m}^2, \quad \tilde{\alpha}_2 = \tilde{\alpha}_3 = 9 \times 10^{-3}\ \text{MPa m}^2. \tag{5.34}$$

The second gradient solution for the shear angle variation ϕ, obtained for the aforementioned values of the second gradient parameters, is shown in Fig. 5.7. For obtaining this solution, Eq. (5.31) was solved with the following additional boundary conditions

- Zero angle variation at the clamped ends of the specimen: $\psi^1 = i_8 = 0$,
- Zero elongation of the fibers at the clamped ends of the specimen: $\psi^2 = i_4 = 1$, $\psi^3 = i_6 = 1$.
- Boundaries on the lateral (top and bottom) surfaces free from micromorphic loads: $\tilde{\beta}_i^{\text{ext}} = 0,\ i = \{1, 2\}$.

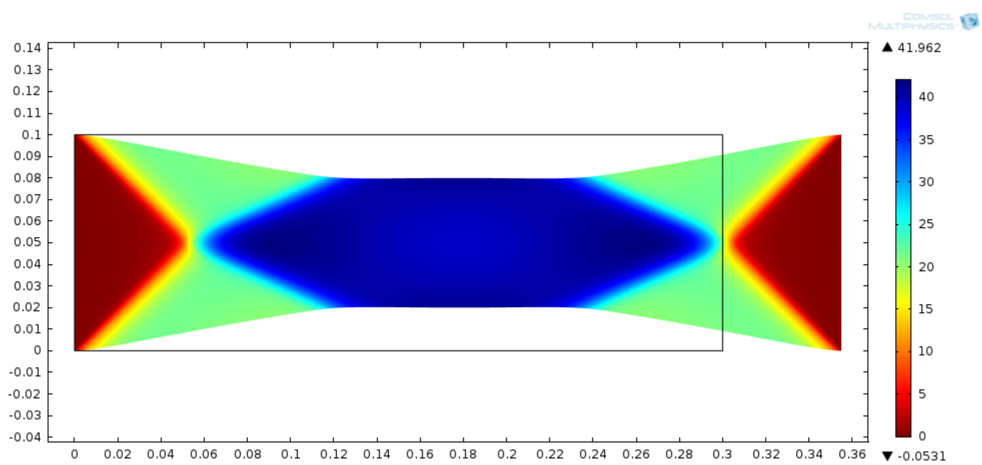

Figure 5.7: Shear angle variation ϕ for an imposed displacement $d = 55\ mm$ obtained with the proposed second gradient theory. The lateral bar indicates the values of ϕ in degrees

It can be noticed that in the second gradient solution shown in Fig. 5.7 the transition zones between different shear regions are regularized and shear boundary layers can be clearly observed, as well as a curvature of the free boundaries on the two free sides. It can be immediately remarked how the solution shown in Fig. 5.7 is, at least qualitatively, very close to the experimental picture shown in Fig.5.5.

We show in Fig. 5.8 the first and second gradient solutions for the shear angle variation along the sections I and II.

It can be clearly seen that, along section I, the first gradient solution (dashed line) produces a sharp variation of the shear angle across the two regions C and B. On the other hand, the second gradient solution (continuous line) clearly regularizes the transition between the zone at zero variation of the shear angle and the adjacent zone. The same arrives in section II, which spans on the whole specimen, in which the transition zones are clearly regularized by the second gradient solution.

In Fig. (5.9) we show the effect of the variation of the shear second gradient parameter $\tilde{\alpha}_1$ on the solution for the shear angle variation ϕ along the sections I and II respectively. It can be seen that

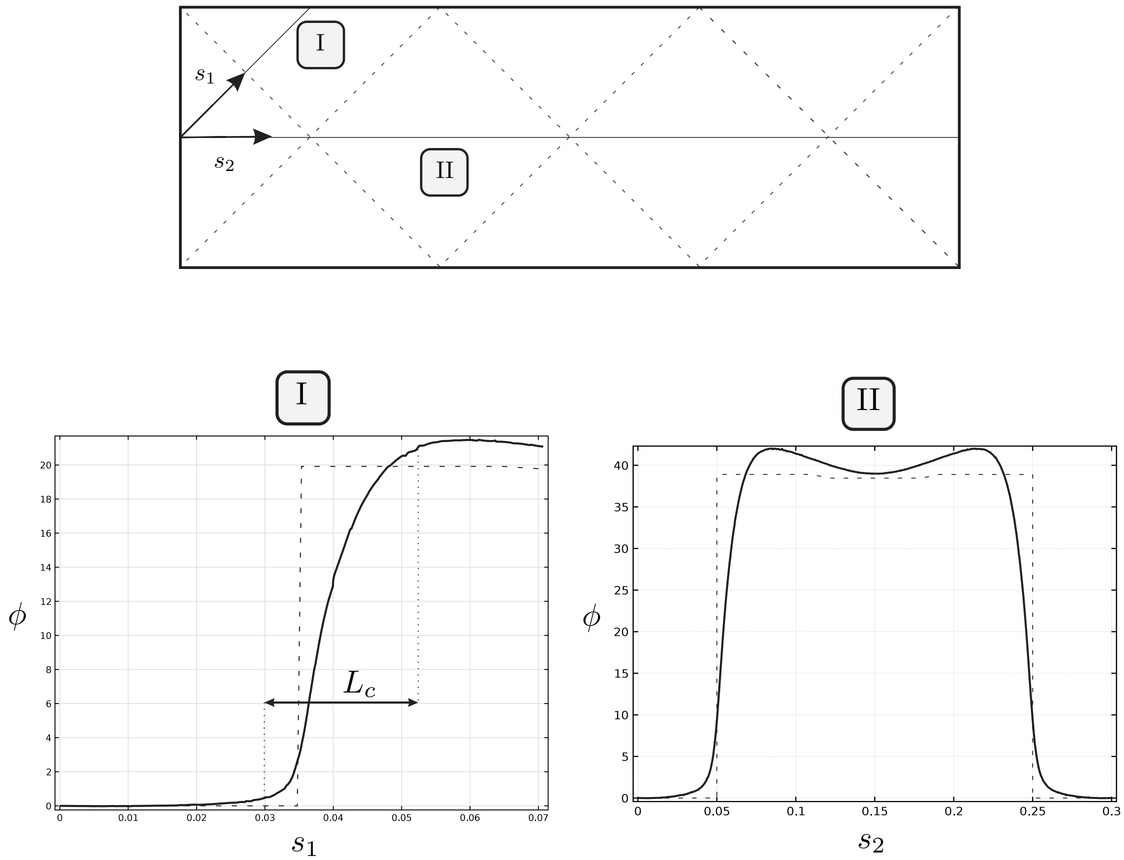

Figure 5.8: Definition of the sections I and II (top) and shear angle variation ϕ for the two sections I and II both for first gradient (dashed line) and second gradient (continuous line).

the effect of increasing the shear second gradient parameter actually lower the value of the shear angle variation so producing more regular transitions from the two regions at different constant shear. This clearly results in an increasing of the characteristic size of the shear boundary layer. It can be also noticed that the value of ϕ increases with $\tilde{\alpha}_1$ in the center of the specimen. We can conclude that the choice of the shear second gradient parameter $\tilde{\alpha}_1$ is directly related to the fact of fixing the thickness of the shear boundary layer. This parameter can be hence easily tuned on the basis of experimental evidences. In the presented numerical simulations, we tuned the shear second gradient parameter $\tilde{\alpha}_1$ in order to have a boundary layer of thickness $L_c \approx 2$ cm, so obtaining the quoted value $\tilde{\alpha}_1 = 3 \times 10^{-5}\,\mathrm{MPa\,m^2}$.

As for the choice of the second gradient elongation parameters, the identification procedure is less direct than that one used for identifying the shear parameter $\tilde{\alpha}_1$. First of all, due to symmetry of material properties in the directions of weft and warp, we set *a priori* that $\tilde{\alpha}_2 = \tilde{\alpha}_3$. Unfortunately, due to the very high tensile stiffness of the yarns, experimental measurements of elongation boundary layers in the fiber directions are not available, as it was instead the case for shear boundary layers (see Fig. 5.5). The precise tuning procedure which allows us to fit the second gradient elongation parameters to experimental measures of elongation boundary layers is henceforth not possible at this stage. Therefore, the value of the parameters $\tilde{\alpha}_2$ and $\tilde{\alpha}_3$ was tuned after performing the parametric study shown in Fig. 5.10 in which the effect of the variation of the second gradient elongation parameter on the value of the shear angle is shown. It can be remarked from this picture that increasing the value of the second gradient elongation parameter results in an overall increase of the shear angle variation ϕ. The value of $\tilde{\alpha}_2$ which gives, in the center of the specimen, the same value of ϕ obtained for the limit first gradient solution shown in Fig. 5.6 was chosen, so resulting in the

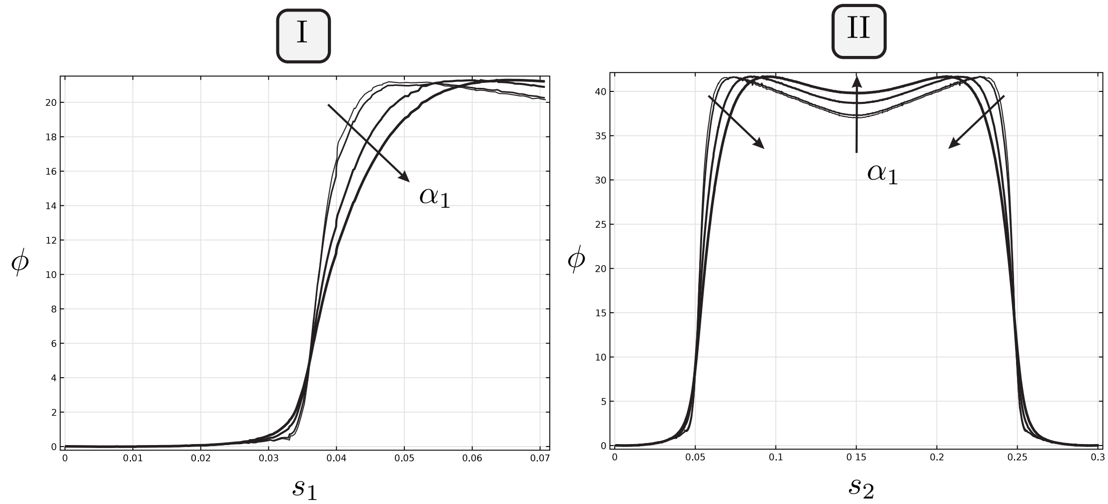

Figure 5.9: Parametric study on the shear second gradient parameter $\tilde{\alpha}_1 \in [7 \times 10^{-6}, 6 \times 10^{-5}]$ $\mathrm{MPa\,m^2}$, taking fixed $\tilde{\alpha}_2 = \tilde{\alpha}_3 = 9 \times 10^{-3}$ $\mathrm{MPa\,m^2}$.

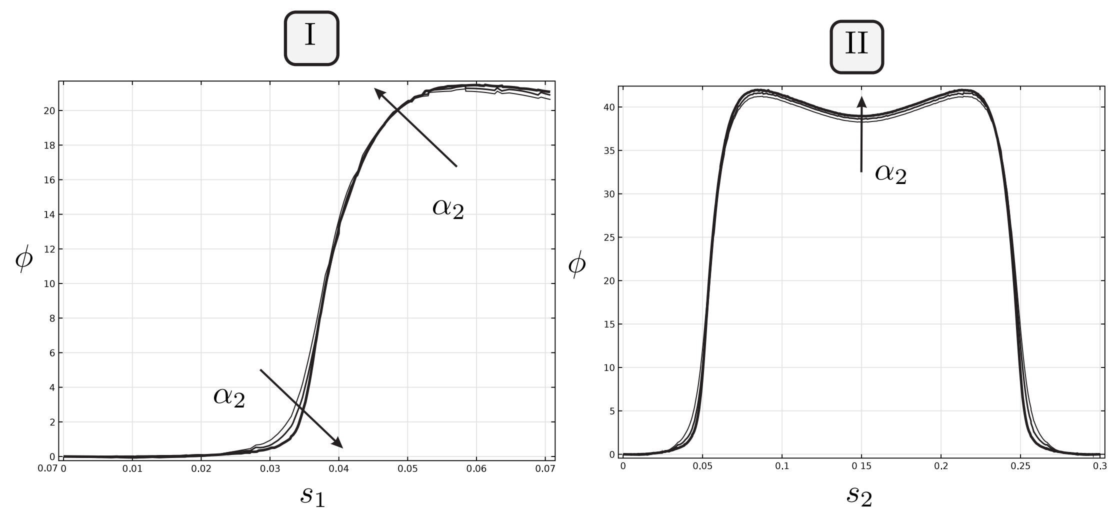

Figure 5.10: Parametric study on the elongation second gradient parameter $\tilde{\alpha}_2 = \tilde{\alpha}_3 \in [3 \times 10^{-3}, 9 \times 10^{-3}]$ $\mathrm{MPa\,m^2}$, taking fixed $\tilde{\alpha}_1 = 3 \times 10^{-5}$ $\mathrm{MPa\,m^2}$.

value $\tilde{\alpha}_2 = 9 \times 10^{-3}$ $\mathrm{MPa\,m^2}$. We obtained, in the performed numerical simulations, an elongation field which is everywhere very small: the maximum value of elongation is of the order of 10^{-3}. We show in figures 5.11 the elongation boundary layers (each corresponding to the elongation in one of the two preferred directions of the fibers) obtained in the performed numerical simulations. In order to precisely reveal the nature of these elongation boundary layers suitable experimental campaigns as well as adapted microscopic models should be developed together with suitable micro-macro identification techniques.

5.5.3 By using first gradient models it is not possible to correctly describe the onset of boundary layers

One could wonder if it is really necessary to introduce micromorphic continuum models to carefully describe the onset of boundary layers in bias tests. In the present subsection we discuss some difficulties which arise if one tries to use the methods discussed in section 5.1. Actually, as shown by Fig. 5.12, although it is indeed possible to describe the onset of some boundary layers still

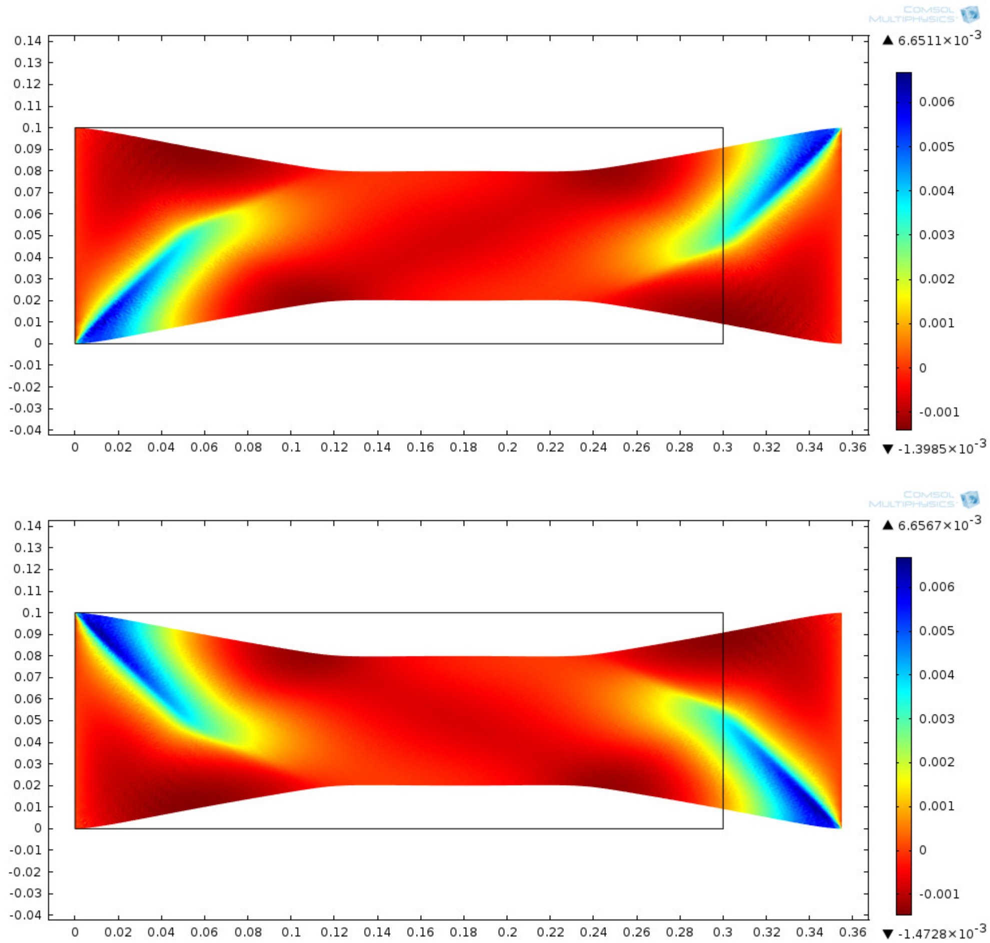

Figure 5.11: Elongations in the direction $+45°$ (top figure) and $-45°$ (bottom figure).

remaining in the framework of first gradient models, it seems very unlikely that with those methods one can catch all experimental features which are present in bias extension tests. In the numerical simulations leading to Fig. 5.12 one can see formation of boundary layers where high gradients of shear and elongation are concentrated even if this simulation is conducted in the framework of first gradient theory. However, the solution is qualitatively and quantitatively different from the first gradient sharp solution shown in Fig. 5.6 so that realistic quantitative values for shear deformations cannot be obtained from it.

Moreover, if one evaluates the reaction force on the fixed clamped end in the last considered case, it can be checked that its value exceeds of a big amount the reaction force which is expected. More particularly, the force evaluated for the limit first gradient solution depicted in Fig. 5.6 is of the order of 5 N which is a sensible force for the bias extension test. On the other hand, if one evaluates the force for the case depicted in Fig. 5.12, this force exceeds from 10 to 100 times the 5 N obtained in the limit sharp first gradient solution, depending on the choice of the mesh. This means that the mesh dependence of the first gradient solution is even more evident when analyzing force than when analyzing deformation. Such a problem on the value of calculated force is not present when considering the second gradient solution shown in Fig. 5.7. This point allows us to conclude that, using first gradient models, it is not possible to correctly describe the onset of boundary layers and that the reaction forces at clamped ends are definitely overestimated as soon as one gets far from the limit first gradient solution shown in Fig. 5.6.

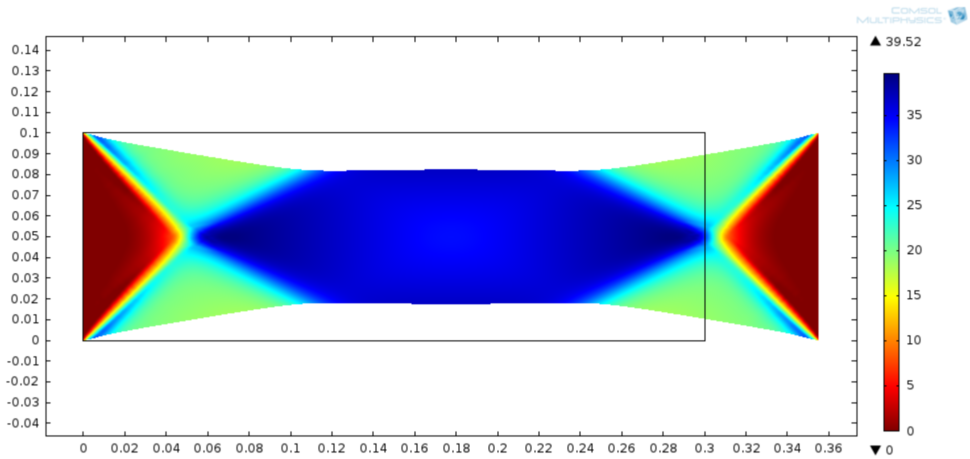

Figure 5.12: Shear angle variation ϕ for an imposed displacement $d = 55\,\text{mm}$ obtained with the first gradient theory and for an arbitrary mesh. The lateral bar indicates the values of ϕ in degrees

5.6 Conclusions

In this chapter a constrained micromorphic theory is introduced which includes, as a particular case, a second gradient model. Particular orthotropic, hyperelastic, constitutive laws are introduced in order to account for the anisotropy of fibrous composite reinforcements undergoing large deformations. The obtained theoretical framework is used to model the mechanical behavior of such fibrous composite materials during the so-called bias extension test.

The first and second gradient solutions are compared showing that the proposed second gradient model is actually able to describe the onset of shear boundary layers which regularize the first gradient sharp transition between two zones at different levels of shear. Moreover, differently from what happens for the first gradient model, the proposed second gradient theory also allows to describe the curvature of the free boundaries of the specimen.

In order to identify the values of introduced second gradient parameters we proceed by inverse approach, performing numerical simulations which correctly fits the experimental data. More particularly, we choose the values of second gradient parameters in order to fit at best the characteristic length of the shear boundary layer which is observed is bias test experiments.

Therefore, the results obtained allow us to estimate the order of magnitude of the second gradient parameters to be used for the considered fibrous materials. These results are promising and justify the need of novel experimental campaigns in order to estimates such gradient parameters for a wider class of composite preforms.

Chapter 6

Second Gradient Modeling of the Three Point Bending of 3D Interlocks

In this chapter we present a simple quadratic second gradient model for the description of the three point bending of thick composite interlocks. In particular, we will address the following points:

- formulate a first 3D extension of the 2D model presented in [DEL14] by introducing suitable quadratic second gradient deformation energy dependences,
- adopt the same deformation energy introduced by [CHA12] for the description of first gradient, hyperelastic, orthotropic constitutive behavior,
- introduce a 3D generalization of the numerical integration scheme proposed in [FER13] to describe the 3 point bending test with fixed cylindrical supports for which [CHA12] supplies experimental evidence and first gradient numerical simulations,
- calibrate second gradient constitutive parameters to describe the experimental mechanical behavior of the 3 point bending of $0°/90°$ and $\pm 45°$ fibrous composite interlocks.

The performed numerical simulations were obtained by interfacing the solid mechanics module (used to model contact and first gradient constitutive behavior) with the weak form PDE module (used to implement second gradient constitutive laws) in COMSOL®. Second gradient effects were obtained by using suitable Lagrange multipliers linking the introduced micromorphic kinematical descriptors to some orthotropic invariants of the right Cauchy-Green deformation tensor.

In conclusion, we can state that the numerical difficulties found when applying Cauchy models are a symptom of their weakness in the modeling capabilities of complex physical phenomena. Introducing second gradient models, one simultaneously obtains a twofold effect i) to enlarge the scope of applicability of continuum theories and ii) to improve the efficiency of introduced numerical integration schemes.

Contents

6.1 Kinematics

In this section we are interested in the introduction of the correct kinematical framework which is needed to describe the deformation of three dimensional interlocks. To do so, we follow the reasonings proposed in [DEL14] for the case of two dimensional networks in which suitable second gradient energies are proposed which account for the effect of yarns' bending stiffness on the deformation of the considered 2D woven fabrics.

Fibrous composite interlocks are constituted by different layers of thin woven fabrics which are held together by a third weaving pattern. To account for the fact that such materials show two privileged material directions, we introduce two orthonormal vectors $\mathbf{D}_1$ and $\mathbf{D}_2$ which represent the warp and weft directions of the yarns constituting the 2D woven fabrics in the reference configuration. These weaving directions are the same for all points in the considered woven specimen. A third direction can be introduced as $\mathbf{D}_3 = \mathbf{D}_1 \times \mathbf{D}_2$: it is worth noticing that while $\mathbf{D}_1$ and $\mathbf{D}_2$ actually identify the pattern of the yarns in the undeformed configuration, the third unit vector $\mathbf{D}_3$ does not necessarily represent a material direction. The quoted set of unit normal vectors is known to be worth to describe the reference configuration of an orthotropic material (see e.g. [RAU09]). Once the Lagrangian unit vectors are introduced, we can define the corresponding Eulerian vectors as:

$$\mathbf{d}_1 = \mathbf{F} \cdot \mathbf{D}_1, \qquad \mathbf{d}_2 = \mathbf{F} \cdot \mathbf{D}_2, \qquad \mathbf{d}_3 = \mathbf{F} \cdot \mathbf{D}_3, \tag{6.1}$$

where $\mathbf{F} = \nabla \boldsymbol{\chi}$ is the gradient of the usual placement map $\boldsymbol{\chi}$. The vectors $\mathbf{d}_1$, $\mathbf{d}_2$ and $\mathbf{d}_3$ are the push-forward in the current configuration of the vectors $\mathbf{D}_1$, $\mathbf{D}_2$ and $\mathbf{D}_3$ respectively. It is worth to stress the fact that, while the vectors $\mathbf{d}_1$ and $\mathbf{d}_2$, represent the current directions of the warp and weft, the vector $\mathbf{d}_3$ cannot be related to privileged directions inside the considered orthotropic material.

We can summarize by saying that the kinematics of the considered continuum is univocally determined by the introduction of a suitably regular placement field $\boldsymbol{\chi} : B_0 \to \mathbb{R}^3$ which maps the Lagrangian configuration $B_0 \subset \mathbb{R}^3$ of the considered body into the 3D Euclidean space. The deformation of the body is hence completely described by means of the deformation gradient $\mathbf{F} = \nabla \boldsymbol{\chi}$ as in classical continuum mechanics. In this framework, if one introduces an orthonormal basis $\{\mathbf{D}_1, \mathbf{D}_2, \mathbf{D}_3\}$, the corresponding deformed vectors $\{\mathbf{d}_1, \mathbf{d}_2, \mathbf{d}_3\}$ are immediately found by means of Eq. (6.1). The fact of identifying two of the Lagrangian material vectors (namely $\mathbf{D}_1$ and $\mathbf{D}_2$) with the reference directions of yarns will be seen to be useful to describe in an intuitive way the deformation of the considered orthotropic material.

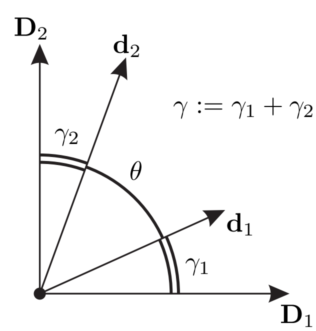

Figure 6.1: Eulerian yarn vectors $\mathbf{d}_1$ and $\mathbf{d}_2$: the angle θ is the angle between yarns in the current configuration, γ is the total angle variation with respect to the reference configuration

In fact, with reference to Fig. 6.1 for the definition of the angles θ and γ, it is possible to remark that the shear strain S can be related to the total angle variation γ according to the formula

$$S = \mathbf{d}_1 \cdot \mathbf{d}_2 = |\mathbf{d}_1|\,|\mathbf{d}_2| \cos(\theta) = |\mathbf{d}_1|\,|\mathbf{d}_2| \sin(\gamma), \tag{6.2}$$

where $\gamma = \gamma_1 + \gamma_2$ is the total angle variation field between the two orders of yarns from the reference configuration to the current one and $|\cdot|$ represents the length of considered vectors. Analogously, $\lambda_1 = |\mathbf{d}_1|$ and $\lambda_2 = |\mathbf{d}_2|$ are a measure of the yarns' stretches: indeed the elongations of the two orders of yarns with respect to the reference configuration can be easily obtained as $\lambda_1 - 1$ and $\lambda_2 - 1$ respectively.

6.2 Second gradient energy density for 3D interlocks

The aim of this section is to introduce constitutive laws which are suitable to describe at best the mechanical behavior of 3D fibrous composite reinforcements. It will be shown that a second gradient constitutive law which is able to account for the in-plane and out-of-plane bending stiffnesses of the yarns is indeed necessary to correctly model the mechanical behavior of such materials. Following what done in [DEL14] for the 2D case, we suppose that the deformation energy density W depends on the deformation tensor and on its gradient by means of the following additive decomposition:

$$W(\mathbf{F}, \nabla\mathbf{F}) = W_{\mathrm{I}}(\mathbf{F}) + W_{\mathrm{II}}(\mathbf{F}, \nabla\mathbf{F}), \tag{6.3}$$

where W_{I} and W_{II} are the first and second gradient energies respectively.

In order to determine a suitable constitutive expression for the first gradient energy W_I, we start recalling the representation theorem for orthotropic materials (see [RAU09]) which states that the first gradient energy for an orthotropic material can take the following functional form:

$$W_{\mathrm{I}}(\mathbf{F}) = W_{\mathrm{I}}(i_1, i_4, i_6, i_8, i_9, i_{10}), \tag{6.4}$$

where

$$\begin{array}{lll} i_4 = \mathbf{D}_1 \cdot \mathbf{C} \cdot \mathbf{D}_1 = \lambda_1^2, & i_6 = \mathbf{D}_2 \cdot \mathbf{C} \cdot \mathbf{D}_2 = \lambda_2^2, & i_8 = \mathbf{D}_1 \cdot \mathbf{C} \cdot \mathbf{D}_2 = S, \\ i_9 = \mathbf{D}_1 \cdot \mathbf{C} \cdot \mathbf{D}_3, & i_{10} = \mathbf{D}_2 \cdot \mathbf{C} \cdot \mathbf{D}_3, & i_1 = \mathrm{tr}(\mathbf{C}), \end{array} \tag{6.5}$$

are the invariants of the right Cauchy-Green deformation tensor for an orthotropic material and where $\mathbf{C} = \mathbf{F}^T \cdot \mathbf{F}$ is the classical right Cauchy-Green deformation tensor. It is worth noticing that the first three invariants respectively coincide with the square of the stretches in the yarns' direction and with the shear strain. The invariants i_9 and i_{10}, on the other hand, are related to the out-of-plane angle variations of the two orders of yarns and their spacial gradient can be related to the out-of plane bending of the yarns. Specific constitutive laws for the first gradient energy which fit available experimental data will be given in the next subsection.

As far as the second gradient energy is concerned, a general class of expressions which can be considered is of the type

$$W_{\mathrm{II}}(\mathbf{F}, \nabla\mathbf{F}) = W_{\mathrm{II}}(\nabla i_1, \nabla i_4, \nabla i_6, \nabla i_8, \nabla i_9, \nabla i_{10}). \tag{6.6}$$

In the next subsection we will point out some reasonings which will allow us to consider simpler constitutive expressions for the second gradient energy which are suitable to describe the overall behavior of the considered interlock subjected to three point bending..

6.2.1 Constitutive choice for the first gradient energy

Following what done in [CHA12], we introduce some specific functions of the introduced invariants which are relatively simple to be determined by means of suitable experimental settings:

$$\begin{array}{lll} I^1_{\mathrm{elong}} = \ln\left(\sqrt{i_4}\right), & I^2_{\mathrm{elong}} = \ln\left(\sqrt{i_6}\right), & I^{\mathrm{p}}_{\mathrm{sh}} = \dfrac{i_8}{\sqrt{i_4 i_6}}, \\ I^{\mathrm{t1}}_{\mathrm{sh}} = \dfrac{i_9}{\sqrt{i_4 i_{11}}}, & I^{\mathrm{t2}}_{\mathrm{sh}} = \dfrac{i_{10}}{\sqrt{i_6 i_{11}}}, & I_{\mathrm{comp}} = \ln\left(\sqrt{\dfrac{i_3}{i_4 i_6}}\right), \end{array} \tag{6.7}$$

where the invariants which have not been previously introduced are defined as

$$i_3 = \det(\mathbf{C}), \quad i_{11} = \mathbf{D}_3 \cdot \mathbf{C} \cdot \mathbf{D}_3. \tag{6.8}$$

Indeed, considering an energy which depends on the quantities appearing in (6.7) is equivalent to consider a functional dependence of the type (6.4). In fact, as shown in [RAU09], the additional two invariants defined in (6.8) depend on the previously introduced ones by means of the following relationships

$$\begin{aligned} i_{11} &= i_1 - i_4 - i_6, \\ i_3 &= \left(i_4 i_6 - i_8^2\right)(i_1 - i_4 - i_6) + 2\, i_8\, i_9\, i_{10} - i_6\, i_9^2 - i_4\, i_{10}^2. \end{aligned} \tag{6.9}$$

The interest of introducing a particular functional dependence of the strain energy density on the invariants (6.5) through the introduction of the quantities (6.7) can be found in the fact that these quantities can be easily measured by means of suitable experimental set-ups. The two quantities I^1_{elong} and I^2_{elong} are directly related to yarns elongations $\lambda_1 = \sqrt{i_4}$ and $\lambda_2 = \sqrt{i_6}$. As for the second quantity, it can be checked that $I^{\text{p}}_{\text{sh}} = \sin(\gamma)$ (see also Eq. (6.2)): this means that it can be directly related to the shear angle variation between yarns. Analogously, $I^{\text{t1}}_{\text{sh}}$ and $I^{\text{t2}}_{\text{sh}}$ represent the out-of-plane angle variations of the two orders of yarns and are thus related to out-of-plane shear modes. Finally, I_{comp} represent a normalized volume variation which can be directly related to a compression deformation mode. The possibility of performing simple elementary measurements on the quantities (6.7) allows the conception of constitutive laws which characterize the behavior of composite interlocks and which show considerable agreement with the available experimental evidences. In [CHA12] it is proposed a constitutive expression of the first gradient deformation energy of the type

$$W_I = W^1_{\text{elong}} + W^2_{\text{elong}} + W_{\text{comp}} + W^{\text{p}}_{\text{sh}} + W^{\text{t1}}_{\text{sh}} + W^{\text{t2}}_{\text{sh}}, \tag{6.10}$$

where

$$\begin{aligned}
W^1_{\text{elong}} &= \begin{cases} \frac{1}{2}\mathrm{K}^0_{\text{elong}}\left(I^1_{\text{elong}}\right)^2 & \text{if } I^1_{\text{elong}} \le I^0_{\text{elong}} \\ \frac{1}{2}\mathrm{K}_{\text{elong}}\left(I^1_{\text{elong}} - I^0_{\text{elong}}\right)^2 + \frac{1}{2}\mathrm{K}^0_{\text{elong}} I^1_{\text{elong}} I^0_{\text{elong}} & \text{if } I^1_{\text{elong}} > I^0_{\text{elong}}, \end{cases} \\
W^2_{\text{elong}} &= \begin{cases} \frac{1}{2}\mathrm{K}_{\text{elong}}\left(I^2_{\text{elong}}\right)^2 & \text{if } I^2_{\text{elong}} \le I^0_{\text{elong}} \\ \frac{1}{2}\mathrm{K}^1_{\text{elong}}\left(I^2_{\text{elong}} - I^0_{\text{elong}}\right)^2 + \frac{1}{2}\mathrm{K}^0_{\text{elong}} I^2_{\text{elong}} I^0_{\text{elong}} & \text{if } I^2_{\text{elong}} > I^0_{\text{elong}}, \end{cases} \\
W_{\text{comp}} &= \mathrm{K}_{\text{comp}}\left(\left(1 - \frac{I_{\text{comp}}}{I^0_{\text{comp}}}\right)^{-q} - q\,\frac{I_{\text{comp}}}{I^0_{\text{comp}}} - 1\right) \\
W^p_{\text{sh}} &= \begin{cases} \mathrm{K}^{12}_{\text{shp}}\left(I^{\text{p}}_{\text{sh}}\right)^2 & \text{if } \left|I^p_{\text{sh}}\right| \le I^{\text{p}0}_{\text{sh}} \\ \mathrm{K}^{21}_{\text{shp}}\left(1 - \left|I^{\text{p}}_{\text{sh}}\right|\right)^{-p} + W^0_{\text{shp}} & \text{if } \left|I^p_{\text{sh}}\right| > I^{\text{p}0}_{\text{sh}} \end{cases} \\
W^{t1}_{\text{sh}} &= \begin{cases} \frac{1}{2}\mathrm{K}^{12}_{\text{sht1}}\left(I^{\text{t1}}_{\text{sh}}\right)^2 & \text{if } \left|I^{t1}_{\text{sh}}\right| \le I^0_{\text{sht1}} \\ \mathrm{K}^{22}_{\text{sht1}}\left(I^{\text{t1}}_{\text{sh}}\right)^2 + \mathrm{K}^{21}_{\text{sht1}}\left|I^{\text{t1}}_{\text{sh}}\right| + W^0_{\text{sht1}} & \text{if } \left|I^{t1}_{\text{sh}}\right| > I^0_{\text{sht1}} \end{cases} \\
W^{t2}_{\text{sh}} &= \begin{cases} \frac{1}{2}\mathrm{K}^{12}_{\text{sht2}}\left(I^{\text{t2}}_{\text{sh}}\right)^2 & \text{if } \left|I^{t2}_{\text{sh}}\right| \le I^0_{\text{sht2}} \\ \mathrm{K}^{22}_{\text{sht2}}\left(I^{\text{t2}}_{\text{sh}}\right)^2 + \mathrm{K}^{21}_{\text{sht2}}\left|I^{\text{t2}}_{\text{sh}}\right| + W^0_{\text{sht1}} & \text{if } \left|I^{t2}_{\text{sh}}\right| > I^0_{\text{sht2}}. \end{cases}
\end{aligned} \tag{6.11}$$

In the previous formulas, all the quantities which have not been introduced before are constant.

It is worth noticing that the elongation energies W^1_{elong} and W^2_{elong} are defined in such a way that a threshold value I^0_{elong} exists for which the yarns' rigidity is smaller for small elongations than for higher ones ($K^0_{\text{elong}} < K_{\text{elong}}$). This constitutive choice allows to take into account the fact that the yarns are not initially straight due to weaving and they can hence initially be elongated more easily. The elongation threshold I^0_{elong} corresponds to the configuration in which the yarns are completely straightened and start showing a higher resistance to deformation. The need of introducing such elongation strain energy densities is related to the fact that they actually carefully describe the response of the woven yarns to elongation. Nevertheless, the elongation of yarns is a mechanism which is definitely less important than the deformation mechanism associated to the angle variations between the two orders of yarns. We can actually say that, in most of the experimental tests, the considered yarns can be considered almost inextensible with respect to the observed predominant shear strains: the energy associated to elongation is negligible when compared to the energy associated to the in-plane and out-of-plane shear of the considered set of yarns. As it will be better pointed out in the next subsection, this feature, which is peculiar of fibrous composite reinforcements, will be essential for choosing a simplified constitutive expression for the second gradient energy.

6.2.2 Constitutive choice for the second gradient energy

In this subsection we specify the constitutive expression which we will use to model the mechanical behavior of 3D composite interlocks. To do so, we start considering some results recently proposed in [DEL14] for 2D woven composites. In the quoted paper, it is shown that a suitable 2D second gradient energy which is able to account for in-plane bending stiffness of the yarns at the mesoscopic scale is of the type

$$W_{\text{II}}(\mathbf{F}, \nabla\mathbf{F}) = \frac{1}{2}A_\lambda\left(|\nabla\lambda_1|^2 + |\nabla\lambda_2|^2\right) + \frac{1}{2}A_S\,|\nabla S|^2\,, \tag{6.12}$$

where A_λ and A_S are positive constants. This energy has been shown to be a good choice for the description of the mechanical behavior of 2D woven composites due to its convexity with respect to $\nabla\mathbf{F}$ which guarantees well posedness of the resulting differential problem. A second gradient energy of this type has also been used in [FER13] to model the bias extension test on 2D woven composites. It is clear that, when considering inextensible yarns, the gradient of elongations are vanishing and the second gradient strain energy density thus reduces to

$$W_{\text{II}}(\mathbf{F}, \nabla\mathbf{F}) = \frac{1}{2}A_S\,|\nabla S|^2 = \frac{1}{2}A_S\,|\nabla i_8|^2\,. \tag{6.13}$$

In [DEL14] it is also shown that, in the limit case of inextensible yarns, an alternative to the strain energy density (6.13) is given by

$$W_{\text{II}}(\mathbf{F}, \nabla\mathbf{F}) = \frac{1}{2}A_g\left(|\mathbf{g}_1|^2 + |\mathbf{g}_2|^2\right), \tag{6.14}$$

where

$$\mathbf{g}_1 = \kappa_1\boldsymbol{\nu}_1, \qquad \mathbf{g}_2 = \kappa_2\boldsymbol{\nu}_2 \tag{6.15}$$

are two vectors which account for the bending of the yarns at the mesoscopic level and A_g is a positive constant. In the last formulas κ_1 and κ_2 are the bending strains of the two orders of yarns and $\boldsymbol{\nu}_1$ and $\boldsymbol{\nu}_2$ are vectors orthogonal to the current yarn directions $\mathbf{d}_1$ and $\mathbf{d}_2$ respectively (see [DEL14] for more details). Direct comparison of equations (6.13) and (6.14) allows to conclude that, in the case of almost inextensible yarns, the fact of considering an energy accounting for the gradient of the shear angle variation is equivalent to consider an energy accounting for the bending of the two orders of yarns at the mesoscopic level. This interpretation is intriguing since it provides a clear interpretation of the deformation mechanisms which take place at the mesoscopic level when considering woven fabrics.

By extension of the previous reasoning, we consider the following expression for the second gradient energy to be used for accounting for out-of plane bending stiffness of the yarns in 3D composite interlocks

$$W_{\mathrm{II}}\left(\mathbf{F},\nabla\mathbf{F}\right)=\frac{1}{2}A_S^{\mathrm{t}1}\left|\nabla i_9\right|^2+\frac{1}{2}A_S^{\mathrm{t}2}\left|\nabla i_{10}\right|^2. \tag{6.16}$$

By this constitutive choice, we are considering that the wires are almost inextensible (small elongations compared to the shear strains) and that the predominant second gradient deformation modes are the out-of-plane bending of the yarns at the mesoscopic level. This is coherent with the usual phenomenology observed when dealing with 3D composite interlocks.

As a matter of fact, the constitutive choice (6.16) for the second gradient strain energy density deserves more accurate investigations in future works in order to be generalized to describe any observable material behavior of thick composite interlocks. Actually, even if the predominant mesostructure-related deformation mechanisms which are activated in the three point bending test are the out-of-plane bending of the yarns, it is possible that other second gradient mechanisms could be activated when considering other loading and/or boundary conditions. In order to explore all these possibilities, other independent macroscopic tests need to be conceived which are able to unveil such supplementary material behaviors taking place at the mesoscopic level. A fully realistic constitutive choice for the generalized elasticity parameters remains a big challenge for mechanicians and it constitutes an open field of research. Despite the simplicity of the constitutive choic made here, non-linear material behaviors are likely to occur also for second gradient deformation mechanisms. If Eq. e(6.16) is well adapted for describing the macroscopic effect of the mesostructure when considering a macroscopic bending of the specimen, it is possible that more general expressions (including a dependence of the elastic second gradient parameters on the first gradient strain and/or more complicated functional expressions for the strain energy density) will be needed to describe the behavior of interlocks when subjected to arbitrary loading and boundary conditions.

6.3 Least action principle and principle of virtual powers

Once the kinematics and the adopted constitutive laws for 3D orthotropic materials have been introduced, we can introduce the action functional as

$$\mathcal{A}=\int_{B_0}W\left(\mathbf{F},\nabla\mathbf{F}\right)\,dB_0=\int_{B_0}\left(W_{\mathrm{I}}\left(\mathbf{F}\right)+W_{\mathrm{II}}\left(\mathbf{F},\nabla\mathbf{F}\right)\right)\,dB_0, \tag{6.17}$$

where W_{I} and W_{II} are constitutively given by (6.10) and (6.16) respectively. Assuming the previous expression for the action functional implies that all inertia effects are neglected and that we are hence considering a static case. As it will be shown in the remainder of the chapter, this assumption is sensible for the applications which are targeted here.

6.3.1 Second gradient theory as the limit case of a micromorphic theory

In this subsection we will present the principle of virtual powers for the considered second gradient material passing through the theory of micromorphic media. The theory of micromorphic media (see [MIN64, ERI01]) is known to be suitable to account for microstructure in elastic materials. This theory is more general than a second gradient one in the sense that the set of unknown kinematical fields is enriched with respect to the classical kinematics based on the displacement field alone. More precisely, supplementary kinematical fields accounting for the motion of the microstructure are provided thus generalizing the classical kinematical framework of Cauchy and second gradient continua. In this chapter, we state the principle of virtual powers for 3D composite interlocks by means of a simple micromorphic model and we use suitable Lagrange multipliers to let the considered micromorphic model tend to the second gradient model presented in the previous sections. The interest of introducing the principle of virtual powers by means of this approach is threefold: i) the presentation via a micromorphic model allows to better catch the physical meaning of the considered internal and external actions, ii) the natural and kinematical boundary conditions which can be used naturally take an intuitive meaning, iii) last but not least, the numerical implementation of the considered generalized problem is easier and the obtained solution is more stable. As far as considering the third quoted advantage of using constrained micromorphic theories to numerically implement second gradient problems, one has to notice that the gain in terms of numerical calculations is evident. Indeed, when considering a differential problem stemming from a micromorphic model, the associated differential equations are of lower order with respect to those which would directly derive from a second gradient model. These lower order equations are obviously easier to be solved from a numerical point of view and the obtained numerical solution will be more stable and precise.

To proceed according to this optic, we introduce the kinematical fields of the considered micromorphic model by means of the two vector functions

$$\boldsymbol{\chi} : B_0 \to \mathbb{R}^3, \qquad \boldsymbol{\psi} : B_0 \to \mathbb{R}^2, \tag{6.18}$$

the first one being the classical placement field introduced before also for the 2nd gradient kinematics and the second one accounting for microscopic motions in the considered continuum. The micromorphic model proposed here is simpler than the classical one proposed by Mindlin and Eringen [MIN64, ERI01] since we only consider here two additional scalar functions instead of the 9 which are introduced in the quoted models. We hence introduce a micromorphic strain energy density which take the following particular form and which is used to implement our numerical simulations:

$$\tilde{W}_{\mathrm{II}}\left(\nabla\boldsymbol{\psi}\right) = \frac{1}{2}A_S^{\mathrm{t1}}\left|\nabla\psi_1\right|^2 + \frac{1}{2}A_S^{\mathrm{t2}}\left|\nabla\psi_2\right|^2, \tag{6.19}$$

where we denoted by $\psi_\alpha,\ \alpha = 1,2$ the components of the vector $\boldsymbol{\psi}$. By direct comparison of the energies (6.19) and (6.16) it can be checked that the proposed micromorphic energy tends to the second gradient one introduced before if $\psi_1 \to i_9$ and $\psi_2 \to i_{10}$. In order to account for such constraints in the weak formulation of the problem, we introduce suitable Lagrange multipliers Λ_1 and Λ_2 which have an associated energy density of the type

$$W_{\mathrm{L}}\left(\mathbf{F},\boldsymbol{\psi},\boldsymbol{\Lambda}\right) = \Lambda_1\left(\psi_1 - i_9\right) + \Lambda_2\left(\psi_2 - i_{10}\right), \tag{6.20}$$

where we clearly set $\boldsymbol{\Lambda} = (\Lambda_1, \Lambda_2)$.

We hence propose to write the action functional of the proposed micromorphic medium as

$$\mathcal{A} = \int_{B_0}\left(W_{\mathrm{I}}\left(\mathbf{F}\right) + \tilde{W}_{\mathrm{II}}\left(\nabla\boldsymbol{\psi}\right) + W_{\mathrm{L}}\left(\mathbf{F},\boldsymbol{\psi},\boldsymbol{\Lambda}\right)\right)\, dB_0, \tag{6.21}$$

where W_{I} is the same energy given in 6.10, while the energies $\tilde{W}_{\mathrm{II}}$ and W_{L} are introduced in terms of the additional kinematical variables as in formula (6.19) and (6.20) respectively. The power of internal forces of the considered constrained micromorphic medium can be written as the first variation of the considered action functional as

$$\mathcal{P}^{\mathrm{int}} = \delta\mathcal{A} = \int_{B_0}\left(\left(\frac{\partial W_{\mathrm{I}}}{\partial F_{ij}} + \frac{\partial W_{\mathrm{L}}}{\partial F_{ij}}\right)\delta F_{ij} + \frac{\partial W_{\mathrm{L}}}{\partial\psi_\alpha}\delta\psi_\alpha + \frac{\partial\tilde{W}_{\mathrm{II}}}{\partial\psi_{\alpha,j}}\delta\psi_{\alpha,j} + \frac{\partial W_{\mathrm{L}}}{\partial\Lambda_\alpha}\delta\Lambda_\alpha\right). \tag{6.22}$$

The power of external forces is easily introduced when considering a micromorphic framework (see e.g. [BLE67]) and in the present case, neglecting body external actions, can take the form

$$\mathcal{P}^{\mathrm{ext}} = \int_{\partial B_0}\left(f_i^{\mathrm{ext}}\delta\chi_i + \tau_i\delta\psi_i\right). \tag{6.23}$$

Indeed, in the performed numerical simulations we assume that the virtual fields $\delta\psi_i$ is arbitrary on the boundary of the considered specimen (vanishing double force: $\tau_i = 0$), while the virtual displacement $\delta\chi_i$ is arbitrary almost everywhere, except on small subparts of the boundary where the displacement is assigned or vanishing. Such small parts of the boundary on which the displacement is vanishing can eventually change during deformation as happens for the contact of simply supported interlocks undergoing large bending deformations. The boundary conditions to be applied to model contact between two deformable continua is of difficult implementation but contact laws are usually already implemented in numerical codes as e.g. COMSOL Multiphysics. We used such tool to model the contact in our numerical three point bending simulations.

The weak formulation of the differential problem for the considered constrained micromorphic medium can be then stated as

$$\mathcal{P}^{\text{int}} = \mathcal{P}^{\text{ext}}, \tag{6.24}$$

where the internal and external power are respectively given by (6.22) and (6.23).

It is worth to remark that, starting from this formulation of the principle of virtual powers and considering arbitrary variations $\delta\Lambda_i$ of the Lagrange multipliers, one gets the bulk constraints which actually let the considered micromorphic model tend to the particular second gradient one previously introduced, namely

$$\psi_1 = i_9, \quad \psi_2 = i_{10}. \tag{6.25}$$

It is clear that, starting from the principle of virtual powers and integrating by parts, one could also obtain the strong form of the bulk equations and naturally associated boundary conditions in duality of the virtual variations $\delta\chi_i$ and $\delta\psi_i$. Nevertheless, since the numerical simulations presented in the following are directly implemented via the weak form (6.24), we do not explicitly write here such strong equations.

6.4 Numerical simulations for three point bending of composite interlocks

In this section we present the numerical results stemming from the application of the proposed second gradient model to the case of three point bending of a composite interlock. The first gradient constitutive parameters appearing in equation 6.11 are assumed to take the values presented in tables 6.1, 6.2 and 6.3, in agreement with the experimental identification proposed in [CHA12]. We remark that the two out-of-plane shear potentials are not symmetric in the sense that the corresponding constants appearing in table (6.3) do not take the same values for the two order of yarns. This fact is due to different weaving patterns in the warp and weft directions and has been experimentally observed in [CHA12].

$\mathrm{K}^0_{\text{elong}}$	$\mathrm{K}_{\text{elong}}$	I^0_{elong}	K_{comp}	I^0_{comp}	q
37.85 [MPa]	816.33 [MPa]	0.0145	7.57×10^{-3} [MPa]	-1.12	2.85

Table 6.1: Constitutive parameters appearing in the elongation and compression energy potentials.

$\mathrm{K}^{12}_{\text{shp}}$	$\mathrm{K}^{21}_{\text{shp}}$	p	I^0_{shp}	W^0_{shp}
0.07575 [MPa]	1.69×10^{-4} [MPa]	3.69	4.2×10^{-3}	-1.69×10^{-4} [MPa]

Table 6.2: In-plane shear constitutive parameters.

$\mathrm{K}^{12}_{\mathrm{sht1}}$	$\mathrm{K}^{22}_{\mathrm{sht1}}$	$\mathrm{K}^{21}_{\mathrm{sht1}}$	I^{0}_{sht1}
0.064945 [MPa]	0.00401131 [MPa]	0.00079691 [MPa]	1.4×10^{-2}

$\mathrm{K}^{12}_{\mathrm{sht2}}$	$\mathrm{K}^{22}_{\mathrm{sht2}}$	$\mathrm{K}^{21}_{\mathrm{sht2}}$	I^{0}_{sht2}
0.0330351 [MPa]	0.0042497 [MPa]	0.000736072 [MPa]	3×10^{-2}

Table 6.3: Out of plane shear constitutive parameters.

Indeed, it must be said that the constitutive expressions for the in-plane and out-of-plane shear potentials (last three equations in 6.11) are slightly different from the ones used in [CHA12]. Nevertheless, the associated stresses (derivatives of the energy with respect to $I^{\mathrm{p}}_{\mathrm{sh}}$, $I^{\mathrm{t1}}_{\mathrm{sh}}$ and $I^{\mathrm{t2}}_{\mathrm{sh}}$) are seen to be almost equivalent. The reason to introduce here a simplified expression for the shear potentials is that a quadratic energy (linear stress) is more easily treated in numerical calculation than an energy in which non-integer powers of the considered invariants appear. All other constitutive laws used here (see Eq. 6.11) coincide with the one proposed in [CHA12].

The physical test we want to reproduce here is a simple three point bending of a composite reinforcement beam with rectangular cross-sections. The considered interlocks are 3D materials (see Fig. 6.2) in which a specific meso-structure with particular ordered patterns can be identified.

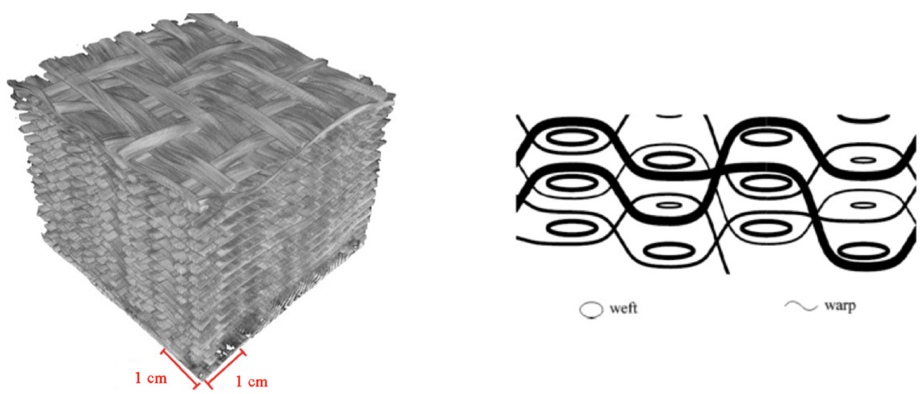

Figure 6.2: Example of 3D woven composite interlock reinforcement [ORL12] and general principle of the interlock weaving pattern.

As it can be inferred from figure 6.2, such materials are realized by different superimposed sheets of 2D woven fabrics which are partially interwoven in the direction orthogonal to the plane of the yarns. More particularly, the weaving in the direction orthogonal to the plane of the yarns is not continuous through the thickness of the specimen and thus cannot be considered as a material direction. For more details about the considered woven materials, we refer to [CHA11b, ORL12] in which the mesostructure of Snecma composite interlocks are described in greater detail.

In this chapter we will focus on two different three types of samples which basically differ one from the other for the direction of warp and weft with respect to the boundaries of the considered specimen. More particularly, we consider a three point 0°/90° bending test (warp and weft directions aligned with the edges of the specimen) and a three point ±45° bending test (the yarn directions form an angle of 45° degrees with respect to the longer sample edge). Numerical simulations showing the effect of the introduced second gradient parameters will be proposed for both cases and a discussion on the need of considering such a generalized continuum theory will be performed.

In all the performed numerical simulations we consider specimens with the dimensions of $200 \times 30 \times 15\,\text{mm}$, and we impose in the middle of the specimen a displacement of 60 mm. As already discussed, since large deformations are imposed to the specimen, the contact law between the specimen and the two cylindrical supports is a crucial point for the correct modeling of the considered problem. More particularly, as far as boundary conditions are concerned, we suppose that external double-forces are vanishing, while the force at the supports are assumed to follow a frictionless contact law which is built-in in the COMSOL code. In the middle of the top surface a displacement is applied which goes from 0 to 60 mm.

As for the values of the second gradient parameters appearing in Eq. (6.16), they are chosen by fitting the performed second gradient numerical simulations with the available experimental data concerning three point bending of $0°/90°$ and $\pm 45°$ composite interlocks. As it will be seen in the following subsections, the values of the second gradient parameters which are needed to fit at best the experimental evidences are not constant but depend on the entity of the macroscopic deformation. This indicates that the constitutive law (6.16) may not be general enough to catch all the possible material behaviors at high strains. Indeed, as far as sufficiently small imposed displacements are considered (up to $30-40\,\text{mm}$), a quadratic constitutive law of the type (6.16) is sufficient to describe quite precisely the overall material behavior. On the other hand, when higher imposed displacements are considered, different values of the second gradient parameters must be chosen to fit at best the experimental shape. Further studies on the formulation of the constitutive behavior of composite interlocks are thus needed which are focused on the development of more complex non-linear second gradient constitutive equations.

6.4.1 Three point $0°/90°$ bending test: the effect of out-of plane yarns' bending stiffness

In this subsection we present the numerical simulations obtained via the proposed linear second gradient model and we compare the obtained solutions with those issued by the classical Cauchy theory.

Figure 6.3 shows the comparison between the experimental tests, the first gradient solution and the second gradient one. It can be immediately noticed that the first gradient solution does not allow to correctly describe the deformation of the two ends of the beam whose deformation significantly deviates from the experimental data. This discrepancy between the experiments and the first gradient solution can be better pointed out in Fig. 6.4.

In this picture the fact that the the two ends of the beam do not correctly lift up results to be quite evident. On the other hand, the better fitting of the second gradient solution with the experimental evidence can be seen in Fig. 6.5.

It can also be remarked in the quoted picture that the fitting between the second gradient solution and the experimental data is performed by using two different values of the second gradient parameter when considering small and high deformations. These observations lead naturally to infer that the second gradient out-of-plane parameters cannot be considered to be constant, but seem to vary with deformation. This allows to conjecture that the second gradient constitutive law should indeed be generalized with respect to the simple quadratic form considered in Eq. (6.16) in order to include material non-linearities also in the second gradient terms. In this chapter, we limit ourselves to the quadratic second gradient constitutive law (6.16) which is able to catch the most important features of the mechanical behavior of considered interlocks with very few elastic constants. On the other hand, we also remark that, in subsequent works, a generalized non-linear constitutive law needs to be formulated for the second gradient energy in order to complete the mechanical characterization of considered materials.

The results obtained by means of the performed numerical simulations are appealing as they strongly suggest that the presence of second gradient terms in the strain energy density of the considered orthotropic material is unavoidable if one wants to correctly model the three point bending

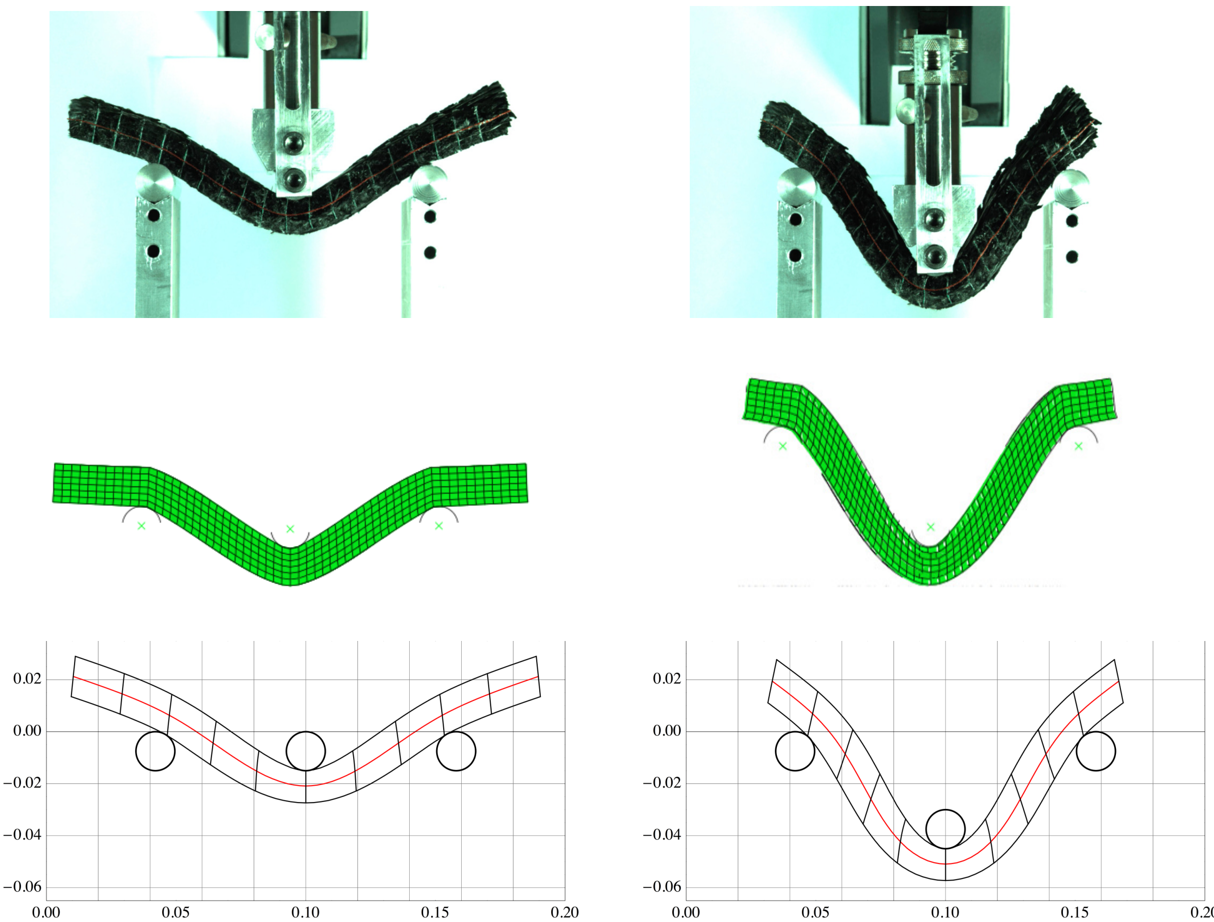

Figure 6.3: $0°/90°$ three point bending for an imposed displacement of for $30\,mm$ (left) and for $60\,mm$ (right). Top: experimental shapes [ORL12], middle: first gradient numerical simulations [CHA12], bottom: second gradient numerical simulations with $A_S^{t1} = A_S^{t2} = 1.2 \times 10^{-5} MPa \times m^2$ (left) and $A_S^{t1} = A_S^{t2} = 5 \times 10^{-6} MPa \times m^2$(right).

of a $0°/90°$ interlock while remaining in a continuum framework. Indeed, it is sensible that the out-of-plane bending stiffness plays a very important role in the deformation of such materials. In fact, the predominant deformation mode in such a test is related to the bending deformation of the order of yarns which are aligned with the longer side of the specimen. The order of yarns aligned with the depth of the specimen has very little influence on the global deformation of the considered sample. The fact that the longer yarns bend and that they posses a non-negligible out-of-plane bending stiffness allow the two ends of the beam to lift up. Such a deformation pattern is well recovered by the second gradient numerical simulations, but not by the first gradient ones (see Fig. 6.3). Moreover, it can be seen in the quoted figure that, as far as the three point bending of a $0°/90°$ specimen is considered, the cross sections of the beam are not orthogonal to its mean axis: this is directly related to the fact that the yarns can be considered almost inextensible in the considered woven composite.

Indeed, as it can be seen in Fig. 6.6, a specimen which behave as an Euler-Bernouilli beam would need that the upper part of the specimen shrink and the lower part elongate in order to let the cross sections stay orthogonal with respect to the mean axis. This shrinking/elongation deformation of the specimen is not possible due to the quasi-inextensibility of the yarns: the inextensibility constraint actually imposes a relative sliding of the yarns and, as a result, a rotation of the cross-sections with respect to the direction orthogonal to the mean axis.

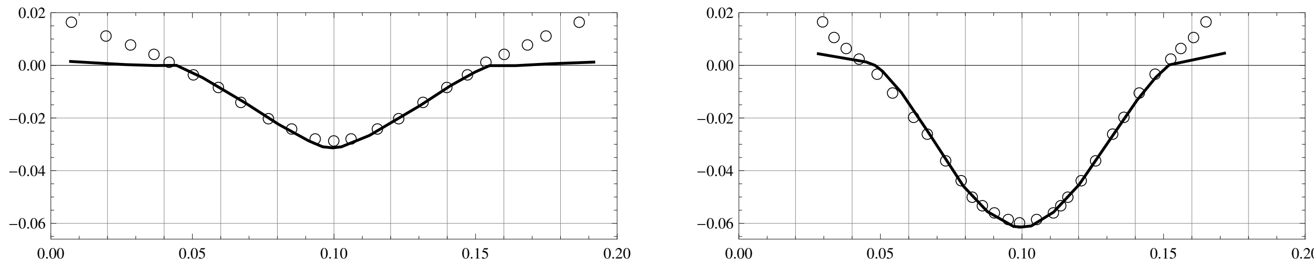

(a) (b)

Figure 6.4: Comparison between experimental data (dots) and first gradient solution: current shape of the mean axis of the specimen for imposed displacement of $30\,mm$ (a) and for $60\,mm$ (b).

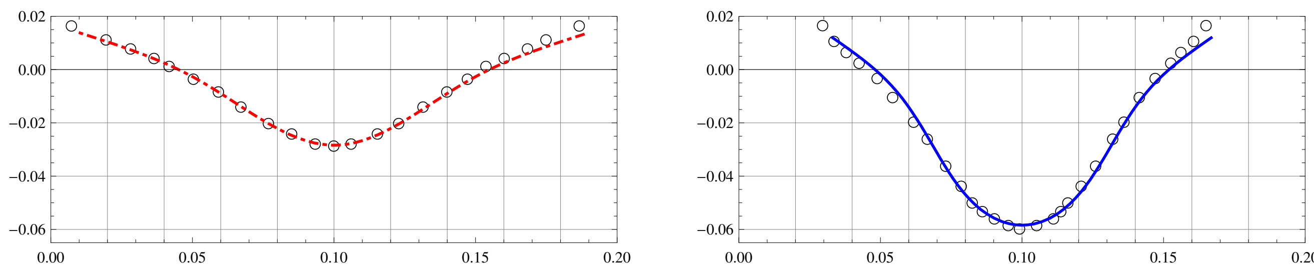

(a) (b)

Figure 6.5: Comparison between experimental data (dots) and second gradient solution: current shape of the mean axis of the specimen for imposed displacement of $30\,mm$ and $A_S^{t1} = A_S^{t2} = 1.2 \times 10^{-5} MPa \times m^2$ (a) and of $60\,mm$ (b) and $A_S^{t1} = A_S^{t2} = 5 \times 10^{-6} MPa \times m^2$.

6.4.2 Three point ±45° bending test

The present subsection is devoted to the comparison between first and second gradient solutions for the ±45° 3 point bending. Figure 6.7 shows a schematic representation of the bending of a ±45° specimen.

It can be seen from this figure that in such a deformation pattern, the upper part of the specimen necessarily undergoes to shrinking, while the bottom part is instead elongated. This change of length of the specimen is not due to elongation of the yarns (which we know to be almost inextensible), but to their pantographic motions. Indeed, it is known (see also Fig. 6.7(b) and (c)) that pantographic structures can increase or decrease their global length without changing the length of the single elements constituting the pantograph itself. Such "pantographic" variation of length of the specimen, coupled to out-of-plane angle variation of the two order of yarns give rise to the overall deformed shape of the ±45° specimen.

Figure 6.8 shows the comparison between the experiments and the first and second gradient solutions for the ±45° specimen for an imposed displacement of $60\,mm$. It can be inferred from this figure that the first gradient solution is closer to the experimental shape than in the 0°/90° case. This means that the second gradient effects due to in-plane and out-of-plane bending of the yarns are definitely less important than in the 0°/90° case. Indeed, this is sensible since the yarns are short compared to the length of the specimen and they can hence deform (rotate) changing their out-of-plane shear angle with no significant bending.

Figure 6.9 shows the experimental deformation of the mean axis together with those obtained via the first and second gradient theories. It is evident that that the two ends of the specimen are partially lifted up even when considering the first gradient solution (which means that some out-of-plane rotation takes place even without bending), but the experimental shape becomes much

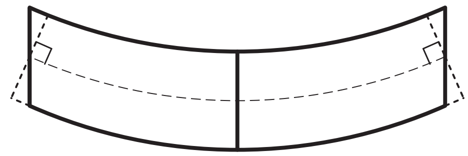

Figure 6.6: Schematic representation of 0°/90° bending test: Euler-Bernouilli hypothesis of cross sections orthogonal to the mean axis is violated.

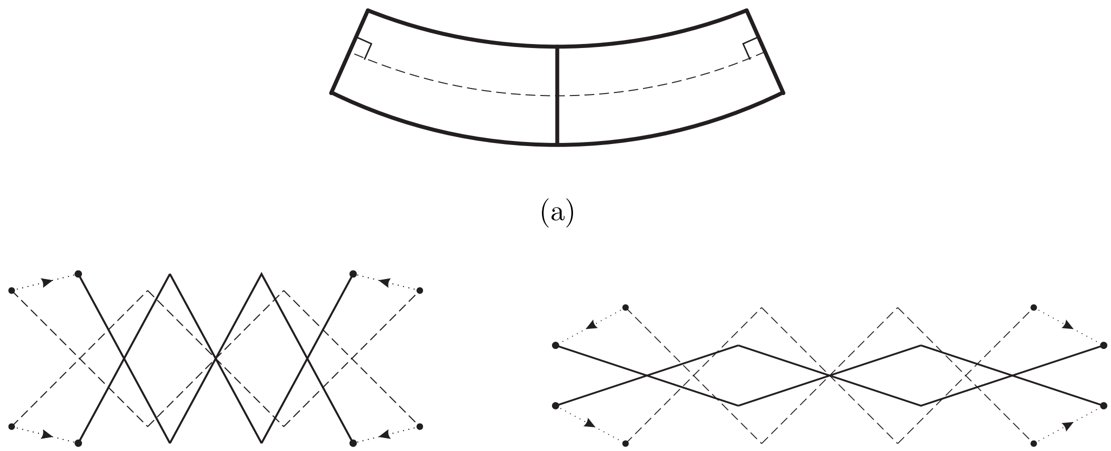

(a)

(b) (c)

Figure 6.7: Schematic representation of (a) ±45° bending test: Euler-Bernouilli hypothesis of cross sections orthogonal to the mean axis is almost verified; (b) and (c) possible motions of panthographic structures allowing for elongation and shrinking of the macroscopic specimen.

closer to the experimental one for a non vanishing value of the out-of-plane shear second gradient parameters. The fact that a partial lift-up of the two ends of the beam takes place even in the case of a first gradient theory is due to the fact that the fibers can rather easily rotate with respect to the vertical direction even without bending, due to their reduced length. Such almost rigid rotation of the fibers produces a non-local transmission of deformation which allows the two ends of the beam to partially lift-up. Nevertheless, a small amount of bending of the yarns can be seen to be present also in the ±45° case. Such effect of the shear bending stiffness can be recognized to be important both for the complete lift of the two ends of the beam and for the curvature of the middle part of the specimen.

Once again, we remark that the value of the second gradient parameter used in the numerical simulations is not the same as the one used for the 0°/90° test. This corroborates the thesis according to which the introduced simple constitutive load must be further generalized in order to account for nonlinear second gradient material behaviors.

6.5 Conclusions

In this chapter we present an orthotropic 3D second gradient model which is suitable to describe the complex mechanical behavior of thick composite interlocks. The need of using such generalized continuum theory is revealed by the study of the three point bending of 3D fibrous composite reinforcements. The considered specimens are parallelepipeds with the dimensions of $200 \times 30 \times 15\,mm$. Two types of specimens are considered which differ for the relative directions between the yarns and the edges of the specimen itself. More particularly, we consider the so-called 0°/90° specimen in which one order of long yarns follows the direction of the longer edge of the specimen,

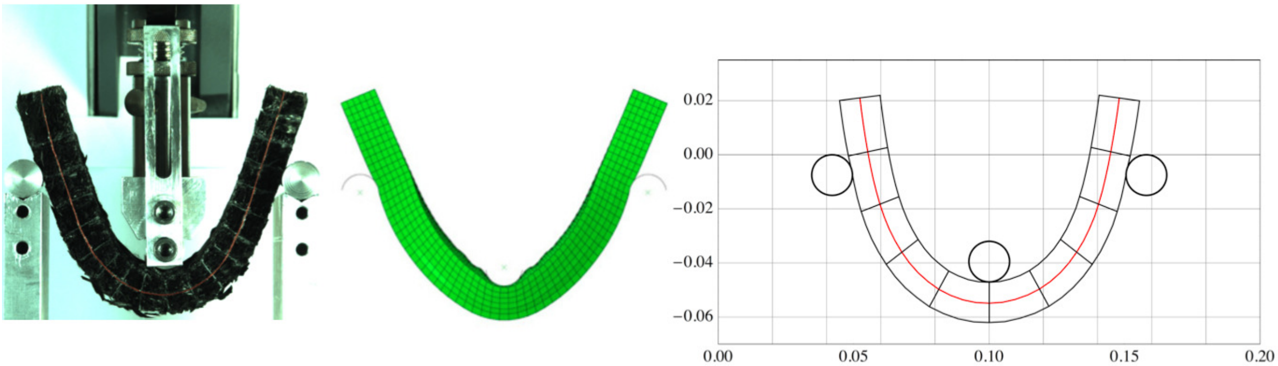

Figure 6.8: $\pm 45°$ three point bending for an imposed displacement of $60\,mm$ (right). left: experimental shape [ORL12], middle: first gradient numerical simulation [CHA12], bottom: second gradient numerical simulation with $A_S^{t1} = A_S^{t2} = 7.5 \times 10^{-6} MPa \times m^2$..

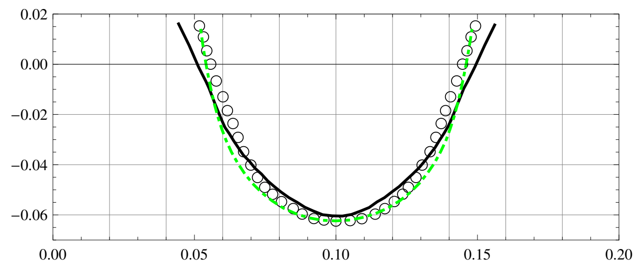

Figure 6.9: Comparison of experimental data with different second gradient solutions for an imposed displacement of $60\,mm$ and $A_S^{t1} = A_S^{t2} = 7.5 \times 10^{-6} MPa \times m^2$

while the second order of shorter yarns is directed along the depth of the specimen itself. The second type of specimen is called $\pm 45°$ and is such that the yarns are directed at $\pm 45°$ degrees with respect to the direction of the longer edge of the sample. In both cases, the specimens are subjected to a classical three point bending test and the experimental results are compared with numerical solutions obtained via first and second gradient continuum theories. It appears clearly from the obtained results that the use of a second gradient theory is useful tool if one wants to correctly model the behavior of composite interlocks subjected to three point bending. Indeed, we show that the fact of including the gradient of the out-of-plane shear angle variations in the strain energy density is directly related to the fact of considering the out-of-plane bending stiffness of the yarns at the mesoscopic level. Such bending rigidity of the mesostructure is crucial to correctly describe the response of the material to the applied external sollicitations. In particular, we show that the out-of-plane bending of the yarns is one of the leading mesoscopic deformation mechanism affecting the macroscopic bending of $0°/90°$ specimens. In fact, when subjected to bending, such materials basically behave as a "package" of superimposed wires which are held together by a second order of shorter yarns which indeed do not intervene directly in the deformation process. The longer wires so bend all together (as happens for the pages of a book when one tries to bend it) and their bending rigidity allows to the two ends of the macroscopic specimen to lift up and to the middle part of the specimen to take its characteristic curvature. A first gradient theory is not able to account for the bending of the mesostructure and hence is not suitable to correctly describe all the mechanisms which intervene in the complex process of deformation of composite interlocks. Moreover, we explicitly point out that the constraint of "quasi-inextensibility" of the yarns is directly related to the fact that a $0°/90°$ specimen does not behave as an Euler-Bernouilli beam in the sense that cross-sections which are initially orthogonal to the mean axis of the beam, do not remain orthogonal during deformation. Indeed, due to large bending deformations, the upper and lower surface of the specimen inevitably have different curvature and cross sections could remain orthogonal to the mean axis if and only if a significant change of length occurred in the direction of the longer edge of the specimen. This is actually impossible, due to the fact that the yarns have a very high extensional rigidity.

Similar reasonings can be repeated also for the $\pm 45°$ specimens, even if the deformation of such materials is more complex to be understood from a phenomenological point of view. We prove that in such a case, the bending rigidity of the yarns intervenes much less on the macroscopic deformation of the specimen, even if it keeps playing some role. Indeed, the main part of the out-of-plane motion of the yarns is accounted for by simple rotations of the yarns with no (or very few) associated bending. Such a deformation mode is possible due to the fact that the yarns are relatively short with respect to the size of the specimen and they can rotate rather easily with respect to the vertical direction. Nevertheless, the fact of considering the bending of the yarns still bring some complements to the complete description of the experimental behavior of the considered materials, both for what concerns the complete lift of the two ends of the specimen and its global curvature. We finally remark the $\pm 45°$ specimens almost behave as Euler-Bernouilli beams. This is possible since changes of length of the specimen are allowed due to pantographic motions of the yarns.

We can summarize by saying that 3D composite interlocks can be correctly modeled by considering the bending stiffness of the yarns by means of second gradient theories. When considering three point bending tests, the influence of the out-of-plane bending stiffness is much higher for $0°/90°$ specimens than $\pm 45°$ ones. We can infer that for orthotropic media with different initial angles between yarns the effect of second gradient terms would be of intermediate importance with respect to the two limit cases presented here.

The results proposed here are a fundamental step for the characterization of the mechanical behavior of thick composite interlocks for the impact that such results can have on the modeling of forming processes of complete engineering components. Nevertheless, the conception of more complex non-linear, second gradient constitutive laws appears to be a crucial point for further investigations.

General Conclusions

The complete characterization of fibrous composite reinforcements must account for the description of their mechanical behavior at the mesoscopic and microscopic scales. In order to consider the presence of lower scales in a macroscopic continuum theory, suitable constitutive laws must be introduced which account for

- the description of the microstructured material at high strains by means of suitable hyperelastic constitutive laws accounting for the orthotropy of the material,
- the description of microstructure-related deformation modes (as the bending of the yarns) by means of second gradient theories.

In order to bring new elements to the constitutive characterization of fibrous composite reinforcements, the hyperelastic constitutive laws proposed in [CHA11b] are complemented here by adding suitable second gradient terms which account for the effect of the bending stiffness of the yarns on the macroscopic mechanical behavior of the considered fibrous composite reinforcements.

Two experimental tests are targeted, namely the bias extension test on 2D fibrous composites and the three point bending of tick composite interlocks, which are simulated by means of a second gradient continuum model. It is shown that, in both the considered cases, the fact of using second gradient theories allows for the description of in-plane and out-of-plane bending modes of the yarns which inevitably have a non-negligible effect on the overall deformation of the considered specimens.

In particular, for the bias extension test, internal boundary layers are individuated which are transition zones between two regions of the specimen in which the shear angle between fibers remains almost constant. In such transition layers in-plane bending of the fibers can be observed which allows for a gradual variation of the angle between the two quoted zones. Such in-plane bending modes are associated to a simple second gradient energy whose elastic coefficients are determined by inverse approach.

The second considered experimental test is the three point bending of composite interlocks. It is seen that in this case a second gradient energy is needed to describe the out-of-plane bending modes of the yarns. The second gradient terms are proved to determine a complete fitting between the numerical simulations and the experimental results. In fact, if the solution obtained by a first gradient theory does not allow for the correct description of the deformation of the two ends of the interlock beam, a second gradient theory cures this inconvenient by providing a more realistic deformed shape of the specimen.

In the light of the previous remarks, we can conclude that the work presented in this thesis actually provides an advancement in the knowledge of the mechanical behavior of fibrous composite reinforcements. Nevertheless some open points still remains open and then need to be addressed in further works. Among them we can list

- Conception of general non-linear, second gradient constitutive laws which allow to univocally characterize the mechanical behavior of considered woven composites for any deformation state (small and very large deformations) and consequently for any set of imposed loads and boundary conditions.

- Inclusion of the inextensibility constraint of the yarns in the adopted second gradient analytical model in order to investigate limit systems which can serve as a reference for more complicated material behaviors.
- Micro-macro identification, i.e. identification of the macroscopic average second gradient coefficients as function of the microscopic mechanical characteristics.
- Rigorous study of the well-posedness (existence and uniqueness) of the second gradient differential problem.

Bibliography

[AIF92] Aifantis E.C., (1992). On the role of gradients in the localization of deformation and fracture. International Journal of Engineering Science, 30:10, 1279-1299.

[AIM09] Aimène Y., Vidal-Sallé E., Hagège B., Sidoroff F., Boisse P., (2009). A hyperelastic approach for composite reinforcement large deformation analysis. Journal of Composite materials, 44:1, 5-26.

[ALI03] Alibert J.-J., Seppecher P., Dell'Isola F., (2003). Truss modular beams with deformation energy depending on higher displacement gradients. Mathematics and Mechanics of Solids, 8:1, 51-73.

[ALT03] Altenbach H., Eremeyev V.A., Lebedev L.P., Rendón L.A. (2010). Acceleration waves and ellipticity in thermoelastic micropolar media. Archive of Applied Mechanics, 80 (3), 217-227.

[ATA97] Atai, A.A., Steigmann, D.J. (1997). On the nonlinear mechanics of discrete networks. Archive of Applied Mechanics, 67:5, 303-319.

[BAL06] Balzani D., Neff P., Schröder J., Holzapfel G.A., (2006). A polyconvex framework for soft biological tissues. Adjustment to experimental data. International Journal of Solids and Structures, 43, 6052-6070.

[BLE67] Bleustein J.L., (1967). A note on the boundary conditions of Toupin's strain gradient-theory. International Journal of Solids and Structures, 3, 1053-1057.

[BOE87] Boehler, J.P., (1987). Introduction to the invariant formulation of anisotropic constitutive equations. In: Boehler, J.P. (Ed.), Applications of Tensor Functions in Solid Mechanics CISM Course No. 292. Springer-Verlag.

[BOE78] Boehler J.P., (1978). Lois de comportement anisotrope des milieux continus. Journal de mécanique, 17.2, 153-190.

[BOI95] Boisse P., Cherouat A., Gelin J.C., Sabhi H., (1995). Experimental Study and Finite Element Simulation Of Glass Fiber Fabric Shaping Process. Polymer Composites, 16:1, 83-95

[CAO08] Cao J., Akkerman R., Boisse P., Chen J., et al., (2008). Characterization of mechanical behavior of woven fabrics: experimental methods and benchmark results. Composites Part A: Applied Science and Manufacturing, 39, 1037-53.

[CAS72] Casal P., 1972. La théorie du second gradient et la capillarité. C.R. Acad. Sci. Paris, Ser. A 274, 1571-1574.

[CIA88] Ciarlet P. G., (1988). Mathematical Elasticity, volume I. Noth-Holland, Amsterdam.

[CHA11a] Charmetant A., Vidal-Sallé E., Boisse P. (2011). Hyperelastic modelling for mesoscopic analyses of composite reinforcements. Composites Science and Technology, 71,1623-1631.

[CHA11b] Charmetant A., (2011). Approches hyperélastiques pour la modélisation du comportement mécanique de préformes tissées de composites. PhD thesis, INSA-Lyon, 2011.

[CHA12] Charmetant A., Orliac J.G.,Vidal-Sallé E., Boisse P. (2012). Hyperelastic model for large deformation analyses of 3D interlock composite preforms. Composites Science and Technology, 72, 1352-1360.

[COS09] Cosserat E., Cosserat F., (1909). Théorie de Corps déformables. Librairie Scientifique A. Hermann et fils, Paris.

[DEG81] deGennes, P.G., (1981). Some effects of long range forces on interfacial phenomena. Journal de Physique Lettres, 42.16, 377-379.

[DEL95a] dell'Isola F., Gouin H., Seppecher P., (1995). Radius and surface tension of microscopic bubbles by second gradient theory. C.R. Acad. Sci. II, Mec. 320, 211-216.

[DEL95b] dell'Isola F., Rotoli G., (1995). Validity of Laplace formula and dependence of surface tension on curvature in second gradient fluids. Mechanics Research Communications, 22, 485-490.

[DEL95c] dell'Isola F., Seppecher P., (1995). The relationship between edge contact forces, double force and interstitial working allowed by the principle of virtual power, C.R. Acad. Sci. II, Mec. Phys. Chim. Astron. 321, 303-308

[DEL96] dell'Isola F., Gouin H., Rotoli G., (1996). Nucleation of Spherical shell-like interfaces by second gradient theory: numerical simulations, European journal of mechanics. B, Fluids, 15:4, 545-568.

[DEL97] dell'Isola F., Seppecher P., (1997). Edge contact forces and quasi-balanced power, Meccanica 32, 33-52.

[DEL00] dell'Isola F., Guarascio M., Hutter K., (2000). A variational approach for the deformation of a saturated porous solid. A second-gradient theory extending Terzaghi's effective stress principle. Archive of Applied Mechanics. 70, 323-337.

[DEL09] dell'Isola F., Sciarra G., and Vidoli S., (2009). Generalized Hooke's law for isotropic second gradient materials. Proceedings of the Royal Society A: Mathematical, Physical and Engineering Science, 465, 2177–2196.

[DEL09a] dell'Isola F., Madeo A., Seppecher P., (2009). Boundary Conditions at Fluid-Permeable Interfaces in Porous Media: A Variational Approach. International Journal of Solids and Structures, 46, 3150–3164.

[DEL12a] dell'Isola F., Madeo A., Placidi L., (2012). Linear plane wave propagation and normal transmission and reflection at discontinuity surfaces in second gradient 3D Continua. Zeitschrift fur Angewandte Mathematik und Mechanik (ZAMM), 92:1, 52-71.

[DEL12b] dell'Isola F., Seppecher P., Madeo A., (2012). How contact interactions may depend on the shape of Cauchy cuts in N-th gradient continua: approach "à la D'Alembert". ZAMP, 63:6, 1119-1141.

[DEL14] dell'Isola F., Steigmann D.J., (2014). A Two-Dimensional Gradient-Elasticity Theory for Woven Fabrics. Journal of Elasticity, DOI 10.1007/s10659-014-9478-1.

[DUM03a] Dumont F.. Contribution à l'expérimentation et à la modélisation du comportement de renforts de composites tissés. Thèse de doctorat LMSP/LM2S, Paris : Université de Paris VI, 2003, 149 p.

[DUM03b] Dumont F., Hivet G., Rotinat R., Launay J., Boisse P., Vacher P.. Mesures de champs pour des essais de cisaillement sur des renforts tissés. Mécanique & Industries, 2003, vol. 4, pp. 627–635.

[DUM87] Dumont J.P., Ladeveze P., Poss M., Remond Y., (1987). Damage mechanics for 3-D composites Composite structures, 8:2, 119-141.

[ERE05] Eremeyev V.A., (2005). Acceleration waves in micropolar elastic media. Doklady Physics 50:4, 204-206.

[ERE13] Eremeyev V. A., Lebedev L. P., Altenbach H. (2013). Foundations of micropolar mechanics. Springer, Heidelberg.

[ERI64a] Eringen A.C., Suhubi, E.S. (1964). Nonlinear theory of simple microelastic solids: I. International Journal of Engineering Science, 2, 189-203.

[ERI64b] Eringen A. C., Suhubi, E. S. (1964). Nonlinear theory of simple microelastic solids: II. International Journal of Engineering Science., 2, 389-404.

[ERI01] Eringen A. C., (2001). Microcontinuum field theories. Springer-Verlag, New York.

[FER13] Ferretti M., Madeo A., dell'Isola F., Boisse P., (2014). Modeling the onset of shear boundary layers in fibrous composite reinforcements by second gradient theory, ZAMP 65, 3, pp. 587-612.

[FOR06] Forest, S., Sievert, R. (2006). Nonlinear microstrain theories. International Journal of Solids and Structures, 43, 7224-7245.

[FOR09] Forest S., (2009). Micromorphic Approach for Gradient Elasticity, Viscoplasticity, and Damage. Journal of Engineering Mechanics, 135:3, 117-131.

[FOR10] Forest S., Aifantis E.C., (2010). Some links between recent gradient thermo-elasto-plasticity theories and the thermomechanics of generalized continua. International Journal of Solids and Structures, 47:(25-26), 3367-3376

[GER73a] Germain, P., (1973). La méthode des puissances virtuelles en mécanique des milieux continus. Première partie. Théorie du second gradient. J. Mécanique 12, 235-274.

[GER73b] Germain, P., (1973). The method of virtual power in continuum mechanics. Part 2: Microstructure. SIAM Journal on Applied Mathematics, 25, 556-575.

[GRE64] Green A.E., Rivlin R.S., (1964). Multipolar continuum mechanics. Archive for Rational Mechanics and Analysis, 17: 2, 113-147.

[HAM13a] Hamila N., Boisse P., (2013). Tension locking in finite-element analyses of textile composite reinforcement deformation. Comptes Rendus Mécanique, 341:6, 508-519.

[HAM13b] Hamila N., Boisse P., (2013). Locking in simulation of composite reinforcement deformations. Analysis and treatment. Composites Part A: Applied Science and Manufacturing,109-117.

[HAR04] Harrison P., Clifford M.J., Long A.C. (2004). Shear characterisation of viscous woven textile composites: a comparison between picture frame and bias extension experiments. Composites Science and Technology, 64, 1453-1465.

[HAS96] Haseganu, E.M., Steigmann, D.J. (1996). Equilibrium analysis of finitely deformed elastic networks. Computational Mechanics, 17:6, 359-373

[HOL00a] Holzapfel, G.A., Gasser, T.C., Ogden, R.W., (2000). A new constitutive framework for arterial wall mechanics and a comparative study of material models. Journal of Elasticity 61, 1-48.

[HOL00b] Holzapfel, G.A., (2000). Nonlinear Solid Mechanics, Wiley.

[ITS00] Itskov M. (2000). On the theory of fourth-order tensors and their applications in computational mechanics. Computer methods in applied mechanics and engineering, 189:2, 419-38.

[ITS04] Itskov M., Aksel N., (2004). A class of orthotropic and transversely isotropic hyperelastic constitutive models based on a polyconvex strain energy function. International Journal of Solids and Structures, 41, 3833–3848.

[LAS88] Lasry D., Belytschko T., (1988). Localization limiters in transient problems.International Journal of Solids and Structures, 24: 6, 581-597.

[LEE08] Lee W., Padvoiskis J., Cao J., de Luycker E., Boisse P., Morestin F., Chen J., Sherwood J., (2008). Bias-extension of woven composite fabrics. International Journal of Material Forming, 1:895-898.

[LUO91] Luongo A. (1991). On the amplitude modulation and localization phenomena in interactive buckling problems. International Journal of Solids and Structures 27:15, 1943-1954.

[LUO01] Luongo A. (2001). Mode localization in dynamics and buckling of linear imperfect continuous structures. Nonlinear Dynamics 25:1, 133-156.

[LUO05] Luongo A., D'Egidio A. (2005). Bifurcation equations through multiple-scales analysis for a continuous model of a planar beam. Nonlinear Dynamics 41:1, 171-190.

[MAD08] A. Madeo, F. dell'Isola, N. Ianiro and G. Sciarra, (2008). A Variational Deduction of Second Gradient Poroelasticity II: an Application to the Consolidation Problem. Journal of Mechanics of Materials and Structures, 3:4, 607-625.

[MAD12a] Madeo A., George D., Lekszycki T., Nieremberger M., Rémond Y., (2012). A second gradient continuum model accounting for some effects of micro-structure on reconstructed bone remodelling. CRAS Mécanique, 340:8, 575-589.

[MAD12b] Madeo A., Djeran-Maigre I., Rosi G., Silvani C., (2012). The Effect of Fluid Streams in Porous Media on Acoustic Compression Wave Propagation, Transmission and Reflection. Continuum Mechanics and Thermodynamics, 25.2-4 (2013): 173-196.

[MAD13] Madeo A., Neff P., Ghiba I. D., Placidi L., Rosi G. (2013). Wave propagation in relaxed micromorphic continua: modeling metamaterials with frequency band-gaps. Continuum Mechanics and Thermodynamics, 1-20.

[MAK10] Makradi A., Ahzi S., Garmestani H., Li D.S., Rémond Y., (2010). Statistical continuum theory for the effective conductivity of fiber filled polymer composites: Effect of orientation distribution and aspect ratio A Mikdam. Composites Science and Technology, 70 :3, 510-517.

[MIK09] Mikdam A., Makradi A., Ahzi S., Garmestani H., Li D.S., Rémond Y., (2009). Effective conductivity in isotropic heterogeneous media using a strong-contrast statistical continuum theory. Journal of the Mechanics and Physics of Solids, 57:1, 76-86.

[MIN64] Mindlin R.D. , (1964). Micro-structure in linear elasticity. Archive for Rational Mechanics and Analysis, 51-78.

[NAD03] Nadler, B., Steigmann, D.J. (2003). A model for frictional slip in woven fabrics. Comptes Rendus - Mecanique, 331 (12), pp. 797-804

[NAD06] Nadler, B., Papadopoulos, P., Steigmann, D.J. (2006). Multiscale constitutive modeling and numerical simulation of fabric material. International Journal of Solids and Structures, 43 (2), pp. 206-221.

[NEF06a] Neff P., (2006). Existence of minimizers for a finite-strain micromorphic elastic solid. Proceedings of the Royal Society of Edinburgh: Section A Mathematics, 136(05), 997-1012.

[NEF06b] Neff P., (2006). A finite-strain elastic–plastic Cosserat theory for polycrystals with grain rotations. International journal of engineering science, 44(8), 574-594.

[NEF07] Neff P., Forest S., (2007). A geometrically exact micromorphic model for elastic metallic foams accounting for affine microstructure. Modelling, existence of minimizers, identification of moduli and computational results. Journal of Elasticity, 87(2-3), 239-276.

[NEF13] Neff P., Ghiba I. D., Madeo A., Placidi L., Rosi G., (2013). A unifying perspective: the relaxed linear micromorphic continuum. Continuum Mechanics and Thermodynamics, 1-43.

[NEF14a] Neff P., Ghiba I.D., Lankeit, J., (2014). The exponentiated Hencky-logarithmic strain energy. Part I: Constitutive issues and rank–one convexity. arXiv preprint arXiv:1403.3843.

[NEF14b] Neff P., Lankeit J., Ghiba I.D., Martin R., Steigmann, D.; (2014). The exponentiated Hencky-logarithmic strain energy. Part II: Coercivity, planar polyconvexity and existence of minimizers. arXiv preprint arXiv:1408.4430.

[OGD84] Ogden R.W., (1984). Non-linear elastic deformations. New York: Wiley and Sons.

[OGD03] Ogden R.W., (2003). Nonlinear Elasticity, Anisotropy, Material Stability and Residual stresses in Soft Tissue. CISM Courses and Lectures Series 441, 65-108.

[ORL12] Orliac J.G., (2012). Analyse et simulation du comportement anisotrope lors de la mise en forme de renforts tissés interlock. PhD thesis, INSA-Lyon, 2012.

[PEN13] Peng X., Guo Z., Du T., Yu W.R., (2013). A Simple Anisotropic Hyperelastic Constitutive Model for Textile Fabrics with Application to Forming Simulation. Composites Part B: Engineering, 52, 275-281.

[PIE09] Pietraszkiewicz W., Eremeyev V.A., (2009). On natural strain measures of the non-linear micropolar continuum. International Journal of Solids and Structures, 46:3, 774-787.

[OSH06] Oshmyan V.G., Patlazhan S.A., Rémond Y., (2006). Principles of structural-mechanical modeling of polymers and composites. Polymer Science Series A, 48:9, 1004-1013.

[PID97] Pideri C., Seppecher P., (1997). A second gradient material resulting from the homogenization of an heterogeneous linear elastic medium. Continuum Mechanics and Thermodynamic, 9:5, 241-257.

[PIO46] Piola G., (1846). Memoria intorno alle equazioni fondamentali del movimento di corpi qualsivogliono considerati secondo la naturale loro forma e costituzione. Modena, Tipi del R.D. Camera.

[PIO14] Piola G., (2014). The Complete Works of Gabrio Piola: Commented English Translation (Vol. 1). Springer.

[PLA13] Placidi L., Rosi G., Giorgio. I., Madeo A., (2013). Reflection and transmission of plane waves at surfaces carrying material properties and embedded in second gradient materials. Mathematics and Mechanics of Solids, DOI: 10.1177/1081286512474016.

[RAU09] Raoult A., (2009). Symmetry groups in nonlinear elasticity: An exercise in vintage mathematics. Communications on Pure and Applied Analysis, 8:1, 435-456.

[RIN07a] Rinaldi A., Lai Y.C., (2007), Damage Theory Of 2D Disordered Lattices: Energetics And Physical Foundations Of Damage Parameter. International Journal of Plasticity, 23, 1796-1825 .

[RIN07b] Rinaldi A., Krajcinovic D., Mastilovic S., (2007). Statistical Damage Mechanics and Extreme Value Theory. International Journal of Damage Mechanics, 16:1, 57-76.

[RIN08] Rinaldi A., Krajcinovic K., Peralta P., Lai Y.-C., (2008). Modeling Polycrystalline Microstructures With Lattice Models: A Quantitative Approach. Mechanics of Materials, 40, 17-36.

[RIN09] Rinaldi A. (2009). A rational model for 2D Disordered Lattices Under Uniaxial Loading. International Journal of Damage Mechanics, 18, 233-57.

[RIN11] Rinaldi A. (2011). Statistical model with two order parameters for ductile and soft fiber bundles in nanoscience and biomaterials. Physical Review E, 83(4-2) 046126.

[RIN13] Rinaldi A. (2013). Bottom-up modeling of damage in heterogeneous quasi-brittle solids. Continuum Mechanics and Thermodynamics, 25, Issue 2-4, 359-373.

[RIV48] Rivlin R.S, (1948). Large elastic deformations of isotropic materials. Philosophical Transactions of the Royal Society A: Mathematical, Physical and Engineering Sciences , vol. 241, pp. 379–397.

[ROS13] Rosi G., Madeo A., Guyader J.-L., (2013). Switch between fast and slow Biot compression waves induced by “second gradient microstructure” at material discontinuity surfaces in porous media. International Journal of Solids and Structures, 50:10, 1721-1746.

[SCH05] Schröder J., Balzani D., Neff P., (2005). A variational approach for materially stable anisotropic hyperelasticity. International Journal of Solids and Structures, 42, 4352-4371.

[SCI07] Sciarra G., dell’Isola F., Coussy O., (2007). Second gradient poromechanics. International Journal of Solids and Structures, 44:20, 6607-6629.

[SCI08] Sciarra G., dell’Isola F., Ianiro N., Madeo A., (2008). A Variational Deduction of Second Gradient Poroelasticity I: General Theory. Journal of Mechanics of Materials and Structures, 3:3, 507-526.

[SEP11] Seppecher P., Alibert J.-J., dell’Isola F., (2011). Linear elastic trusses leading to continua with exotic mechanical interactions. Journal of Physics: Conference Series, 319.

[SET64] Seth B.R. (1964). Generalized strain measure with applications to physical problems. In: Reiner M., Abir D.. Second-Order Effects in Elasticity, Plasticity and Fluid Dynamics. Pergamon Press, Oxford, 162-172.

[SIL97] Silhavy M., (1997). The Mechanics and Thermodynamics of Continuous Media. Springer.

[SPE84] Spencer A.J.M., (1984).Constitutive theory for strongly anisotropic solids, in Continuum Theory of Fibre- Reinforced Composites, CISM International Centre for Mechanical Sciences Courses and Lecture Notes, 282, Spencer A.J. M. Ed., Springer.

[STE92] Steigmann D.J, (1992). Equilibrium of prestressed networks. IMA Journal of Applied Mathematics (Institute of Mathematics and Its Applications), 48:2, 195-215.

[STE02] Steigmann D.J, (2002). Invariants of the stretch tensors and their application to finite elasticity theory. Mathematics and Mechanics of Solids, 7:4, 393-404.

[STE03] Steigmann D.J, (2003). Frame-invariant polyconvex strain-energy functions for some anisotropic solids Mathematics and Mechanics of Solids, 8:5, 497-506.

[TOU64] Toupin R., (1964). Theories of elasticity with couples-stress. Archive for Rational Mechanics and Analysis, 17, 85-112.

[TRI86] Triantafyllidis N., Aifantis E.C.A., (1986). Gradient approach to localization of deformation, I. Hyperelastic materials. Journal of Elasticity, 16:3, 225-237.

[HIL70] Hill R., (1970). Constitutive inequalities for isotropic elastic solids under finite strain. Proceedings of the Royal Society of London. A. Mathematical and Physical Sciences, 314(1519), 457-472.

FOLIO ADMINISTRATIF

THESE SOUTENUE DEVANT L'INSTITUT NATIONAL DES SCIENCES APPLIQUEES DE LYON

NOM : FERRETTI DATE de SOUTENANCE : 07/11/2014
(avec précision du nom de jeune fille, le cas échéant)

Prénoms : Manuel

TITRE : Non-Linear Mechanics of Generalized Continua and Applications to Composite Materials

NATURE : Doctorat Numéro d'ordre : AAAAISALXXXX

Ecole doctorale : Mécanique, énergétique, Génie civil, Acoustique

Spécialité : Mécanique, Génie mécanique, Génie civil

RESUME :

La microstructure des matériaux est un levier essentiel pour l'optimisation des propriétés mécaniques des structures. Le passage à la description continue de la matière conduit souvent à une simplification trop drastique de la réalité et à une perte significative d'informations. Les développements de la mécanique des milieux continus, des moyens de calcul numérique et des techniques expérimentales permettent aujourd'hui de rendre compte des effets d'échelle observés en mécanique des matériaux et des structures. Le but primaire de cette thèse a été celui de développer un modèle continu de gradient supérieur pour intégrer dans la modélisation continue la morphologie complexe des microstructures ainsi que les longueurs caractéristiques associées. Ce modèle continu généralisé a ensuite été utilisé pour décrire en détail le comportement mécanique des renforts de composites textiles.
Des simulations numériques qui montrent l'importance des termes de deuxième gradient pour la correcte description du comportement mécanique de ces matériaux ont été développées dans le cadre de cette thèse à l'aide du software COMSOL Multiphysics.
Il a été montré que des théories de deuxième gradient sont nécessaires pour intégrer dans la modélisation continue l'effet de la flexion des mèches au niveau mesoscopique. Ceci a été mis en évidence pour le cas du "bias extension test" et de la flexion trois points d'un interlock 3D de composite.
Pour le cas du "bias extension test", les termes de deuxième gradient permettent la description de certaines couches limites qui déterminent une zone de transition entre deux régions à angle de cisaillement constant.
Pour ce qui concerne la flexion trois points des interlocks de composite, il a été montré que les termes de deuxième gradient sont nécessaires pour décrire correctement la déformée des deux extrémités de la poutre et la courbure au milieu de l'échantillon.
Dans les deux exemples traités, l'effet de la flexion des mèches à l'échelle mesoscopique est le mécanisme principal donnant lieu aux effets de deuxième gradient.

MOTS-CLES : Renforts fibreux de composite, théories de second gradient, milieux continus général- isés, bias extension test, flexion trois points d'un interlock de composite.

Laboratoire (s) de recherche :
LaMCoS, INSA-Lyon, France.
Université de L'Aquila, Italie.

Directeur de thèse:
BOISSE Philippe, INSA-Lyon, France
LUONGO Angelo, Université de L'Aquila, Italie

Composition du jury :
BOISSE Philippe, DELL'ISOLA Francesco, LUONGO Angelo, MADEO Angela, REMOND Yves, RUBINO Bruno